NASA CR-72641

FINAL REPORT

DEVELOPMENT OF LOW COST ABLATIVE NOZZLES FOR SOLID PROPELLANT ROCKET MOTORS

VOLUME I

by

J. R. Mathis and R. C. Laramee

THIOKOL CHEMICAL CORPORATION
WASATCH DIVISION
Brigham City, Utah

Prepared for

NATIONAL AERONAUTICS AND SPACE ADMINISTRATION

12 February 1970

CONTRACT NAS3-10288

NASA Lewis Research Center
Cleveland, Ohio
J. J. Notardonato, Project Manager

NOTICE

This report was prepared as an account of Government-sponsored work. Neither the United States, nor the National Aeronautics and Space Administration (NASA), nor any person acting on behalf of NASA:

A.) Makes any warranty or representation, expressed or implied, with respect to the accuracy, completeness, or usefulness of the information contained in this report, or that the use of any information, apparatus, method, or process disclosed in this report may not infringe privately-owned rights; or

B.) Assumes any liabilities with respect to the use of, or for damages resulting from the use of, any information, apparatus, method or process disclosed in this report.

As used above, "person acting on behalf of NASA" includes any employee or contractor of NASA, or employee of such contractor, to the extent that such employee or contractor of NASA or employee of such contractor prepares, disseminates, or provides access to any information pursuant to his employment or contract with NASA, or his employment with such contractor.

Requests for copies of this report should be referred to

National Aeronautics and Space Administration
Scientific and Technical Information Facility
P.O. Box 33
College Park, Md   20740

FINAL REPORT

DEVELOPMENT OF LOW COST ABLATIVE NOZZLES
FOR SOLID PROPELLANT ROCKET MOTORS

VOLUME I

by

J. R. Mathis and R. C. Laramee

THIOKOL CHEMICAL CORPORATION
WASATCH DIVISION

Prepared for

NATIONAL AERONAUTICS AND SPACE ADMINISTRATION

FOREWORD

The research and development work described herein was conducted by Thiokol Chemical Corporation under NASA Contract NAS3-10288. The work was done under the management of the NASA Project Manager, Mr. J. J. Notardonato, NASA-Lewis Research Center.

This program was conducted at the Wasatch Division under the management of Mr. E. L. Bennion with Mr. E. L. Gray as the project engineer. Principal investigators were Mr. J. R. Mathis and Mr. R. C. Laramee. Motor manufacturing was supervised by Mr. L. S. Jones.

The program final report consists of two volumes. Volume I contains the text and Volume II the illustrations and tables as referenced in the text.

ABSTRACT

The object of this program was to investigate and evaluate low cost materials and processes applicable to full sized nozzles for 260 in. solid rockets.

Over 20 materials were subjected to increasingly severe tests, consisting of mechanical, physical, and thermal properties and evaluation in nozzles of three different sizes, ranging in throat diameter from 0.34 to 8.1 inches. Resulting data were analyzed, and the better performing materials were employed in the design and performance prediction of four full sized nozzles for 260 in. solid rockets.

Conclusions are that acceptable full sized nozzles can be fabricated at substantially lower cost than those produced in the past.

TABLE OF CONTENTS

Page

TABLE OF CONTENTS (Cont)

SUMMARY

The objective of this program was to develop and evaluate low cost materials and processes suitable for use in ablative nozzles for large, 260 in. diameter solid propellant rocket motors.

The program was initiated with a survey of available low cost materials and processes which showed potential for large low cost nozzles. Forty-three materials were seriously considered for inclusion in this program, encompassing seven basic groups of materials: carbon cloth binder, graphite particle binder, fiberpaper phenolic, silica cloth binder, asbestos binder, paper binder, and miscellaneous. Twenty-one materials were finally selected as candidates and subjected to evaluation. The materials were subjected to a series of screening tests consisting of mechanical properties at both ambient and elevated temperatures, physical properties, and thermal properties. In addition, each material was fabricated into three individual test nozzles which were subsequently static tested on a TU-379 materials screening motor. Erosion and char rates of the materials were then calculated and plotted versus total heat flux or heat transfer coefficients. Fabrication techniques for the materials were also explored during the fabrication of the nozzles and test specimens.

Following the evaluation of results from these tests, 10 materials were selected for further evaluation in nozzles tested on the TU-622, a larger, more severe materials evaluation motor. The 10 materials were LCCM-2610 (graphite particle phenolic), LCCM-4120 (graphite particle phenolic), SP-8057 (Pluton H-1 Fabric phenolic), 4C1686 (carbon cloth polyphenylene), WB-8251 (Avceram C/S cloth phenolic), MXSC-198 (Avceram C/S cloth epoxy novolac), SP-8030-96 (heavyweight silica cloth phenolic), MXS-198 (silica cloth epoxy novolac), 23RPD (Asbestos/cork phenolic), and SMS-21 (Kraft paper phenolic). Each nozzle consisted of three basic components: inlet, throat, and exit cone. Depending upon the material being evaluated, the throat diameters ranged from 1.41 to 1.74 inches. Each component employed a different fabric orientation, providing a means of comparison for a single material in different orientation as well as an opportunity to evaluate different fabrication methods with the same material. The exit cones were oriented parallel to the centerline of the nozzle, the throats 45 deg and the inlets 90 degrees. The nozzles were evaluated after firing, and erosion and char rates for each material were calculated and plotted versus a heat transfer coefficient or total heat flux.

Following the testing and evaluation of these 10 nozzles, six large subscale nozzles with approximately an 8 in. throat were fabricated and static tested at Edwards AFB (RPL) on modified Stage II Minuteman motors. A total of 14 materials and three fabrication concepts were encompassed in the six nozzles. Five materials

1

were preselected from a previously conducted, similar program, while the remaining materials and the three fabrication concepts evolved from the work described in this report. Each nozzle contained five major liner components and two backup insulative components as shown below in the materials/components matrix.

Nozzle No.	1	2	3	4	5	6
Submerged Liner	FM-5272	MXA-6012	23RPD	KF-418	KF-418	SP-8030-96
Nose	WB-8217	4C-1686	SP-8057	KF-418	SP-8030-96	FM-5272
Inlet	WB-8217	4C-1686	SP-8057	SP-8030-96	LCCM-2626	SP-8030-96
Throat	MX-4926	LCCM-2626	SP-8050	SP-8030-96	LCCM-2626	SP-8057
Forward Exit	SP-8050	LCCM-2626	SP-8057	23RPD	LCCM-2626	KF-418
Aft Exit	KF-418	LCCM-2626	SP-8030-96	MXS-198	LCCM-4120	FM-5272
Throat Backup	MXA-6012	23RPD	FM-5272	SP-8030-96	23RPD	KF-418
Exit Overwrap	MXA-6012	MXB-6001	23RPD	KF-418	KF-418	FM-5272

With the assistance of the previously plotted erosion rate versus total heat flux or heat transfer coefficient curves determined from TU-379 and TU-622 nozzle firings, predicted erosion rates for each material in each nozzle location were made and subsequently compared to actual rates determined after firing of each of the larger nozzles. The curves were then corrected as necessary and utilized in the design of full sized nozzles for a 260 in. diameter motor.

Several significant achievements were made during the fabrication and testing of the six large nozzles. Components fabricated of a number of smaller segments, rather than one monolithic part, were successfully tested in two nozzles. These components contained longitudinal as well as radial joints. Components fabricated under autoclave pressure were successfully tested in all six nozzles, and some successful components were fabricated under vacuum pressure only. From a materials viewpoint, silica cloth phenolic was wholly satisfactory as the throat in one nozzle, exhibiting very uniform erosion at a maximum rate of approximately 20 mils per second. Canvas phenolic, a very low cost material when compared to other ablative materials ($1.35 per pound) performed as well as silica in the exit cone and backside insulated liners in a total of four nozzles.

Following the testing and evaluation of the materials in the six subscale nozzles, four full scale low cost material nozzles for use on 260 in. diameter

solid rocket motors were designed along with a baseline nozzle incorporating standard materials. The materials employed in the low cost nozzles were selected through the employment of a special rating method derived for this purpose. Cost/ performance effectiveness studies were performed on these nozzle designs and compared to the baseline nozzle as well as a nozzle design supplied by NASA-Lewis.

Based on the work performed in this program, several significant conclusions were drawn, as outlined below.

Nozzle ablative and insulative materials cost savings of from 69 to 76 percent can be realized on large 260 in. booster nozzles by utilizing the lower cost materials "standard" carbon cloth and silica cloth materials and Pluton H-1 carbon cloth phenolic, low cost reinforcement materials such as canvas and paper phenolic, and the low cost carbonaceous materials developed by Thiokol. Additional savings can be realized by employing lower cost fabrication methods proven in this program, consisting of curing components at pressures entirely within autoclave range or by employing epoxy novolac resin curing at 1 atmosphere pressure. It was further shown in this program that savings can be realized in the manufacture of large nozzles through the utilization of a segmented concept in which the components are assembled of smaller segments rather than being fabricated of one monolithic piece. It was also shown that performance of a segmented throat, containing longitudinal joints, is totally unaffected by the joints.

MATERIALS SELECTION

To thoroughly survey the field of new and improved materials, formal letters were written to the suppliers of insulation materials requesting recommendations for lightweight, low cost materials to be used in the various areas of a large nozzle. Personal contact was also encouraged in these letters. Table 1 contains a list of the vendors contacted. Previous results and test data on these materials were reviewed, especially results obtained in the Nomad series of nozzles fabricated and evaluated by Aerojet-General Corporation under USAF Contract AF 04(611)-11646.

A large number of materials was considered, with over 40 being listed for final consideration, as shown on Table 2. The materials recommended from this group for use in the initial evaluation phases of this program are denoted by an asterisk and then isolated on Table 3. The materials were divided into general classifications or families, such as asbestos-binder or low cost carbonaceous. Every effort was made to select representative materials from each of these families in order to preclude the possibility of overlooking a promising type of material and to guarantee a representative cross section of all currently available materials.

The materials were selected on the basis of available information examined in the light of past experience by Thiokol engineering personnel. As many factors as possible were considered, such as cost, availability, performance, tentative fabrication methods, and experience with similar materials.

Some families of materials were not considered for this program for various reasons. Graphite cloth reinforced and regraphitized materials were not considered primarily because of their extra cost and because carbon cloth will perform adequately and reliably in a large nozzle, eliminating the need for testing these somewhat higher performance materials. Woven cloths, such as Avceram C/S fabric, containing a codeposit of carbon and silica, were also eliminated from original consideration for similar reasons. Although their performance in the Nomad program had been comparable to a straight carbon cloth-phenolic tape, there was not a significant cost advantage over the carbon cloth materials. In addition, none of these materials were recommended by any of the preimpregnating facilities queried, probably because of their cost.

Two fibertape materials produced by Fiberite Corporation, MSCS-313 (carbon and silica) and MXSA-313 (silica and asbestos) were not selected at this time. It was felt that these two materials, which are blends of carbon, silica, or asbestos fibers, were merely logical extensions of the basic materials MSC-313, MXS-313 and MXA-313, which were selected. If the basic materials showed promise later in the program, the two blends of these materials could be easily added.

4

An inquiry was also made to IIT Research Institute concerning a trowelable carbonaceous composite material, but information received was inadequate due to proprietary considerations and consequently the material was not considered.

The following 19 materials were approved by NASA for test evaluation.

Material	Type	Supplier
LCCM-2610	Graphite powder phenolic	Thiokol Chemical Corp
LCCM-4113	Graphite particle NBR phenolic	Thiokol Chemical Corp
LCCM-4120	Graphite particle phenolic	Thiokol Chemical Corp
LCCM-(reinforced)	Graphite particle phenolic, reinforced	Thiokol Chemical Corp
MXS-313	Silica fiberpaper phenolic	Fiberite Corporation
MXA-313	Asbestos fiberpaper phenolic	Fiberite Corporation
MXC-198	Carbon cloth epoxy novolac	Fiberite Corporation
4C-1686	Carbon cloth polyphenylene	Coast Mfg & Supply
4C-2530	Avceram C/S phenolic	Coast Mfg & Supply
FM-5072LD	Carbon cloth phenolic (silica microballoons)	U.S. Polymeric
SP-8057 (Pluton)	Pluton H-1 phenolic	Armour Coated Products
MXS-198	Silica cloth epoxy novolac	Fiberite Corporation
SP-8030-48 and -96	Silica cloth phenolic	Armour Coated Products
4S-5186	Silica cloth polyphenylene	Coast Mfg & Supply
4065	Silica cloth NBR phenolic (phenolic microballoons)	Narmco

5

Material	Type	Supplier
4A-6385	Asbestos polyphenylene (ceramic microballoons)	Coast Mfg & Supply
23-RPD	Chrysotile asbestos phenolic (cork filler)	Raybestos-Manhattan
WB-7605	Microbestos DS phenolic	Western Backing
SMS-21	Kraft paper phenolic	Thiokol Chemical Corp

Three of the above materials (SMS-21, 4C-2530, and SP-8057) were not included in the original recommendation by Thiokol, but were included in the material test matrix as a result of additional consultation with NASA.

In addition to the 19 materials selected for initial test evaluation, another six materials, originally recommended by Thiokol, were to be held in abeyance for evaluation in the subsequent task, Subscale Nozzle Evaluation. All six of these materials received extensive exposure in the Nomad program under USAF Contract AF 04(611)-11646. They performed well in the Nomad nozzles and it was jointly agreed by NASA and Thiokol that preliminary screening and evaluation of these materials would be redundant. Consequently, these materials were incorporated directly into the first subscale nozzle, employing Nomad obtained data for design information. Subsequent subscale nozzles contained some number of these six materials as well as materials derived by Thiokol. Table 4 contains a listing of these materials. Included in the table is a listing of Nomad nozzle exposures through Nozzle No. 8.

MATERIALS SCREENING AND EVALUATION

Quantities of each material were ordered from the suppliers for the 19 materials selected by NASA-Lewis and Thiokol in the Materials Selection phase of this program. A sufficient amount of each material was ordered to allow screening tests to be performed.

The materials screening and evaluation tests consisted of determining physical and mechanical properties of the materials at temperatures up to 600°F and erosion and char performance testing in TU-379 motor nozzles.

Upon receipt of a material from a vendor, flat laminates were fabricated, from which tensile, shear, and compression specimens could be machined. Illustrations of these test specimens are contained in Figures 1 and 2. The specimens were machined from the laminates in both the warp (parallel) and fill (perpendicular) directions, so that test data could be obtained in both the strong (warp) and weak (fill) directions of the materials. Testing was accomplished on a Riehle Screw Power Universal Testing Machine, Model FS. An oven was employed for the high temperature tests. The specimens were brought to temperature in the oven and then tested while still inside the oven. A summary of the data thus obtained is contained in Tables 5 thru 8.

Examination of the data contained in these tables indicates that the fabric re-inforced materials generally possess greater strength in the warp direction than in the fill direction, which is to be expected. This is also true for the fibrous materials such as asbestos which were obtained in tape form, indicating that at least some degree of fiber orientation occurs during processing of the raw material. All materials were affected by high temperatures, decreasing in strength with increasing temperature.

In tensile strength properties, the carbon, silica, and asbestos reinforced phenolic materials retained over 50 percent of their strength at 600°F. In compressive and interlaminar shear properties, strength retention of the asbestos and silica materials was even more impressive, with up to 100 percent of strength retention at 600°F. The carbon reinforced materials were less spectacular, showing strength retention in the range of 25 to 50 percent.

Nozzle inlet and exit cone components for TU-379 motors were also fabricated from each of the selected materials. An illustration of the TU-379 motor assembly is contained in Figure 3, and a detailed sketch of the nozzle is contained in Figure 4. Basically, the TU-379 is a small, cartridge loaded, end burning, materials screening motor which operates at an average pressure of about 400 psi for approximately 15 seconds. As can be seen in Figure 4, the fabric type materials were oriented 45 deg to the centerline in the inlet and 60 deg to the centerline in the exit. The throat material in all test firings was HLM-85 graphite. Solid billets were fabricated of each material and then machined to the proper configuration. In all cases, vendor

7

recommendations were followed with regards to cure conditions. A brief summary of these conditions is contained in Table 9.

During the fabrication of TU-379 components, one material was eliminated from further evaluation because of processing difficulties encountered. The material, WB-7605, was Johns Manville's Microbestos DS impregnated with a phenolic resin by Western Backing Company. Examination of this material on receipt indicated that the material had not been impregnated, but only coated with resin. In addition, the coating was nonuniform. Some areas were heavily coated and exhibited the characteristics of flypaper, while other areas appeared not to be coated at all. Flat laminates, up to 0.5 in. thick, were satisfactorily fabricated of this material; however, repeated attempts to manufacture a TU-379 inlet cone billet were unsuccessful. This billet was 4.2 in. high by 3 in. in diameter with all plies oriented at a 45 deg angle. During cure, all resin flow appeared to be to the outside diameter between plies with no flow through the plies. Consequently, a number of delaminations occurred, each at a ply which appeared to be uncoated. As a result of this experience, Thiokol recommended and received approval that the material be eliminated from the program. In place of this substance, a material designated as MXCS-198, from Fiberite Corp, was substituted. The material was Avceram C/S fabric impregnated with epoxy novolac resin. It theoretically combined the advantages of a low cost, high performance fabric with a resin system requiring only vacuum bag pressure for cure. As it later developed, this material was not received in time for TU-379 nozzle testing.

Following the fabrication and assembly of the TU-379 nozzles of the various materials, they were static tested. Three nozzles of each material were tested in order to obtain adequate data and to compensate for irregularities and questionable results which might occur in a single firing. After static test, the nozzles were disassembled and each inlet cone and exit cone was cut in half lengthwise and measured for char and erosion along its length at 0.1 in. intervals or stations. An erosion and char profile was then made for each individual component. Figures 5 and 6 illustrate the forms on which these measurements were made and recorded. This data, which is quite voluminous, will be kept on file and supplied on request.

For the purposes of this report, however, the erosion and char rates of each material were averaged for the three cones of each material at representative stations. These more condensed data are included in Table 10.

As would be expected, the carbon and graphite reinforced materials underwent the least erosion. Examination of the data in Table 10 indicates that LCCM-2610 experienced no erosion whatsoever while the most erosion was experienced by LCCM-4120 in the inlet. The remainder of the carbon cloth materials were in between. The only NBR modified material in this group, LCCM-4113, suffered extreme erosion in both inlet and exit and consequently was eliminated. One carbon cloth material, MXC-198, employed an epoxy novolac resin and was cured under vacuum bag pressure only. Although this material performed poorly, with erosion as high as 28 mil/sec, it was felt that the basic difficulty was in the fabrication and not the material itself.

A higher flow version of the material would have performed more satisfactorily. The two Avceram C/S reinforced materials experienced erosion approximately midway between carbon reinforced and silica reinforced materials. Silica and asbestos reinforced materials performed as was expected, eroding in the range of 14 mil/sec for silica and 19 mil/sec for asbestos, except for 23-RPD (asbestos/cork phenolic) which experienced the surprisingly low erosion rate of 13 mil/seconds.

Figures 7 thru 11 illustrate typical cross sections of fired TU-379 nozzles of each material compared to other materials of the same family. Both erosion and char depth can be seen on the sections, as well as fabric orientation in the two components.

With the completion of the above tests and data reduction and correlation, the material screening and evaluation phase of the program were completed. An examination of the data obtained on the materials tested in this task resulted in the recommendation to NASA-Lewis of 10 materials to be more fully evaluated in the Evaluation of Most Promising Materials program phase.

Table 11 presents a listing of the 10 recommended materials together with a brief description and comment on each. Nine of these materials were subsequently approved by NASA-Lewis. The 10th material, 4065 (silica NBR phenolic), was replaced by SMS-21 (Kraft paper phenolic).

Although previously mentioned tables contain some information pertaining to the recommendation or rejection of individual materials for additional follow-on evaluation, it is advisable here to briefly discuss each material tested in this phase of the program, indicating its particularly favorable and unfavorable points.

For simplification, the materials are grouped into families and compared to each other within these families, since an attempt was made to select representative materials from each family for continued evaluation. Materials marked with an asterisk (*) are those originally recommended by Thiokol for follow-on test evaluation. It should be noted that some of the points mentioned here were verified by subsequent testing while other points were discredited.

Family No. 1 - Low Cost Carbonaceous Materials

LCCM-2610.* - This material exhibited fairly high char (30 mil/sec) but absolutely no erosion in subscale TU-379 firings. Previous firings in 4 and 8 in. throat nozzles had previously demonstrated the outstanding characteristics of this material.

LCCM-4113. - This material, which employed an NBR modified phenolic resin system, exhibited rather poor mechanical properties (tensile strength $<$ 500 psi). In addition, severe erosion ($>$ 100 mil/sec) was encountered in TU-379 motor firings. Consequently, this material was rejected.

LCCM-4120.* - This material underwent medium erosion (10 mil/sec) in TU-379 tests. The material unquestionably charred, but its makeup is such that the char could not be visibly measured. The material is very low in cost ($0.75/lb) and can be cast and cured at vacuum bag pressure. As with LCCM-2610, the LCCM-4120 has also performed well in larger nozzles. Its mechanical properties were adequate (tensile strength of 2300 psi), particularly when its low curing pressures were also taken into consideration.

Family No. 2 - Carbon Cloth Reinforced Materials

SP-8057.* - The reinforcement in this material is Pluton H-1 fabric, possessing a high surface area and consequently a resin content in excess of 50 percent. A resin content of 50 percent results in lower prepreg price. The material handled very well and was comparable in performance to standard carbon cloth phenolic materials with resin contents of 34 percent. Erosion and char properties as measured by TU-379 firings were very good (5 and 17 mil/sec, respectively). Apparently this material could be used as a direct substitute for the best carbon phenolic materials with no loss of performance.

FM-5072LD. - Performance of this material was equivalent to that of any standard carbon cloth phenolic material with an erosion rate of 9 mil/sec. The specific gravity of this material was in the range of 1.1 to 1.3 as compared to 1.4 to 1.5 for standard materials. The high cost of the material, however, did not warrant its use.

4C-1686.* - Erosion rate of 4.5 mil/sec was equivalent to standard materials, and the TU-379 inlet erosion was the lowest found in this family. The material handled well and was easy to fabricate into uniform parts having a specific gravity of approximately 1.3.

MXC-198. - The outstanding feature of this material was its low pressure cure capability of 15 psi. Cost was reasonable when its fabrication potential was considered. The sample evaluated possessed insufficient flow, causing delaminations and excessive erosion (28 mil/sec) when tested in TU-379 motors. Higher flow of resin would make this a desirable material. This specific material was not recommended for continued evaluation because of its cost, but the same resin was recommended below with silica reinforcement.

Family No. 3 - Silica Reinforced Materials

SP-8030-96.* - The double weight fabric allowed a fast fabrication time. The material handled well and produced consistent, uniform parts. It is a typical standard silica phenolic material at a lower cost than other standards ($4.90/lb vs $5.90/lb).

4S-5186. - This material is a good handling double weight material producing good parts. It had a slightly higher erosion rate (14.1 mil/sec) and slightly lower char rate (17.4 mil/sec)than the above material and was considered a good second choice to SP-8030-96 at a somewhat higher cost.

MXS-313. - This material was composed of impregnated silica fibers in a mat or felt form. As such, it allowed for very fast thickness buildup, although there was a correspondingly high bulk factor. Resultant parts were very low in specific gravity (0.8). Excessive erosion (>100 mil/sec) in TU-379 tests eliminated this material from further consideration.

4065.* - This material was recommended solely on the basis of its low density (1.0). As a flexible NBR modified phenolic, it had limited application potential in some nozzle areas. Erosion and char characteristics (27 mil/sec) were adequate considering the material's low density. The material fabricated very well, providing fast buildup and uniform parts.

MXS-198.* - The outstanding feature of this material was its potential in reduced fabrication costs through its low pressure (vacuum bag) curing requirements. In addition, the material was procured with a double weight fabric reinforcement, resulting in shorter fabrication time. The material sample evaluated had too low a flow in the resin, resulting in delamination during firing in the TU-379 motor. Despite this, erosion and char rates were adequate (34 and 52 mil/sec, respectively). A higher resin flow version of this material was to be obtained for subsequent evaluation.

Family No. 4 - Avceram C/S Reinforced Materials

WB-8251.* - This material had excellent handling and fabrication characteristics and very uniform erosion and char rates (8 and 15 mil/sec, respectively) when evaluated in TU-379 firings.

4C-2530. - This product was very similar to above material, with an erosion rate of 12 mil/sec and tensile strength properties of 7,600 psi. This material would be a good second choice.

MXCS-198.* - This material was not specifically evaluated as it was not thought of until too late for inclusion in this program phase, but it nevertheless was recommended for evaluation in the following phase. The material combined Avceram C/S reinforcement with epoxy novolac resin, which results in a material possessing great potential. Avceram C/S reinforcement had so far produced excellent results in both this program and the previously conducted Nomad program. Epoxy novolac resins performed well in the Nomad program and offer a substantial reduction in fabrication costs because of their ability to cure at vacuum bag pressures. It was because of the potential of this material that it was recommended for evaluation.

11

Family No. 5 - Asbestos and Paper Reinforced Materials

MXA-313. - This material possessed a high density (1.6) and exhibited non-uniform char in the TU-379 inlet cones in an area immediately adjacent to the graphite throat insert. Because of its thickness, the material produced a fast buildup in part fabrication, but it also had a high bulk factor. This material would be a good second choice.

4A-6385. - This material had the highest erosion and char rates (19 and 22 mil/sec, respectively) and lowest density (1.4) of any asbestos materials evaluated. The material fabricated well, but the improved char characteristics claimed for the polyphenylene resin system did not materialize.

23-RPD.* - This material had the best erosion and char properties (13 and 15 mil/sec, respectively) of any materials in the family. Areas not exposed directly to exhaust in TU-379 firings showed amazingly low char. The material fabricated easily into uniform parts and would make an excellent backup material.

WB-7605. - As was stated previously in this report, this material delaminated severely during part fabrication and was consequently dropped from further consideration.

SMS-21. - This material possessed good erosion and char properties (9 and 15 mil/sec, respectively). Overall, a very good material with one outstanding deficiency: it had no drape whatsoever. As a result, wrinkles in parts were a certainty. For this reason, the material was not recommended.

Nine of the 10 materials recommended by Thiokol for additional evaluation were subsequently approved by NASA-Lewis. The 10th material, 4065 (silica NBR phenolic), was replaced by SMS-21 (Kraft paper phenolic) by NASA-Lewis.

Following the final selection of the 10 materials, a TU-379 performance summary was made. Erosion and char rates of each of the 10 materials were selected at six locations in the nozzle and corrected to reflect the average pressure and time of all the motors tested. The resultant data is presented in Table 12.

Both corrected and uncorrected values are contained in this table. Examination of the data in this table indicates that correction of the erosion and char values to a standard has not significantly altered any of the values. None were changed by more than one mil/second.

Following is a relative ranking of the material as provided by the correct maximum erosion rates at nozzle Station 9 (the forward interface with the graphite throat).

Ranking	Material	Erosion Rate (M/S)
1	LCCM-2626, Graphite particle phenolic	0.0
2	4C-1686, Carbon polyphenylene	3.6
3	SP-8057, Carbon phenolic	4.6
4a	WB-8251, Carbon-silica phenolic	7.9
4b	SMS-21, Paper phenolic	7.9
5	LCCM-4120, Graphite particle phenolic	9.7
6	23-RPD, Asbestos phenolic	12.2
7	SP-8030-96, Silica phenolic	13.5
8	MXS-198, Silica epoxy novolac	25.8

It is noted that the tenth material, MXCS-198, was not ranked since it had not been evaluated at this point in the program.

EVALUATION OF MOST PROMISING MATERIALS

Upon approval by NASA-Lewis of the 10 materials recommended for additional evaluation, sufficient quantities of each were ordered to fabricate a complete nozzle liner assembly - inlet, throat and exit cone. Primary emphasis during this phase of the program was placed upon the fabrication and testing of TU-622 nozzles. The TU-622 motor (Figure 12) is a relatively large materials evaluation motor, containing approximately 250 lb of propellant in an end-burning configuration. The nozzle for this motor (Figure 13) is divided into three major areas for materials performance evaluation: inlet, throat, and exit cone. In addition, two design configurations were developed to equalize the test vehicle operating parameters (average pressure and burning time) among the ten nozzle assemblies. It was anticipated that the erosion rate of the "black material", i.e., carbon, graphite particle and Avceram C/S reinforced materials, would range from 0 to 10 mil/sec; whereas the erosion rate of the "white materials", i.e. silica, asbestos and paper reinforced materials, would range from approximately 12 to 18 mil/sec when evaluated in the TU-622 nozzle throat. To compensate for this material category performance variation, the throat diameter was set at 1.74 in. in the nozzle assemblies containing black materials, and the throat diameter was set at 1.41 in. in the nozzle assemblies containing the white materials.

The nozzle area components employed different fabric orientation: (1) the inlet was perpendicular to the centerline, (2) the throat was 45 deg to the centerline, and (3) the exit cone was parallel to the centerline. The inlet and throat components were fabricated by cutting plies to a pattern, laying the plies up in a compression tool, and curing in a press. Inserts were employed in the compression tools to obtain the proper fabric orientation. Although these components were cured in a press because of their size, a maximum pressure of 225 psi was utilized in order to simulate autoclave pressures. The exit cones, on the other hand, were tape wrapped on a mandrel and cured in an autoclave. A cure summary of all the TU-622 components and materials is contained in Table 13.

Generally, the majority of these components fabricated well, with little or no difficulty encountered. Only a few parts presented any major problems. Table 14 lists the nozzles and summarizes the problems (or lack of problems) encountered in their fabrication and the solution to the problems. Problems were encountered in forming the exit cones of the nozzles assigned to evaluate materials WB-8251, MXCS-198 and MXS-198. In the interest of program schedule requirements, readily available materials were used in their place. The exit cone of the WB-8251 material evaluation nozzle was replaced with LCCM-2626 formed into a segmented design as illustrated in Figure 14. This material was an improved version of LCCM-2610 in that a dry powder resin was employed rather than a standard wet resin, which required an additional staging and grinding operation. The exit cone of the MXCS-198 material evaluation nozzle was replaced with LCCM-2610 which was also formed into a segmented design.

The exit cone of the MXS-198 material evaluation nozzle was replaced with LCCM-2610 formed into a cylinder with the internal surface subsequently machined to a monolithic cone configuration. The segmented exit cone configuration was incorporated into this phase of the program to obtain a relative performance comparison between segmented and nonsegmented nozzle components. A problem was also encountered in forming a quality throat component from MXS-198. Standard silica cloth phenolic materials, MX-2600 and Astrolite 1401P, were substituted and formed into a two piece liner throat insert.

Following the fabrication and assembly of the 10 nozzle assemblies, they were static tested on TU-622 motors designed to operate at an average chamber pressure of 400 psia over a 30 to 35 sec web burn time. Figures 15 thru 34 offer views of these nozzles after firing and prior to post-fire performance analysis. Pressure-time records of the TU-622 motors are contained in Figures 35 thru 44. After the nozzles were static tested, the fired components were removed from the steel shell and when necessary, bonded back together. One lengthwise cut was then made on the assembly, cutting each nozzle exactly in half. Cutting the nozzles this way exposed the char depth so that it could be measured. Photographs of these cross sections, in which the char and ply orientations can be clearly seen, are shown in Figures 45 thru 54. Erosion and char measurements were made on the cross sections at 0.5 in. intervals or stations along their entire length, as illustrated in Figure 55.

After static firing of the motor assemblies, a visual examination and general assessment of the performance of each nozzle was made. Comments concerning the results of this examination follow, with a brief performance summary of each of the program candidate materials.

LCCM-2610. - This material experienced low, uniform erosion (max 4 mil/sec) with some localized spalling. Several cracks were also visible, but in all cases they were formed during cooldown. This material was clearly one of the better performers.

4C-1686. - This material also underwent low, uniform erosion (max 4.7 mil/sec) and was completely free of spalling. A few cooldown cracks occurred, but overall the material was excellent in appearance and was considered a very good performer.

WB-8251. - This material was tested in the inlet and throat only. In these locations it performed fairly well, producing uniform erosion in the throat (7.8 mil/sec) and fairly uniform erosion in the inlet (7 mil/sec) with only some grooving. No spalling or cracking occurred.

SP-8057. - This material produced fairly uniform erosion (ranging from 1 to 7 mil/sec), with only a few localized areas of spalling. A large amount of cracking or delaminating took place, all of it during cooldown. Considering the high 50 percent resin content of this material it performed well.

MXSC-198. - The material performed fairly well (6 mil/sec), producing uniform erosion in the inlet and throat, which were the only two areas where it was tested. Some localized grooving took place, but considering the vacuum bag low pressure cure, the material was a good performer.

LCCM-4120. - This material experienced fairly uniform erosion overall, with a fairly high amount of localized pitting and spalling. Some grooving in the throat occurred. Despite its appearance, the material produced very good overall erosion resistance (5.6 mil/sec at the throat).

SP-8030-96. - This material produced fairly high erosion (max 17 mil/sec), as would be expected. On the other hand, the erosion and char rates were extremely uniform for ply oriented 45 deg upstream with no spalling or cracking. If the higher erosion is acceptable, this would be an excellent material.

MXS-198. - As previously described in this report, this material was tested only in the inlet. In this location it performed very well, producing uniform erosion with very minor grooving. The degree of erosion (13 mil/sec) is comparable to a standard silica phenolic material in the area where evaluated.

23-RPD. - This material performed well in all areas, exhibiting uniform erosion with no cracking or spalling and with a maximum erosion rate of 16.2 mil/sec, similar to that of a silica phenolic material. It appeared to have a low char strength.

SMS-21. - This material seemed to produce a uniform erosion except in areas containing wrinkles, which were numerous. Severe grooving or gouging occurred in these areas. The material also seems to possess little or no char strength and erodes about as fast as it chars. At the throat, the erosion rate was 18.2 mil/sec; the char rate was 26.3 mil/seconds.

Also tested in these motors were three exit cones not originally included in the test matrix. A brief description of their performance follows.

One-Piece LCCM-2626. - This material, an improved processing version of LCCM-2610, exhibited performance identical to that of LCCM-2610. Based on this test, LCCM-2626 was substituted for the remainder of this program.

Segmented LCCM-2610 and Segmented LCCM-2626. - These two components were identical in performance. Each consisted of four quarter-segments bonded together and overwrapped. Both exhibited extremely uniform erosion and were totally unaffected by the presence of the longitudinal seams or joints between segments. Their performance was identical to that of one-piece LCCM-2610 exit cone discussed above.

Detailed erosion and char data on each individual nozzle are contained in Tables 15 thru 24.

Following the nozzle post-test operations, a material erosion and char performance analysis was conducted (Table 25). Erosion and char rates of the materials in nozzles one thru 10 were calculated at seven stations along the nozzle and correct to standard nozzle conditions (average web burn time pressure of 466 psia, initial throat diameter of 1.74 in. and a web burning time of 33.2 seconds). Nozzle No. 5, as reflected in Table 25, was selected as the standard. As previously mentioned, slight variations existed between the design of "white material" nozzle and the "black material" nozzle. As a result of these variations (throat diameter and inlet angle), the planes along the nozzle in which the performance measurements were taken differ slightly between the two designs. For example, the distance between Station (plane) 1 and Station 2 is 0.5 inch. However, the area ratio at Station 1 is equivalent to the area ratio at Station 2, i.e., 10.65 as compared to 10.63 respectively.

Following is an erosion rate performance comparison summary of the 10 materials by nozzle area - inlet, throat, and exit cone.

Material	Inlet	Throat	Exit Cone	Rank
LCCM-2610	2.4	3.9	0.6	1
LCCM-4120	4.6	4.9	1.3	3
4C-1686	2.4	4.5	0.0	2
SP-8057	5.8	6.2	1.3	4
WB-8251	9.0	9.5	Not Tested	6
LCCM-2626	Not Tested	Not Tested	0.0	1
MXSC-198	4.7	7.2	Not Tested	5
SP-8030-96	16.4	18.2	8.9	7
23-RPD	18.6	20.6	12.9	9
SMS-21	15.6	23.4	18.1	10
MXS-198	7.0	Not Tested	Not Tested	8

The above erosion rates were calculated from measurements taken at Stations 8 and 9 (inlet), 15 and 16 (throat), and 17 and 19 (exit cone). The smaller station number at each nozzle area represents the plane in which the white materials were measured whereas the higher station number at each nozzle area represents the plane in which the black materials were measured. The plane of measurement was constant

17

by material category for all material with the exception of MXS-198, which was measured at Station 2. Station 2 is located 3 in. forward of Station 8 at a less severe area ratio.

In general, the materials families performed as anticipated with the better performers being the graphite particle and carbon reinforced materials followed by the Avcerams C/S, silica, asbestos and paper reinforced materials, respectively.

In evaluating the erosion performance of the materials tested in the TU-622 motors, the materials were also separated into two groups: (1) those with low test erosion rates and a high material carbon to oxygen (C/O) ratio, and (2) those with high test erosion rates and a low material C/O ratio.

The carbon/oxygen ratio is reported in AFRPL - TR-67-287 report, Investigation and Evaluation of Motor Insulation for Multiple Restart Application, November 1967, pp 112 thru 127. A summary of the influence of ingredients on performance and properties indicated that ablation rates decrease with an increasing C/O ratio. The carbon and oxygen are the percent by weight found in the virgin composite materials. Thus the TU-622 nozzle materials were divided into high and low C/O ratio materials. The carbon reinforcements are 94 to 99 percent carbon, while the silica reinforcements are 99 percent silica (S_1O_2). Thus a carbon cloth phenolic would be called a high C/O ratio material, while the silica cloth phenolic is called a low C/O ratio material.

The two groups included the following materials, which were also classified by the TU-622 throat plane erosion rates.

High C/O Ratio Materials	Throat Plane Erosion Rates Uncorrected (mil/sec)
LCCM-4120 (Graphite particle phenolic)	4.3
LCCM-2610 (Graphite particle phenolic	3.9
4C-1686 (Carbon cloth polyphenylene)	4.5
SP-8057 (Carbon cloth phenolic)	5.4
WB-8251 (Avceram C/S cloth phenolic)	6.9*
MXCS-198 (Avceram C/S cloth epoxy novolac)	5.6*

*Avceram materials do not precisely fit either group as they exhibit a low
    carbon to oxygen ratio (low carbon content) and a low erosion rate.

Low C/O Ratio Materials	Throat Plane Erosion Rates Uncorrected (mil/sec)
SP-8030-96 (Double thickness silica cloth phenolic)	15.8*
MXS-198 (Silica cloth epoxy novolac) MXS-2600 (Silica cloth phenolic)	13.2**
23-RPD (Cork filled asbestos phenolic)	15.8
SMS-21 (Paper phenolic)	18.3

The predicted erosion rate for high C/O ratio materials*** is equal to:

$$\frac{h/cp\,(\beta)\,12,000}{\rho}$$

----

*The silica cloth throat was oriented 45 deg upstream.

**The apparent erosion at the throat plane is low because the actual throat of the nozzle shifted to the entrance plane of the exit cone.

***McDonald, A.J.; and Hedman, P.O.: Determination of the Mechanism of Graphite Erosion in Solid Propellant Combusion Gases and Resulting Effects on Heat Transfer Phenomena. Paper presented at Thiokol Chemical AVAA, Aerospace Sciences Meeting (N.Y., N.Y.), Jan 20-22, 1964.

The h/cp (convective heat transfer coefficient) for the initial pretest nozzle contour of high C/O ratio TU-622 nozzles with a throat diameter of 1.74 in. is shown in Figure 56. The Propellant Blowing Coefficient, a function of the propellant composition (β) for the motor (TU-622) is 0.110 for the density ranges (ρ) of the materials listed above. Generally, the actual erosion line will fall under the theoretical erosion line as the carbonaceous materials are mixed with a phenolic resin binder high in carbon and low in oxygen content.

The theoretical and actual erosion performance of the six high C/O ratio materials evaluated in this program are shown in Figures 57 thru 66 for both the TU-379 and TU-622 Material Test Motors. For those materials with both TU-379 and TU-622 performance data, the actual TU-622 curve is superimposed over the TU-379 performance data to inspect for material reproducibility. The TU-622 motor had each of the 10 materials, with exceptions as previously mentioned, tested alone throughout the entire nozzle and was consequently considered more accurate for material performance than the TU-379 nozzle with its noneroding HLM-85 graphite throat and test materials forward and aft of the throat.

No actual erosion lines were drawn for the WB-8251 and MXSC-198 silica carbon cloth materials. The data scatter indicated a material close to the ideal high C/O ratio theoretical line, probably due to the SiO_2 (no carbon, high oxygen) silicon dioxide added to the carbon cloth. However, the composite material is actually relatively low in the C/O ratio with a 65 percent silica and 35 percent carbon reinforcement and, as a result, does not precisely fit into either of the C/O groups.

The MXSC-198 and LCCM-2610 materials do not show TU-379 erosion performance since the former was not tested and the latter exhibited no erosion.

A summary of the erosion performance and reinforcement/resin ratio for each carbonaceous material is given in Table 26. The better performing materials in the high C/O group were LCCM-2610 and 4C-1686.

The low C/O ratio materials have no actual predicted erosion rate formula, and the erosion rate is consequently graphed vs the total heat flux (Q_T) to provide some meaningful data (Figures 67 thru 70). The total heat flux is defined by the following equation:

$$Q_T = Q_R + Q_C$$

where

$$Q_R = Q_{Radiation} = \sigma \epsilon (T_g^4 - T_w^4)$$

$$Q_C = Q_{Convective} = h (T_{aw} - T_w)$$

σ = Stefan-Boltzmann constant

ϵ = Emissivity

h = Convective heat transfer coefficient = h/cp x (cp)

T_g = Gas temperature

T_{aw} = Adiabatic wall temperature

T_w = Wall temperature

The T_W (wall temperature) and ϵ (emissivity) are best estimates based on previous material test experience and research evaluation. The initial, pretest h (convective heat transfer coefficient) for the low C/O ratio TU-622 nozzles (D_t = 1.41 in.), is shown in Figure 67 and for TU-379 nozzles (D_t - 0.34) in Figures 68 and 70.

The actual erosion performance line for each low C/O ratio material tested on the TU-379 or TU-622 motor is shown in Figures 71 thru 78. No attempt was made to use the least squares curve fit for either high C/O ratio or low C/O ratio materials due to time and cost limitations. The curves are based on best engineering judgment. For those materials with both TU-622 and TU-379 curves, the TU-622 curve is super-imposed over the TU-379 performance data for verification. The silica and asbestos materials appear the most consistent in both TU-379 and TU-622 nozzle erosion performance.

A summary of the erosion performance and reinforcement/resin ratio for each low C/O ratio material is given in Table 27. The SMS-21 paper and 23-RPD asbestos appear to exhibit the lowest erosion but the silica SP-8030-96 with a higher reinforcement to resin ratio shows the best correlation of data on both the TU-379 and TU-622 nozzle tests.

These curves, for both the high C/O ratio and the low C/O ratio materials, were subsequently employed in task II of the program, Subscale Nozzle (D_t = 8.0 in.) Evaluation, to predict performance of the materials tested in those nozzles. The curves were then modified as required by the data gained from the subscale nozzle tests and again utilized in the performance predictions for full scale, 260 in. booster motor nozzles. Details are provided in the respective sections of this report.

Additional measurements were made of high temperature properties of representative materials previously evaluated. Graphs of mechanical properties of the materials versus temperature are contained in Figures 79 thru 87. The mechanical properties tested were:

Ultimate Tensile Strength (fill and warp direction)

Ultimate Compressive Strength (fill and warp direction)

Ultimate Interlaminal Shear Strength (fill and warp direction)

The room temperature properties (rounded off) of the materials are listed below.

Material	Ult Tens (psi) Warp	Fill	Ult Comp (psi) Warp	Fill	Ult Int Shr (psi) Warp	Fill
WB-8251 Carbon Silica	9,000	7,000	30,000	27,000	686	468
LCCM-4120 Graphite Particle	1,000		9,000		117	
LCCM-2610 Graphite Particle	1,000		13,000		192	
SMS-21 Paper	12,500	12,000	23,500	22,500	787	555
23-RPD Asbestos	19,800	11,000	15,500	14,000	1,750	1,060
SP-8057 Carbon	6,800	5,000	28,500	27,000	590	455
4C-1686 Carbon	18,500	14,000	13,000	14,500	1,290	1,020
MXS-198 Silica	10,000	10,000	34,500	24,000	1,305	728
SP-8030-96 Silica	6,000	4,000	23,000	28,000	640	370

The ultimate compressive strengths are higher than the ultimate tensile strength except for 23-RPD and 4C-1686 materials. In addition, the warp strengths are higher than the fill strengths for all materials for the three types of strength tests.

Firm data on all materials were employed up to 600°F, and extrapolations were made from this point to the approximate fusion sublimation temperature of the material, except for the selected materials mentioned below, which were tested up to 1,950°F.

A total of 30 compression tests at temperatures as high as 1,950°F were also performed on selected materials. Resultant data are contained in Table 28. The six materials tested at 1,200°F and 1,950°F show the following compressive strengths.

Materials	Average Ultimate Compressive Strength (psi)	
	1,200°F	1,950°F
SP-8030-96 Silica	3,510	2,720
23-RPD Asbestos	1,970	1,900
4C-1686 Carbon	2,670	1,730
LCCM-2626 Graphite Particle	2,050	3,580
LCCM-4120 Graphite Particle	2,360	2,230
KF-418 Canvas	260	Burned Out

In all cases, the test specimens were exposed in air to the test temperature for a period of 15 to 20 sec and then were compressed to failure at a rate of 0.05 in. per minute.

All specimens burned vigorously during the test, and the two specimens fabricated from canvas cloth phenolic (KF-418) were essentially destroyed before any appreciable load could be measured.

Thermal property tests were conducted on five representative materials. These tests were thermal conductivity, specific heat, and coefficient of thermal expansion. The resultant data from these tests are presented in Tables 29 and 30 and in Figures 88 thru 92.

The thermal conductivity tests were run at 32° F and 207° F with the following results.

Materials	Average Thermal Conductivity $\left(\dfrac{Btu/in.}{ft^2\text{-sec °F}} \right) \times 10^{-4}$	
	32°F	207°F
23-RPD Asbestos	2.29	2.05
4C-1686 Carbon	5.07	4.37
SP-8030-96 Silica	3.46	2.38
SP-8057 Carbon	4.56	4.32
LCCM-2626 Graphite Particle	10.66	11.82

The carbonaceous materials (4C-1686, LCCM-2626, SP-8057) showed the highest average thermal conductivity. In addition, all values decreased going from 32°F to 207°F except LCCM-2626.

The specific heat tests were run at 32°, 144°, 200°, 300°, 600°, and 900°F. The test results at the minimum and maximum temperature level are shown below.

Materials	Average Specific Heat (Btu/lb/°F)	
	32°F	900°F
23-RPD Asbestos	0.384	0.363
4C-1686 Carbon	0.304	0.377
SP-8030-96 Silica	0.315	0.305
SP-8057 Carbon	0.328	0.376
LCCM-2626 Graphite Particle	0.269	0.355

The carbonaceous materials showed an increase in specific heat between 32° and 900°F, while the asbestos and silica materials showed a decrease in specific heat.

The coefficient of thermal expansion (CTE) tests were run between room temperature (80°F) and 1,500°F. The recorded values (rounded off) at 80°F and 1,500°F are reported below.

Materials	Coefficient of Thermal Expansion (in./in./°F x 10^{-6})	
	80°F	1,500°F
4C-1686 Carbon	+ 5.8	+0.6
SP-8057 Carbon	+14.0	-1.5
LCCM-2626 Graphite Particle	+ 8.2	-3.7
SP-8030-96 Silica	+ 4.0	-0.7
23-RPD Asbestos	+ 1.2	-7.4

All the materials show a decrease in the coefficient of thermal expansion going from 80°F to 1,500°F. The plus sign indicates length increase while the minus sign indicates a length decrease. Generally, the carbonaceous materials exhibit a higher CTE and a greater range of values than the silica and asbestos materials.

Table 31 lists the materials which were candidates for continued testing in subscale nozzles. A total of 16 materials is contained in this list, 10 of which were carryovers from the Evaluation of Most Promising Materials program. Although these 10 materials were all candidates, three of them were virtually eliminated by difficulties encountered in the fabrication and testing of TU-622 nozzles. Two of these materials, WB-8251 and MXSC-198, contained Avceram C/S fabric as reinforcement. More than half of the nozzle components fabricated from these materials experienced severe cracking and delaminations, regardless of the type construction employed. Tape-wrapped parts cracked across plies and delaminated along plies, while laid-up parts delaminated severely along plies, regardless of their orientation. It is felt that the reinforcement contains the built-in stresses typical of silica which are relieved through rapid heat dissipation typical of carbon, resulting in cracks and delaminations. A gradual, stepped-up cure cycle with a long cooldown cycle under pressure could have been developed to eliminate this difficulty, but such development work would have been beyond the scope of this program. The third material was SMS-21, a Kraft paper phenolic. Although inexpensive, this material was most difficult to handle, and the very thin ply thickness (0.0035 in.) resulted in excessive fabrication time. In addition, wrinkled parts were a certainty with this material since the construction of the paper fabric is such that it has absolutely no bias. Consequently, any unevenness in fabrication results in a distortion in the form of wrinkles. The only possible method of preventing this is to substitute a crepe paper which possesses some bias. Another material recommended, FM-5272, has this combination.

SUBSCALE NOZZLE EVALUATION

Employing the mechanical and thermal property data, the material performance information, and the fabrication data obtained in the Materials Screening and Evaluation program phase, Thiokol designed and fabricated six subscale nozzles having a throat diameter slightly over 8 in. The nozzle assemblies were then transported to Edwards AFB (RPL) where they were static tested, using modified Stage II Minuteman motors as test vehicles. After testing, the nozzles were returned to Thiokol, where detailed postfiring analyses were performed.

These subscale nozzles represented an intermediate step between materials laboratory testing and evaluation and the utilization of these materials in full sized nozzles for 260 in. diameter booster motors. Nozzle tests provided materials performance data under actual large nozzle operating conditions. This information was then in turn used in the design and performance predictions of full 260 in. booster nozzles.

The materials considered for use in these nozzles were the 10 materials evaluated in the Evaluation of Most Promising Material program phase, and six materials previously selected from the Nomad program (AF 04(611)-11646) and held in abeyance for possible use in these nozzles.

In the Subscale Nozzle Task, 13 of the 16 candidate materials were actually tested in six nozzles attached to a modified Stage II Minuteman motor (Figure 93). The 13 materials were applied to the six nozzles and 36 liner components based on an engineering evaluation of the following data.

    1.   TU-379 and TU-622 material cost effectiveness rating.

    2.   TU-379 and TU-622 material visual examination.

    3.   TU-379 and TU-622 erosion performance curves.

    4.   AFRPL Nomad subscale material tests.[1]

The subscale nozzle was designed to use the AFRPL/Nomad steel structural shell and to meet the NASA-Lewis design criteria.

---

[1]AFRPL-TR-67-310, "Evaluation of Low Cost Materials and Manufacturing Processes for Large Solid Propellant Nozzles," 1967.

An aerothermodynamic analysis (Appendix A) provided the liner wall convective heat transfer coefficient (h/cp), wall total heat flux (Q_T), and wall thermal gradient. In addition, a structural analysis provided the stress factors of safety for the motor case, closure, and nozzle structure. Using the TU-379 and TU-622 erosion performance curves and the wall h/cp or Q_T, the material subscale erosion rate was predicted.

The subscale motor test data included pressure and thrust vs time plots, material erosion/char profiles, depths and rates, and a visual material examination. This information, in addition to the material raw material cost and specific gravity, was used to rate and select the best cost effectiveness materials for the 260 in. nozzle.

Materials and Design

Six subscale nozzles (throat D_t = 8.12 in.) and one steel Wing I Stage II Minuteman aft closure were designed and fabricated by Thiokol. Two AFRPL nozzle steel shells were supplied GFE to Thiokol by NASA-Lewis in support of nozzle assembly manufacture.

The selected materials for the six subscale nozzles included LCCM-2626, LCCM-4120, SP-8057, 4C-1686, SP-8030-96, MXS-198, 23-RPD, SP-8050, WB-8217, MX-4926, MXA-6012, KF-418 and FM-5272. As previously mentioned, selection of the latter six materials was based on their performance in the AFRPL/Nomad.

For purposes of review and clarification throughout the remainder of the report, the basic high pressure cure graphite particle phenolic material evaluated in this program had three variations as summarized below.

Material Identification	Material Compounding and Forming Process	Exposure			
		Laboratory Tested	TU-379 Tested	TU-622 Tested	Subscale Motor Tested
LCCM-2610	Mixed wet, staged, ground, and molded. 1,000 psi; 320° F cure.	Yes at R.T.	Yes	Yes, solid and segmented.	No
LCCM-2626	Mixed dry and molded. 1,000 psi; 320° F cure.	Yes at elevated temperature.	No	Yes, solid and segmented.	Yes, solid and segmented.
LCCM-2626X	Mixed dry and molded. 850 psi; 320° F cure.	Yes at R.T.	No	No	Yes

LCCM-2626 was developed to simplify the LCCM-2610 formulating and mixing process. However, the LCCM-2626X designation of the material resulted from a component part fabrication process variation from the LCCM-2626 material process. LCCM-2626X was cured at 850 psi rather than 1,000 psi (LCCM-2626 cure pressure) due to the limited press tonnage available to handle the large subscale components. The LCCM-2626X material was accepted for use based on comparable laboratory mechanical properties.

Mechanical Properties	LCCM-2626	LCCM-2626X
Tensile strength (psi)	2,900	3,435
Tensile modulus (psi x 10^6)	1.66	1.73
Elongation (%)	0.22	0.26

The aft closure shell was a one piece forging of 4120 steel, normalized (average of three tensile tests, U.T.S. = 124,233 psi) and machined to final configuration (Figure 94).

The subscale nozzle design (Figure 95) was designed to meet the following criteria.

Throat diameter = 8.12 in.   Inlet length = 4.03 in.
Exit cone half-angle = 17.5 deg   Inlet expansion ratio = 2.77
Exit cone expansion ratio = 8.40

Two nozzle designs (I and II) were provided for the subscale nozzle test program to reflect the two different fabrication processes (tape wrap and molding) used with low cost materials. Design I used predominantly tape wrapped materials in solid liner rings or cones, while Design II used exit cone molded materials in one and four segment liner rings or cones, as shown in Figure 95 - Sheet 3.

A 13 material matrix for the six nozzles is presented in Table 32. Four Design I and two Design II nozzles were fabricated. Some materials, such as MX-4926, were tested in only one nozzle location, while others, such as SP-8057, were tested in four nozzle locations. The area ratio (ϵ) for the liner component interfaces is also listed in Table 32.

A two dimensional aerodynamic exhaust gas flow analysis (Appendix A) for the motor assembly internal contour (propellant grain, aft closure insulation, and nozzle liner) at time zero and end of action time was used to establish an average nozzle wall, convective heat transfer coefficient, h/cp (Figure 96). The letters relate the h/cp to the nozzle wall location. A one dimensional thermodynamic analysis (Appendix A) using the convective heat transfer coefficient and the wall material physical-chemical properties provides thermal gradients for three nozzle materials (canvas, paper, carbon) at four planes of Nozzle No. 1. The total ablative wall thickness (Figure 97) varies from 2.90 in. at the nose Ⓑ to 2.00 in. at the submerged liner Ⓐ , to insure that the structure steel is maintained at room temperature.

The nozzle thermal analysis sections and a typical thermal gradient at the throat section are shown in Figures 97 and 98. A two-dimensional structural discontinuity analysis, using the aerodynamic nozzle wall pressure profile at the maximum motor pressure, provided the maximum hoop and meridional stresses, the maximum radial deflection and the minimum margin of safety on the case shell wall (Figure 99). The minimum margin of safety (M.S.) of 0.25 required, occurred at the case cylinder wall at interface 1-2 with a M.S. = 0.33. The maximum two plane (axial and circumferential) stress was 150,000 psi with a material allowable stress of 200,000 psi.

As originally designed, the aft closure had a maximum stress of 54,540 psi at the 15-16 interface. After a design modification to accommodate the case-closure insulation sleeve and rebored flange bolt holes (Figure 100) the maximum stress in the closure still occurred at Section 15-16 and increased to 72,055 psi. The M.S. after the closure modification was an acceptable +0.52. Stress levels at other low M.S. interfaces in the case, closure, and nozzle shell, due to closure modification, showed negligible changes. The minimum margin of safety still occurred at interface 1-2 in the case with a M.S. = 0.33.

Fabrication

Summaries of the materials, fabrication methods, and cure cycles used in fabricating the components for the six subscale nozzles are contained in Tables 33 thru 38. Prior to the initiation of component fabrication, detailed planning logs were written for the fabrication and cure of each component. For all Nozzle No. 1 components, this information was obtained from the materials suppliers and through data published in Nomad nozzle reports, in which all these particular materials had previously been used. For the other five nozzles, this information was obtained in the preceding phases of this program, particularly during the fabrication of TU-379 and TU-622 nozzles.

Components for four of the six nozzles fabricated in this program task were made from materials having the same form, that is, tape or broadgoods. The handling of these materials was identical for the fabrication of a specific part. A brief description of the fabrication of components for these four nozzles (No. 1, 3, 4, and 6) follows.

The exit cone assembly was fabricated of 6 in. wide warp tape wrapped parallel to the centerline of a steel conical shaped mandrel and autoclave cured. Wrapping was initiated by attaching the tape to a cylindrical starting section of the small end of the conical mandrel and wrapping the material up the forward portion of the mandrel until the material transition point was reached (approximately 4:1 expansion ratio). At this point the material was changed and wrapping was continued until the proper length was reached. The wrapped cone was then enclosed in a vacuum bag and cured in an autoclave at 225 psi. Following cure, a full skim

machine cut was made on the outside of the cone to provide a smooth, even surface for the overwrap. The cone, still on the steel mandrel, was reinstalled in the tape wrapper and tape (1 1/2 to 2 1/2 in. wide) was wrapped over the full length of the cone. A vacuum bag was again installed, and the overwrapped cone was autoclave cured at 225 psi. After cure, the part was removed from the mandrel and radiographically inspected. A tabulation of the results of this radiographic inspection, for all nozzle components, is contained in Table 39. The part was then machined to its net configuration and stored for final assembly of the nozzle. Figure 101 illustrates a typical exit cone.

The throat was fabricated of patterns cut from broadgoods which were plied up in a compression mold and cured in a press. The doughnut shaped mold contained ring inserts machined at a 45 deg angle to provide the proper ply orientation. Each pattern represented 130 deg of a full revolution in the mold, and was installed in the mold end-to-end with other patterns. In this manner, the joints in successive plies did not overlap each other, but rather spiraled incrementally around the part. When the calculated number of plies had been installed, the top ring insert, again at a 45 deg angle, was installed and the mold was placed in a press. Sufficient pressure to supply 225 psi to the part was applied, and the part was cured. Following cure, the part was radiographically inspected. The OD of the part was then machined to fit into the backup insulation sleeve.

The throat backup sleeve was formed by wrapping 5 in. wide warp tape over a cylindrical mandrel and curing, under vacuum, in an autoclave at 225 psi. Radiographic inspection of the part was then performed. The inner diameter of this part was subsequently machined, and the previously fabricated throat insert was bonded into it with Epon 934 adhesive. After adhesive cure, the throat and backup assembly were machined to final configuration except for the throat diameter, which was machined during the final internal contour machining operation. A typical throat and backup assembly is illustrated in Figure 102.

The inlet was fabricated in the same manner as the throat, except that the mold was designed so that the ply orientation was 90 deg to the centerline. This part was also cured in a press, with sufficient pressure applied to the mold to produce 225 psi on the part, thereby simulating autoclave pressure. The part was subjected to radiographic inspection after cure. It was then rough machined (Figure 103) and retained for final installation and contour machining.

The nose ring consisted of 5 in. wide warp tape wrapped parallel to the centerline on a cylindrical mandrel. When sufficient material had been wrapped, the part was enveloped in a nylon film vacuum bag and autoclave cured under vacuum and 225 psi. Following cure, the part was X-rayed. It was then rough machined and retained for final assembly. An illustration of this part is contained in Figure 104.

The backside liner was fabricated by wrapping 6 in. wide warp tape onto a conical shaped steel mandrel. Wrapping was initiated on a cylindrical starter section at the small end of the cone and progressed up the length of the conical mandrel.

The part was then staged in an autoclave for a number of hours, removed, and reinstalled in the tape wrapper. Another wrap was then made with 3 in. wide warp tape to obtain the proper part thickness. Following the second wrap, the part was cured in an autoclave under vacuum and 225 psi. Radiographic inspection of the cured part followed. The part was then rough machined and retained for final assembly (Figure 105).

An exception to the above descriptions occurred during fabrication of the exit cone for Nozzle No. 4. The forward portion, using 23-RPD tape, was wrapped as described. It was then fully cured in an autoclave under vacuum and 225 psi. The aft portion of the cone was then wrapped with MXS-198, an epoxy novolac impregnated silica tape. This material was cured in an oven under vacuum bag pressure only. The part was then skim cut, overwrapped, and autoclave cured as previously described.

The components for a specific nozzle assembly were dry fit into the steel nozzle shell prior to final installation to insure proper fit to the shell and to each other. Brass shim stock, 1 in. square by 0.010 in. thick, was employed to maintain uniform gaps between segments. Poorly fitting components were reworked until a proper fit was obtained.

The exit cone was then coated with Epon 934 adhesive and emplaced in the steel shell, which had also been coated with a thin film of Epon 934. Pressure was exerted to hold the cone in place until the adhesive cured. The remaining parts were then also coated with Epon 934 and bonded to the steel shell and to each other in the same fashion. Following cure of the adhesive, the nozzle assembly was installed in a vertical tracer lathe and the final nose and throat contour was machined. The same tracer template was utilized in the contouring of all six subscale nozzles to insure uniformity.

Illustrations of the four completed nozzle assemblies are contained in Figures 106 thru 119. Some discrepancies occurred in the final assembly of these nozzles. The discrepancies and their resolutions are summarized below and in Table 40. The exit cone of Nozzle No. 1 was undersize on its OD, causing it to fit too far forward in the steel shell. The situation was alleviated by applying a silica filled epoxy polyamide to the cone, curing it, and remachining the OD to print. During final machining of the internal contour of Nozzle No. 3, the tracer slipped off the template, causing a groove 0.080 in. deep to be gouged in the throat in the aft section. The groove was sanded out manually. The backside liner of Nozzle No. 4 was machined incorrectly, preventing its seating properly on the steel. The part was remachined for proper fit to the steel, which caused a gap to open between the aft end of the part and the steel shell. This gap was filled in with an asbestos filled epoxy polysulfide. Also on Nozzle No. 4, the exit cone liner debulked excessively, resulting in the part being thinner than specified. This was corrected by increasing the thickness of the overwrap.

Nozzle No. 2 incorporated a radical departure from standard nozzle fabrication concepts. The outstanding feature of this nozzle was the segmented exit cone, fabricated of the dry mix version of Thiokol's LCCM-2610 low cost molding compound, LCCM-2626. A total of 12 segments or pieces were employed in the fabrication of this cone. Three tiers of four segments each were fabricated, assembled, and installed in the metal nozzle shell. A series of photographs was made, following the construction of the middle tier (Figures 120 thru 128).

There are two basic methods by which such segments can be fabricated. The first method consists of molding the segments to the net configuration desired, while the other method consists of molding blanks and machining the segments to configuration. Since the first method requires relatively complex tooling, it is more applicable to a production rather than a development program. Consequently, the second or alternate approach was employed in this program. Work was initiated by press molding several large cylinders of the exit cone material (Figure 120). The cylinders were then cut into thirds, and four mating segments for each of the three tiers were machined (Figure 121). As illustrated in Figure 122, the ID of the segments was cylindrical at this point, to facilitate assembly of the segments on a tape-wrapping mandrel (Figure 123). Epon 934 adhesive was employed at the extreme outer edges of the joints to bond the segments together. When the adhesive was cured, the clamps were removed and the mandrel was installed in the tape-wrapping machine (Figure 124). The OD of the segments, which was machined to a net configuration on the conical portion, was then overwrapped with 7581/MIL-R-9299 glass phenolic tape, as illustrated in Figures 125 and 126. The overwrapped tier of segments was then vacuum bagged, autoclave cured, and removed from the mandrel (Figure 127). Following similar fabrication of the other two segmented tiers, interface joints were machined into the tiers and they were bonded together with Epon 934 adhesive (Figure 128). The final conical OD was then machined and the exit cone was installed into the steel nozzle shell. Following installation of the remaining nozzle components, the internal contour of the nozzle was machined. Illustrations of the completed nozzle assembly are shown in Figures 129 thru 133. Figures 129 and 130 illustrate the staggering of the joints between the segments in the three tiers. Each joint was offset 30 deg from the corresponding joint in the preceding tier to interrupt any unusual gas flow which could conceivably form at one of the joints. It is significant that the joints were both longitudinal and radial.

The throat for this nozzle was also fabricated of LCCM-2626, press molded and machined in one piece. The remainder of the components for this nozzle were fabricated as previously described in this report for Nozzles No. 1, 3, 4, and 6.

Nozzle No. 5 was constructed in a configuration similar to that of Nozzle No. 2. The exit cone consisted of three one-piece tiers assembled together and installed into the steel nozzle shell. The aft and middle tiers were constructed of LCCM-4120. The material was packed into a large, cylindrically shaped mold. When the required amount of material had been installed, a nylon film vacuum bag was installed, vacuum was applied, and curing effected in an oven at one atmosphere

pressure (13 psi). The resulting cured billets were very similar in appearance to those illustrated in Figure 120. The forward tier of the exit cone was fabricated of LCCM-2626, which was press molded into a cylindrical billet.

The molded billets were then machined to accept a tape overwrap and over-wrapped with a 7581/MIL-R-9299 glass phenolic tape prepreg. The overwrapped billets were enclosed in a nylon film vacuum bag and the overwrap was cured in an autoclave at 225 psi. After cure, each tier was machined to a net configuration on the forward and aft face, and the three tiers were bonded together with Epon 934 adhesive. Following a room temperature cure of the adhesive, the cone was machined to final configuration and retained for final assembly.

The throat was fabricated of four segments of press molded LCCM-2626. A solid billet of LCCM-2626 was first molded in a press under 1,000 psi pressure. This billet was then machined into four quarter-segments. The segments were then assembled onto a tape-wrapping mandrel. Epon 934 adhesive was applied at the extreme outer edges of the joints to bond the segments together. When the adhesive had cured, the mandrel was installed in a tape-wrapping machine and the segments were overwrapped with 23-RPD tape. The overwrapped segmented insert was then vacuum bagged, autoclave cured, and removed from the mandrel. Finally, it was machined to its net configuration and retained for final installation and contour machining. The resulting assembly contained four longitudinal joints.

The inlet was also fabricated of LCCM-2626. The same tool was used for the inlets of the other five nozzles, which were all fabricated from broadgoods materials. In this case, however, a preweighed amount of the LCCM-2626 molding compound was added to the mold, the top insert was installed, and the inlet ring was press molded at 1,000 psi. Following cure and radiographic inspection, it was machined and stored for final assembly.

The remainder of the components for this nozzle were fabricated as previously described, as was the final assembly of the nozzle. The completed nozzle assembly is illustrated in Figures 134 thru 138.

Performance Prediction

The subscale material performance prediction (erosion rate) varies with the liner material and where the specific material is located in the nozzle. To predict an erosion rate for a specific material in the subscale nozzle location a number of steps were completed as outlined below.

1. Obtain the TU-622 design curve for the specific material
    (erosion rate vs $\dfrac{h/cp\,\beta\,12,000}{\rho}$ for carbonaceous materials
    or erosion rate vs Q_T for canvas, paper, silica and asbestos).

Typical carbon and silica design curves are shown in
Figures 139 and 140, respectively.

2. Plot the calculated subscale aerodynamic convective heat
    transfer coefficient (h/cp) or total heat flux (Q_T) vs nozzle
    axial length. Identify the specific nozzle material appli-
    cation areas on the graphs (Ref Figures 141 thru 144).

3. Identify the subscale nozzle area A, B, C, D, E, G, where
    the material is to be tested and the subscale aerodynamic
    curve for the specific material (Q_T for asbestos, silica,
    paper and canvas and h/cp for carbonaceous).

4. Obtain the value (h/cp) or (Q_T) for the material applied at
    an axial distance to the throat in the subscale nozzle. If
    the value h/cp is used for carbonaceous materials, the
    additional terms of (β) propellant blowing coefficient,

$$\beta = \frac{\text{molecular weight carbon}}{\text{molecular weight propellant gas mixture}}$$

(Mole fraction of
H_2O, O_2, O and OH
in propellant gas
mixture.)

= dimensionless blowing coefficient.

and material density ρ (lb/cu ft) must be determined.

5. Obtain the subscale material erosion rate from the TU-622
    material design curves (Step 1) using the $\dfrac{\text{h/cp} \quad \beta \quad 12,000}{\rho}$
    or (Q_T) parameter.

6. To predict a subscale nozzle erosion profile, repeat the first
    five steps for the other materials at different axial locations
    to predict the maximum erosion rate for each nozzle area.

To illustrate the use of the material performance graphs, the six subscale
nozzles are shown in Figures 145 thru 150 with predicted vs actual erosion rates.
The actual erosion profile for each nozzle has no scale. The actual erosion pro-
file and erosion rates were taken from the subscale nozzle plane between the pro-
pellant starpoint and propellant star valley at the stations indicated. The predicted
erosion rate curves were obtained from the TU-622 material design curves and the
subscale aerodynamic parameter (h/cp or Q_T curves), as shown in Figures 57 thru
66 for carbonaceous materials and Figures 71 thru 78 for non or low carbonaceous
materials.

In general, the predicted erosion rates from the TU-622 material design
curves and subscale aerodynamic parameters are lower than the actual erosion
rates. The difference can be explained by the fact that the TU-622 material design
curves are based on a fixed external thick liner nozzle configuration while the actual

34

erosion rates were obtained from a fixed submerged thin liner nozzle. The submerged nozzle erosion rates historically are approximately 1.5 times higher than the external nozzle erosion rates in the nose, inlet and throat nozzle areas.[1]

In addition, the thick TU-622 liner provided an excellent heat sink for the graphite particle phenolic materials. Generally, a thick (4 in.) heat sink, high thermal conductivity material will exhibit a lower inside heated wall surface and a lower erosion rate than a thin (2 in.) heat sink material, by a factor 1.5 to 3.0. Thus, it is possible that a LCCM material tested in the TU-622 thick fixed external throat material could show a 2.25 to 4.50 erosion rate increase in a thin fixed submerged throat application. However, four materials, LCCM-2626, LCCM-2626X, 23-RPD and SP-8030-96 (Table 41) showed a predicted vs actual erosion rate difference that requires special mention.

The LCCM-2626 graphite particle material in the subscale nozzles No. 2 and 5 inlet and throat exhibited a higher actual erosion than the predicted erosion by a factor of 2.45 to 3.31. However, because it is a heat sink material and the subscale nozzle was submerged, the allowable erosion factor increase is 3.38. Thus, the material is reproducible and acceptable.

The LCCM-2626X graphite particle material in the subscale nozzles No. 2 and 5 forward, middle and aft exit cone exhibited a higher actual erosion than the predicted erosion by a plus factor of 4.72 to 10.18. At one nozzle area the material exhibited less than the predicted erosion by a factor of -16.11. The allowable erosion factor increase in an exit cone application for a heat sink material is 2.25. While the -16.11 factor is acceptable, the material reproducibility is questionable. The high +4.72 to +10.18 erosion factor increase is unacceptable and indicates nonreproducibility. It must be concluded that the material at its present development level is unsuitable for the forward, middle and aft exit cone nozzle areas.

The 23-RPD asbestos material in the subscale Nozzle No. 4 forward exit exhibited a higher actual erosion to predicted by a factor of 2.69, while the material in the submerged liner exhibited less actual erosion than predicted by a factor of 0.64. In both areas the acceptable erosion factor is 1.00. The material is not reproducible in either area. The material's lower erosion in the submerged liner area is acceptable, but of questionable reproducibility. The higher material erosion in the forward exit is unacceptable and unreproducible. It must be concluded that the material as a submerged liner is acceptable with reservations, but must await further material development before it can be used in the forward exit cone.

The SP-8030-96 silica material in the subscale Nozzle No. 3 aft exit exhibited a higher actual erosion to predicted by a factor of 3.04. The acceptable erosion

---

[1]Thiokol Report, TWR-1710, "A Method for the Preliminary Sizing of Nozzle Liners," B. Enserink, 28 Jan 1968.

factor is 1.00. One special factor enters into this materials evaluation. The material prediction is based mainly on the TU-622 erosion rate plotted vs total wall heat flux. As shown in Figure 151, the TU-622 initial and final surface dimensions differ greatly at the throat and very little at the inlet and aft exit cone. Thus, the throat area ratio and Mach number remain essentially the same at the throat, while the inlet and aft exit cone area ratio decreases and Mach number increases. Since the total wall heat flux is proportional to the Mach number, the total wall heat flux increases during the TU-622 test. An average total wall heat flux is calculated for the material erosion design curve as shown in Figure 71 for the aft exit cone, but a larger allowable erosion factor is needed to be fair to the material. It is doubtful the factor would be as high as 3.04 (2.13/0.70) but since the material is reproducible in other areas where used in the subscale nozzle (submerged liner, nose, inlet and throat), it is recommended that the material be accepted for the aft exit cone.

Test

The six Thiokol designed and fabricated nozzle assemblies, after a final QC inspection, were shipped to the AFRPL test site at Lancaster, California. In addition, a Thiokol designed and fabricated aft closure was also shipped to AFRPL to attach the nozzle to the loaded case assembly.

At the test site the aft closure was insulated with a maximum of 3.50 in. of U.S. General Tire V-61 (asbestos fiber reinforced epoxy-polysulfide NBR rubber). The nozzle and insulated closure were bolted together and the subassembly bolted to a modified surplus Stage II Wing I Minuteman motor that had the original four nozzles and aft closure assembly previously removed.

The motor assembly is shown in a sequence of Figures 152 thru 154 with the motor tested in a horizontal one component thrust test stand, with two pressure transducers to measure aft or head end chamber pressure. The initial throat and exit planes were measured in two planes, 90 deg to each other. Camera coverage from the test bay wing walls was provided during the test.

After the motor test firing and a gaseous nitrogen motor quench, the nozzle was visually inspected to determine overall materials condition. Nozzle throat and exit diameter measurements were taken in two planes, 90 deg to each other, and photographs of the nozzle exit cone were obtained before removing the nozzle from the motor. After removal of the nozzle from the motor, the inlet was photographed. Any unusual or unexpected material was transmitted to a Thiokol representative before shipment to Thiokol for detailed post-test analysis in the Thiokol furnished shipping container.

The average web pressure and web time for each of the six motors is listed in Table 42. The average web pressure ranged from 384 to 471 psia and the web time spread was 56.2 to 61.0 seconds.

The pressure time envelope for six subscale motor firings is shown in Figure 155. The maximum chamber pressure was 523.4 psia or 510 psig.

Post-Test Evaluation

A major objective of the program was to determine the accuracy with which the existing analytical techniques predicts the low cost ablative system performance. To this end, it was essential that the performance of the test nozzles in this program be accurately determined, and that the measured performance be critically compared to the predicted performance.

The final step in the evaluation was to recommend specific ablative systems for each section of the 260 in. motor nozzle. The following steps describe the detailed post-test analysis.

The post-test evaluation of each nozzle involved 13 separate operations, as outlined below.

1. The nozzle was inspected while still on the fired motor. It was photographed, visually inspected, and removed from the motor.

2. The nozzle was removed from the motor and shipped to Thiokol.

3. The nozzle was photographed in detail and visually inspected by engineering personnel and the steel exit plane plate was removed.

4. Important nozzle diameters (throat, inlet, and exit) and axial lengths were measured and compared to the pretest dimensions for preliminary performance evaluation to verify char and erosion measurements which will be taken on the sectioned nozzle in Step 10.

5. Three erosion planes (propellant starpoint, star valley and between starpoint and star valley) were marked for later cross section cutting with a diamond saw.

6. The nozzle assembly was placed in an oven at 500° F for 12 hr to break down all adhesive bond interfaces.

7. After the nozzle assembly was removed from the oven and allowed to cool, the components were separated from the nozzle structure shell and inspected.

8. All nozzle components except the steel shell were cut in three planes, inspected and photographed.

9.   The three-cut nozzle component planes were planed true and sanded.

10. For erosion lines, the liner surfaces were traced on the nozzle drawing. The char lines were measured by laying a scale on the sectioned surfaces, measuring from the outside surface, and marking the char line on the nozzle drawing. Erosion and char depths for each material were taken from the nozzle drawing.

11. Illustrations of the cut planes were made to display the erosion and char depths of the materials along the initial inside nozzle material wall surface. The erosion and char depths were divided by web time to calculate erosion and char rates.

12. The steel shell was refurbished for the next nozzle assembly. All other nozzle components were stored.

13. Photographs, erosion and char data, inspection report, pressure and thrust profiles, and fired material test results were accumulated, evaluated, and reported.

A summary of the post-test evaluation for each of the six NASA-Thiokol nozzles shows the performance of all the 48 liner components tested. Each ablative liner will be rated for erosion/char integrity at the following performance levels:

Excellent
Very good
Good
Fair to good
Fair
Poor to fair
Poor.

A material in a specific nozzle ablative area with a rating below fair is eliminated for consideration in the 260 in. nozzle in the area where tested.

Each insulation sleeve (liner backup) will be rated for integrity at the following performance levels:

Very satisfactory
Satisfactory
Adequate.

A material in a specific nozzle insulation area with a rating below satisfactory is eliminated for consideration in the 260 in. nozzle in the area where tested.

In the discussion of the material components, a uniform erosion rate indicates that the maximum erosion rate variation in the three cut planes is under 5.0 mil/second. When discussing the structural integrity, the following terms are used to describe the components. A definition and picture of each term is also included.

Delamination – Tape wrapping – separation between two or more adjacent parallel cloth plies by the lack of, loss of, or breaking of the resin bond.

Molding – continuous separation between many graphite particles by the lack of, loss of, or breaking of the resin bond. The separation is parallel to the inside surface or radial.

Cracks – Tape wrapping – breaking of one or more cloth plies and bonding resin in or out of the plane of the cloth.

Molding – continuous separation between many graphite particles by lack of, loss of, or breaking of the resin bond on the inside or outside diameter surface.

THROAT TAPE WRAPPING

EXIT CONE MOLDING (OD)

40
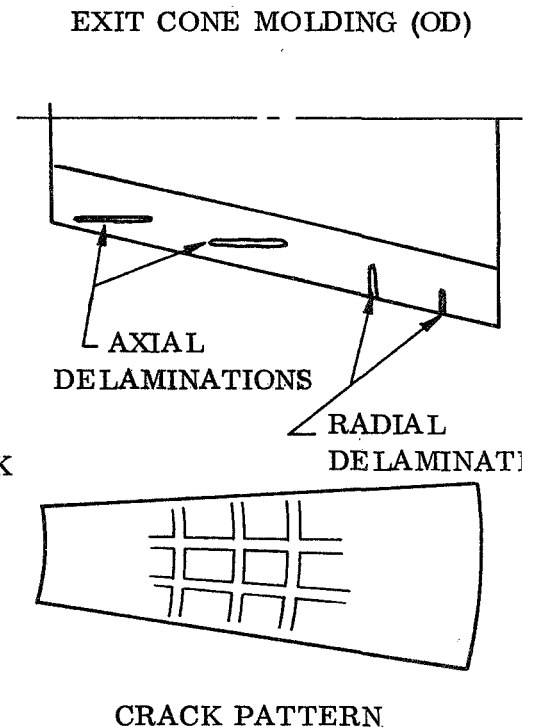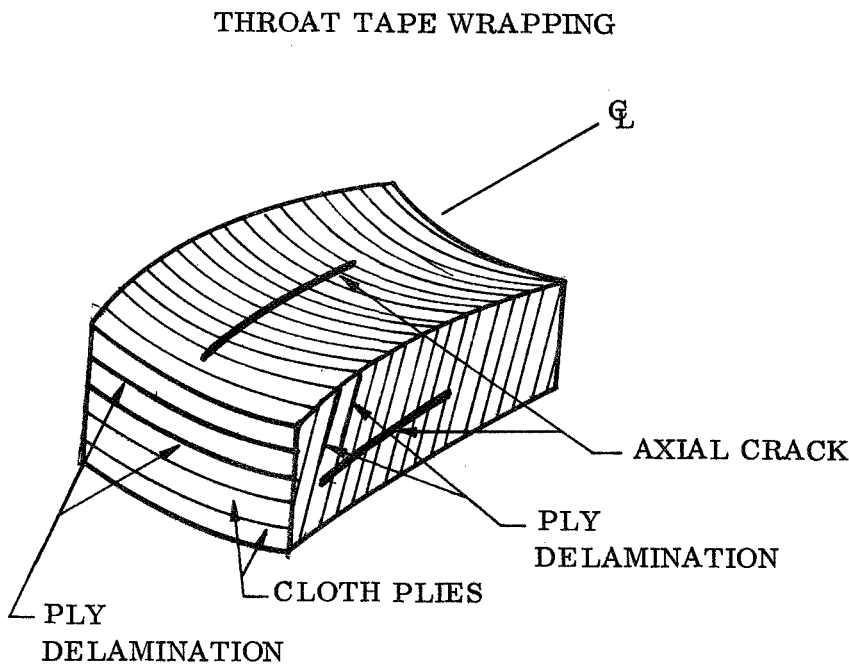
Spalling – <u>Tape wrapping and molding</u> – shallow loss of material locally exceeding the normal erosion depth.

Gouging – <u>Tape wrapping and molding</u> – deep loss of material in concentrated area exceeding the normal erosion depth.
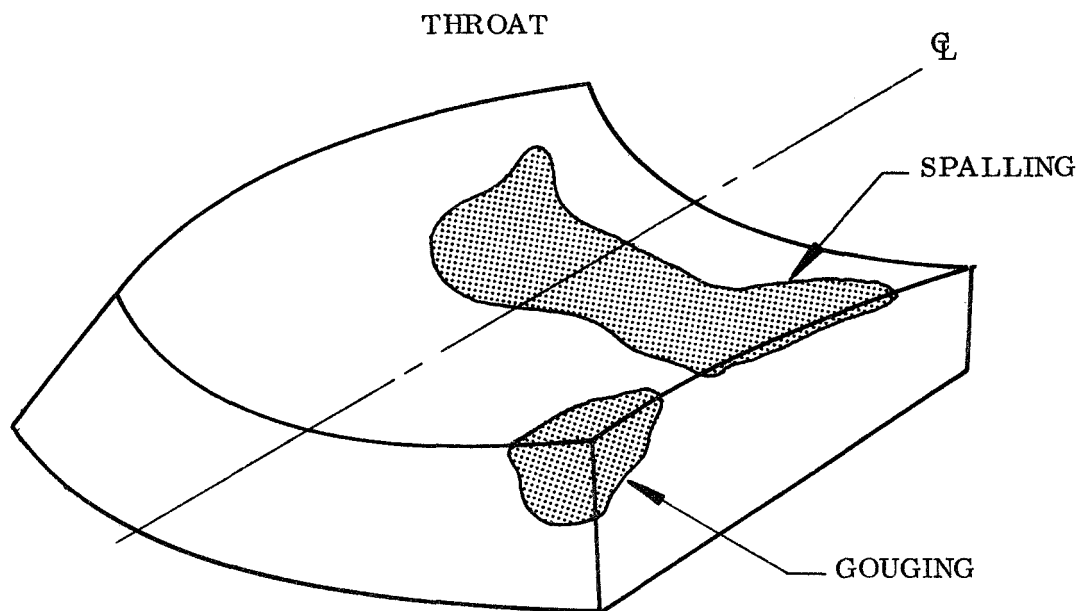
Nozzle No. 1, post-test inspection. - Six materials from the AFRPL-Nomad program were applied to the following six ablative and two backup liner nozzle areas.

Submerged OD	FM-5272	Paper phenolic
Nose	WB-8217	Carbon phenolic
Inlet	WB-8217	Carbon phenolic
Throat	MX-4926	Carbon phenolic
Forward exit	SP-8050	Carbon phenolic
Aft exit	KF-418	Canvas phenolic
Exit cone insulation	MXA-6012	Asbestos phenolic
Inlet throat insulation	MXA-6012	Asbestos phenolic

The test motor pressure versus time trace showed the following operating conditions.

Maximum pressure	520 psia
Average web time pressure	471 psia
Web time	56.8 sec

The post-test nozzle condition was very good, with all six materials exhibiting at least good or satisfactory performance. Three materials were rated excellent. Figures 156, 157, and 158 show the submerged and exit cone liners as received from AFRPL testing facility. Figures 159 and 160 show plane 2-3, one of the three nozzle section profiles.

The actual erosion/char profiles, depths and rates taken at three planes (propellant starpoint, between propellant starpoint and star valley, and star valley) are illustrated in Figures 161, 162, and 163. The notes include data changes and design changes made since publication of the monthly reports.

During nozzle assembly, a gap (B) Figure 161 between the throat and forward exit cone, was filled with adhesive. In nozzle disassembly operations, the weak FM-5272 paper phenolic char layer, (C) Figure 161, fell off in small pieces. Thus, the erosion line is an estimate based on measuring the thickness of the paper phenolic char layer pieces. At location (A) Figure 163 in the forward exit cone, a chip of the forward exit cone was lost during nozzle disassembly, with the erosion depth and rate estimated.

The erosion/char rates are summarized for the three planes in Figure 164. The web time was used in calculating the erosion/char rates. The notes include changes to the data since published in the monthly reports and design changes noted on each individual sectional plane. A performance summary of each nozzle component as discussed below is contained in Table 43.

The FM-5272 paper phenolic submerged OD liner, tape wrapped parallel to centerline, showed very good performance. Low uniform erosion and char rate performance are shown below by the station +1.0 values.

	Erosion Rate M/S	Char Rate M/S
Plane 1-2	1.75	5.63
2-3	2.81	6.68
3-3	2.63	6.51

A typical characteristic of the material is a very weak char layer that flaked off during nozzle disassembly in a 500° F oven. Subsequent to the loss of the char layer in the oven, shallow surface cracks and local internal ply delaminations occurred. In addition, during nozzle disassembly operations with a 500° F oven, the liner cracked due to the thermal expansion of the steel shell. The structural integrity of the virgin material was good, but only fair in the char material.

Figure 156 shows the submerged OD liner with char layer still intact, while Figure 159 shows the sectional liners in plane 3-2 with the loss of the char layer.

The typical scalloped erosion pattern close to the nozzle flange as shown in Figure 156 is due to the four-point star grain configuration. The longest axial erosion profile (Figure 162) is in the axial plane of the propellant star valley. The shortest axial erosion profile (Figure 161) is in the plane of the propellant starpoint. Virgin liner material is visible in Figure 156 adjacent to the nozzle flange due to the protective V-61 Elastomeric closure insulation as shown in Figure 93.

Three special radioactive ablation gages developed by TRW systems group under contract to AFRPL[1] were installed in the submerged liner. Following the motor test, the gages were removed from the nozzle, pulling away the char layer locally (Figure 156).

The WB-8217 carbon phenolic nose, tape wrapped parallel to centerline showed good performance. The material exhibited a uniform erosion and char rate as shown below by the station -3.0 and -8.0 data.

	Erosion Rates M/S		Char Rates M/S	
	Station -3.0	Station -8.0	Station -3.0	Station -8.0
Plane 1-2	1.23	9.67	8.62	13.19
2-3	2.28	10.55	10.55	16.89
3-3	1.75	8.79	8.44	15.83

---

[1]Static Test Firing of Four Low Cost Ablative Nozzles on Stage II Minuteman Motors, W. Payne, A. Bassoni, Technical Report, AFRPL TR-69-60, April 1969.

The material showed local surface gouging and ply delaminations between station
-8.0 and -7.0 (Figure 157). One delamination extends into the virgin material
(Figure 160). Local spalling and ply delamination in the char also occurs at
station -4.0 to 0.0. Several axial cracks in the char layer extend back from
station -7.0 to station 0.0. Usually the cracks and delaminations occur during
the heat soak of motor cooldown after static test as evidenced by the lack of
aluminum oxide deposits in many of the surface openings. The structural integrity
of the virgin material was excellent, while the char material was only fair.

The WB-8217 carbon phenolic inlet, a flat laminate 90 deg to centerline,
showed excellent performance. The material exhibited a uniform erosion and
char rate as shown below by station -4.0 data.

	Erosion Rate M/S	Char Rate M/S
Plane 1-2	9.67	15.13
2-3	8.44	15.48
3-3	11.78	15.83

The material showed a single circumferential ply delamination in the char at
station -4.0 (Figures 156, 157, and 160). In addition, several smaller delami-
nations occurred from station -7.0 to -5.0 in the char layer. Two delaminations
extend into the virgin material at stations -3.0 and -7.0. Light surface spalling
exists at station -8.0. The component showed excellent structural integrity of
the virgin material and very good integrity in the char layer.

The MX-4926 carbon phenolic throat, a layup 45 deg to centerline down-
stream, showed excellent performance. The material exhibited a uniform erosion
and char rate as shown below by the station -3.0 data.

	Erosion Rate M/S	Char Rate M/S
Plane 1-2	8.97	14.25
2-3	9.15	14.78
3-3	9.32	14.95

The material showed several circumferential ply delaminations in the char layer,
between station -2.0 to +4.0. The component showed very good structural integrity.

The SP-8050 carbon cloth phenolic forward exit cone, tape wrapped parallel
to centerline, showed excellent performance. The material exhibited a uniform
erosion and char rate, as shown below by the station +6.0 data.

	Erosion Rate M/S	Char Rate M/S
Plane 1-2	3.51	12.31
2-3	3.69	13.02
3-3	2.46 Est	9.50 Est

The material also showed several circumferential ply delaminations in the char layer as shown by Figure 158. The component showed excellent structural integrity in the virgin material and very good integrity in the char layer.

The KF-418 canvas phenolic aft exit, tape wrapped parallel to centerline, showed very good performance. The material exhibited a uniform erosion and char rate as shown below by the station +32.0 data.

	Erosion Rate M/S	Char Rate M/S
Plane 1-2	1.75	4.39
2-3	0.52	4.75
3-3	1.05	5.10

The material also showed local wide internal delaminations that occurred during fabrication. A characteristic of the material is a weak char as evidenced by the irregular eroded wall surface, the loss of char layer adjacent to the cut sections, and the porous char underneath the carbon cloth forward exit cone interface with the canvas phenolic. Small local gouging occurred at station +36.0 as shown by Figure 158. The structural integrity of the component was good.

The exit cone and inlet throat backside insulation of MXA-6012 asbestos phenolic, tape wrapped parallel to centerline, provided satisfactory steel insulation and ablative liner support, although many local ply delaminations were noticeable in the three sectioned planes.

It is recommended that all six standard materials be evaluated for use in the 260 in. nozzle in the areas where tested. The recommendation is based on their erosion/char performance and the material structural integrity.

Nozzle No. 2 post-test evaluation. - Four materials evaluated in the material screening tests and one material from the AFRPL-Nomad Program were applied to the following six ablative and two backup liner nozzle areas.

Submerged OD	MXA-6012	Asbestos phenolic
Nose	4C-1686	Carbon polyphenylene
Inlet	4C-1686	Carbon polyphenylene
Throat	LCCM-2626	Graphite particle phenolic

Forward exit		
Middle exit	LCCM-2626X	Graphite particle phenolic segmented
Aft exit		
Exit cone insulation	1581	Glass phenolic
Inlet throat insulation	23-RPD	Asbestos phenolic-cork filled
End retainer ring	FM-5063	Carbon cloth phenolic

The test motor pressure versus time trace showed the following operating conditions.

Maximum pressure	502 psia
Average web pressure	466 psia
Web time	57.5 psia

The post-test nozzle condition was fair to good with all materials exhibiting good to very good performance in at least one nozzle area. Figures 165 thru 168 show the submerged OD liner, inlet and exit cone as received from AFRPL testing facility. The main performance difference between test Nozzle No. 1 (standard materials nozzle) and this nozzle is the higher exit cone erosion in the segmented three tier LCCM-2626X liner material. Figures 169 and 170 show one of the three nozzle section profiles for the submerged liner (plane 1-3) and the exit cone liners (nominal erosion plane).

The actual erosion/char profiles, depths, and rates for the submerged liner in three planes are shown in Figures 171 thru 173. The notes indicate data changes, now published in the monthly reports, and that no char depth was visible for the LCCM-2626 throat material.

The maximum, minimum, and nominal exit cone erosion planes are shown in Figures 174 thru 176 with the same type of general notes as the submerged liners. The erosion/char rates are all summarized for the three submerged and exit cone planes in Figure 177. The notes finalize the changes made from the monthly reports and define the erosion and char depths. A performance summary of each nozzle component as discussed below is contained in Table 44.

The MXA-6012 asbestos phenolic submerged liner, tape wrapped parallel to the nozzle centerline, showed good performance. The material exhibited a uniform erosion and char rate as shown by the following station 0.0 data.

	Erosion Rate M/S	Char Rate M/S
Plane 1-2	9.57	11.13
1-3	8.87	10.00
2-3	5.22	7.30

The material also showed many local ply delaminations that probably occurred during fabrication (Figure 170). In addition, during the nozzle disassembly operations with a 500° F oven, the liner cracked in one plane due to the thermal expansion of the steel shell. In subsequent disassembly operations, the liner was further delaminated at station 0.0. The structural integrity of the liner was good.

The 4C-1686 carbon polyphenylene nose, tape wrapped parallel to center-line, showed good performance. The material exhibited a uniform erosion as shown below with station -8.0 and -3.0 data.

	Erosion Rate M/S		Char Rate M/S	
	Station -3.0	Station -8.0	Station -3.0	Station -8.0
Plane 1-2	9.74	8.70	12.70	17.40
1-3	6.96	6.61	14.44	15.48
2-3	6.78	8.17	12.18	18.79

The 4C-1686 erosion, when compared to the standard WB-8217 carbon phenolic evaluated in subscale Nozzle No. 1, was higher at station -3.0 and lower at station -8.0. The erosion pattern is the reverse of the usual carbon cloth nose perform-ance. The material also showed circumferential ply delaminations in the char from station -8.0 to 0.0. The delaminations are small at station -8.0 but much wider at station 0.0 (Figures 165, 167, and 170). Local gouging of the surface material also occurred at station -8.0. The structural integrity of the virgin material was excellent, while the char material was only fair.

The 4C-1686 carbon polyphenylene inlet, a flat laminate layup 90 deg to nozzle centerline, showed good performance. The material exhibited uniform erosion and char as shown below by station -4.0 data.

	Erosion Rate M/S	Char Rate M/S
Plane 1-2	9.57	19.66
1-3	9.96	19.50
2-3	9.57	22.62

The material showed many circumferential ply delaminations in the char layer throughout the length of the part. Several delaminations extended into the virgin material at station -4.0. The structural integrity of the virgin material was excellent, but only fair in the char material. The sectioned component is shown in Figure 170, while Figure 166 shows the inlet before the nozzle was disassembled.

The LCCM-2626 graphite particle phenolic throat, molded at 1,000 psia and 325° F, showed very good performance. The material exhibited a uniform erosion as shown below by the stations -1.0, 0.0, +2.0, and +4.0 data.

47

Erosion Rate M/S				
	Station -1.0	Station 0.0	Station +2.0	Station +4.0
Plane 1-2	7.48	6.09	5.22	5.04
1-3	9.32	8.70	9.22	7.83
2-3	9.22	8.52	7.33	7.30

The material also showed local spalling of the wall surface between station +2.0 to +4.0. Internal delaminations running parallel to the surface occurred at the same station location (Figure 170). The structural integrity of the component was very good.

The LCCM-2626X graphite particle phenolic forward exit was molded at 850 psi and 325° F as a billet, cut, segmented, and bonded together as a four segment ring and overwrapped with glass cloth phenolic

As explained in the subscale fabrication phase section, the exit cone segments were made from four molded 8 in. ID to 26 in. OD 11 in. high rings. The four rings each made three segments or a total of 12 segments. The 12 segments were then machined to form three complete segmented rings of four segments per ring. The exit cone as shown below is formed with three segmented LCCM rings.
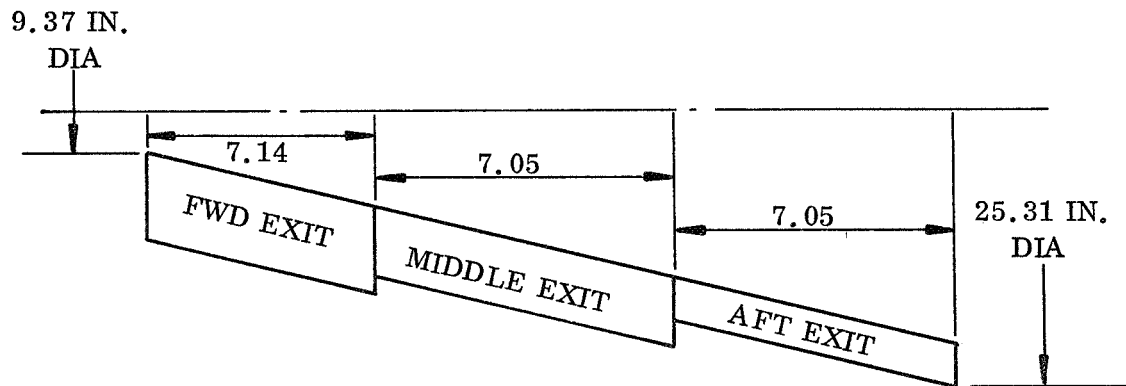
Only one mold tool was required to form the initial four molded 26 in. diameter rings. However, the press (200 tons) could only supply a 850 psi surface pressure load. The resulting cured material, designated as LCCM-2626X, represents a process variation to the LCCM-2626 material which had been characterized at a cure pressure of 1,000 psi. Based upon the prime nozzle objective of demonstrating an exit cone segmented ring fabrication method rather than material performance demonstration, the variation was accepted.

The LCCM-2626 throat ring was cured at 1,000 psi. Because the initial molded ring was smaller than the exit cone molded rings, the smaller molding area allowed a higher surface pressure with the same 200-ton press.

48

The material performance of the LCCM-2626X forward exit cone showed fair performance. The erosion rates were nonuniform at each station as shown below by the station +10 and +12 data.

	Erosion Rate M/S	
Plane	Station +10.0	Station +12
Maximum	9.00	15.50
Nominal	12.20	13.50
Minimum	8.50	5.70

No char layer was visible in the sectioned ring. In addition, the ring showed many internal parallel-to-surface delaminations as reflected in Figure 169, and internal surface gouging and spalling as shown in Figure 167. The white arrows in Figure 167 show the circumferential interface surfaces between the three segmented exit cone rings and the axial interface joint of the four segments in each of the three segmented rings. The circumferential and axial joint interfaces showed no more erosion than the adjacent parent material, thus supporting the segmented ring fabrication concept from a performance standpoint. The structural integrity of the segmented rings after test was only fair, due to the many internal delaminations and the uneven erosion caused by spalling and gouging.

The LCCM-2626X graphite particle phenolic middle exit cone molded at 850 psi and 325° F showed fair performance. The material showed a nonuniform erosion rate as reflected below by the station +20.0 data.

	Erosion Rate M/S
Maximum	19.5
Nominal	14.3
Minimum	10.8

The material also exhibited surface gouging and spalling, and internal local axial wall delaminations. The axial and circumferential joint lines again showed no more or no less erosion than the surrounding parent material. The sectioned middle exit cone is shown in Figure 169, and the internal exit cone wall surface is shown in Figure 167. The structural integrity of the segmented ring was only fair due to the internal delaminations and the surface spalling and gouging.

The LCCM-2626X graphite particle phenolic aft exit cone, molded at 850 psi and 325° F showed fair performance. The material experienced a nonuniform erosion rate as shown below by the station +32.0 data.

49

Erosion Rate M/S

Maximum	+16.2
Nominal	-3.3
Minimum	+6.6

The minus sign indicates a radial wall thickness increase due to the shrinkage of the heated material. The material also exhibited surface gouging and spalling (Figures 167 and 168) and internal delaminations running parallel to the wall surface (Figure 169). The axial and circumferential joint interfaces were satisfactory. The structural integrity of the segmented ring was only fair, due to the delaminations, spalling and gouging.

The large nonuniform erosion and loss of LCCM-2626X in the three tiered segmented exit cone is documented by the four large thrust variations during motor operations (Figure 178) starting at 15 sec as compared to the thrust performance of Nozzle No. 3 with normal exit cone erosion performance.

The FM-5063 carbon cloth phenolic end ring, tape wrapped parallel to centerline, performed satisfactorily.

The exit cone backup insulation 1581 glass phenolic (Figure 169) and the inlet-throat 23-RPD insulation (Figure 170), both tape wrapped parallel to the nozzle centerline, show the material performed very satisfactorily in supporting the ablative liner and insulating the steel shell with no delaminations or cracks.

In summary, three materials, MXA-6012, 4C-1686, and 23-RPD are recommended for further evaluation in the nozzle material areas where they were tested. In addition, a fourth material, LCCM-2626, is recommended for the nozzle throat area, but further development is recommended before the LCCM-2626X material can be used in the exit cone. The recommendations are all based on the material erosion/char performance, the material integrity during static test, and the comparison of the actual to the predicted erosion rates (Figure 146).

Nozzle No. 3 post-test inspection. - Five materials from the screening and evaluation program phase were applied to the following six ablative and two backup insulation liner nozzle areas.

Submerged OD	23-RPD	Asbestos phenolic cork filled
Nose	SP-8057	Carbon phenolic
Inlet	SP-8057	Carbon phenolic
Throat	SP-8050	Carbon phenolic
Forward exit	SP-8057	Carbon phenolic
Aft exit	SP-8030-96	Silica phenolic
Exit insulation	23-RPD	Asbestos phenolic
Inlet throat insulation	FM-5272	Paper phenolic

The test motor pressure versus time trace showed the following operating conditions.

Maximum pressure	524 psia
Average web time pressure	476 psia
Web time	56.2 sec

The post-test nozzle condition was very good with all five materials exhibiting good to excellent performance in all the nozzle areas. Figures 179 thru 182 show the submerged liners and exit cone as received from AFRPL testing facility. Figures 183 and 184 show one of the three nozzle section profiles for the submerged and exit cone liners. In terms of material performance, Nozzle No. 3 compared very favorably to Nozzle No. 1, the standard baseline material nozzle.

The actual erosion/char profiles, depths, and rates are shown for the ablative liners in three planes in Figures 185 thru 187. The notes indicate the data changes since the data were reported in the monthly reports. The erosion/char rates are summarized for the three nozzle profile planes in Figure 188. The notes finalize the data changes and define the erosion/char depths.

The performance of each nozzle liner is summarized on Table 45 and discussed by component in greater detail below.

The 23RPD submerged liner, tape wrapped parallel to centerline, showed very good performance. The material exhibited a uniform erosion and char rate as shown below by the station +2.0 data.

	Erosion Rate M/S	Char Rate M/S
Plane 1-3	5.69	7.12
1-2	7.12	8.18
2-3	7.47	7.83

A characteristic of the material is the very thin char layer exhibited after static test. Several axial wrinkle lines were apparent after static test on the charred outside surface where the material had bunched together during the fabrication debulking and curing operations (Figure 183). The structural integrity of the virgin and char material was excellent.

The SP-8057 nose, tape wrapped parallel to centerline, showed good performance. The material exhibited a uniform erosion and char rate as shown below by the station -3.0 and -8.0 data.

51

	Erosion Rate M/S		Char Rate M/S	
	Station -3.0	Station -8.0	Station -3.0	Station -8.0
Plane 1-3	3.91	12.09	8.89	15.66
1-2	3.91	11.56	9.78	17.80
2-3	4.44	11.56	8.89	21.30

The material showed circumferential gouging at station -7.0 to -8.0, local light spalling at station 0.0 to -3.0, and fine line axial cracks from station -8.0 to 0.0 as reflected in Figures 179, 180, and 183. The spalling, gouging, and cracks all occurred in the char layer. In addition, ply delaminations occurred in the char layer from station -8.0 to 0.0. One ply delamination extended into the virgin material at station -7.0. Many of the char cracks and delaminations occurred during the heat soak of the tested motor cooldown and the subsequent 500° F oven heat nozzle disassembly operation. The structural integrity of the virgin material was excellent while the char material was good.

The SP-8057 carbon phenolic inlet, a flat laminate 90 deg to centerline, showed very good performance. The material exhibited a uniform erosion and char rate as shown below by the station -8.0 data.

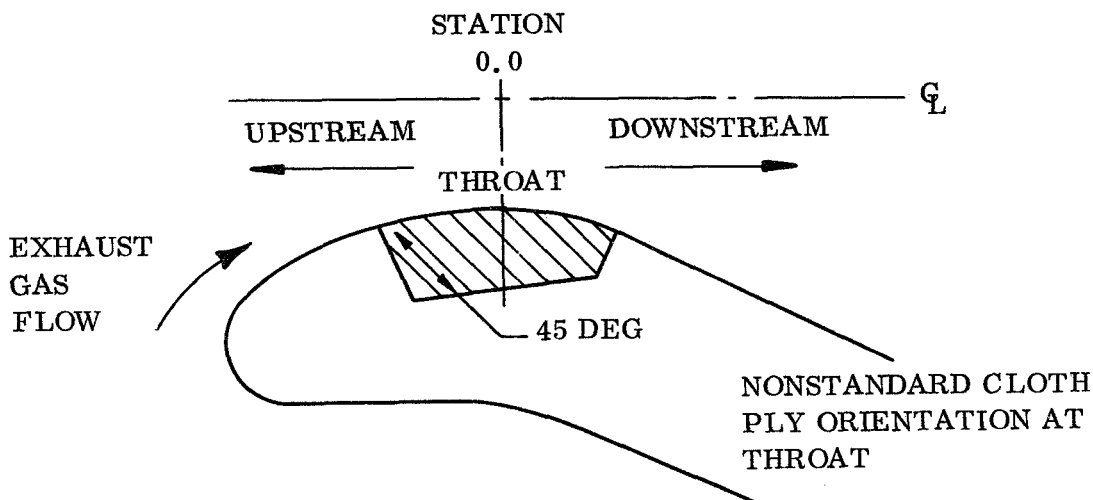|	Erosion Rate M/S	Char Rate M/S
Plane 1-3	10.32	15.66
1-2	13.52	16.90
2-3	12.81	17.43

The material exhibited several ply delaminations at station -3.0 to -2.0 that penetrated through the char layer and extended circumferentially around the ring as shown in Figures 180 and 183. Some local gouging occurred at the forward interface with the nose at station -8.0. The internal wall surface was very smooth. The structural integrity of the virgin material was excellent, while the char layer was very good.

The SP-8050 carbon phenolic throat, laid-up 45 deg to centerline upstream, showed excellent performance. The material exhibited a uniform erosion and char rate as shown below by the station -3.0 data.

	Erosion Rate M/S	Char Rate M/S
Plane 1-3	10.67	17.43
1-2	10.67	18.68
2-3	12.09	17.80

The material showed only one circumferential delamination at station -2.0 in the char layer. The structural integrity of the virgin and char material was excellent. The internal wall surface was very smooth.

It is interesting to note that the SP-8050 carbon throat billet was machined so that the ply angle was 45 deg upstream not downstream as shown below.

STATION
0.0

UPSTREAM   DOWNSTREAM $\mathcal{C}_L$

THROAT

EXHAUST
GAS
FLOW

45 DEG

NONSTANDARD CLOTH
PLY ORIENTATION AT
THROAT

A comparison of two carbon cloth phenolic throat materials (SP-8050 and MX-4926) erosion rates per ply orientation and resin reinforcement ratio are shown below.

Nozzle No.	Throat Material	Cloth	Resin	Station 0.0 Erosion Rate 45 deg Upstream (mil/sec)	Station 0.0 Erosion Rate 45 deg Downstream (mil/sec)	Resin (%)	Cloth (%)	Web Time (sec)	Average Web Pressure (psia)
1	MX-4926	Hitco or Union Carbide Carbon Cloth	MIL-R-9299 Type II Phenolic	--	8.09	30	70	56.8	471
3	SP-8050	Hitco Carbon Cloth	MIL-R-9299 Type II Phenolic	9.78	--	30	70	56.2	476

The SP-8050 performance should be close to that of MX-4926 due to the cloth raw material and resin/cloth percentage similarity. Yet the SP-8050 shows a 21 percent increase in erosion rate over the MX-4926 due to the difference in the ply orientation direction with respect to the direction of the gas flow.

The SP-8057 carbon cloth phenolic forward exit cone, a parallel to center-line tape wrap, showed very good performance. The material exhibited a uniform erosion and char rate as shown below by the station +6.0 data.

	Erosion Rate M/S	Char Rate M/S
Plane 1-3	3.55	8.89
1-2	4.09	9.78
2-3	3.55	9.25

The material showed several circumferential delaminations in the char layer and many localized ply delaminations in the virgin material as shown in Figures 181, 182, and 184. The aft edge of the liner (station +26) showed local circumferential delaminations and several axial surface cracks.

The structural integrity of the virgin material was good and very good in the char layer.

The SP-8030-96 silica cloth phenolic aft exit cone, a parallel to centerline tape, showed very good performance. The material exhibited a uniform erosion/char rate as shown below by the station +27.0 data.

	Erosion Rate M/S	Char Rate M/S
Plane 1-3	4.80	6.94
1-2	4.82	7.12
2-3	3.91	6.40

The material had one delamination at the station +26.0 interface with the forward exit cone extending through the char and virgin material. The structural integrity of the virgin and char material was very good. The exit cone backside insulation, 23-RPD asbestos phenolic, proved to be very satisfactory with only very small ply delaminations.

The inlet/throat backside insulation, FM-5272 paper phenolic, performed adequately as backup insulation and throat support but showed numerous localized ply delaminations in the virgin material as large as 0.015 in. that probably occurred during fabrication. The two sleeves are reflected in the sectioned nozzle sections as shown by Figures 183 and 184.

In summary, it is recommended that all five materials be evaluated for use in the 260 in. nozzle in the areas where tested. The recommendation is based on their erosion/char performance, the structural integrity of the material and the comparison of the actual to predicted erosion rates (Figure 147).

Nozzle No. 4 post-test inspection. – Three low cost materials evaluated in the material screening tests and one standard AFRPL-Nomad material were applied to the following six ablative and two backup liner nozzle areas.

Submerged OD	KF-418	Canvas phenolic
Nose	KF-418	Canvas phenolic
Inlet	SP-8030-96	Silica phenolic
Throat	SP-8030-96	Silica phenolic
Forward exit	23-RPD	Asbestos phenolic cork filled
Aft exit	MXS-198	Silica epoxy novolac
Exit cone insulation	KF-418	Canvas phenolic
Inlet/throat insulation	SP-8030-96	Silica phenolic

The test motor pressure versus time trace showed the following operating conditions.

Maximum pressure	478 psia
Average web time pressure	384 psia
Web time	61.0 sec

The post-test nozzle condition was rated fair to good with all but one of the four materials exhibiting fair to good performance in at least one nozzle area. As a forward exit cone liner, the performance of the 23-RPD material was poor: however, this material demonstrated very good performance as a submerged OD liner in Nozzle No. 3. Figures 189 thru 192 show the submerged liners and exit cone as received from AFRPL testing facility. Figure 193 shows one of the three nozzle section profiles for the submerged and exit cone liners.

The main performance difference between Nozzle No. 1, standard material nozzle, and this nozzle was the loss of the forward exit cone liner material (23-RPD) through high uniform erosion, the localized erosion of the canvas KF-418 and silica SP-8030-96 materials in the nose and inlet, and the high uniform erosion of the SP-8030-96 material throat. The higher throat erosion is reflected by a decrease in maximum pressure and average web time pressure and an increase in web time.

The actual erosion/char profiles, depths, and rates for the ablative liners in three planes are shown in Figures 194, 195, and 196. The notes indicate the fabrication changes from the standard Design I nozzle, the data changes since last reported in the monthly reports, and variation in the canvas phenolic erosion and char at the initial nose slightly forward of station -8.0. The erosion/char rates are summarized for the three nozzle profile planes in Figure 197. The notes finalize the data changes and define the erosion/char depths.

55

A performance summary of each nozzle liner as discussed below is contained in Table 46.

The KF-418 canvas phenolic submerged liner, tape wrapped parallel to center-line, showed very good performance. The material exhibited a uniform erosion/char rate as shown by the following station 0.0 data.

	Erosion Rate M/S	Char Rate M/S
Plane 2-1	5.90	7.50
2-3	4.92	8.19
3-1	7.37	10.33

A characteristic of the material is a weak char layer which breaks away locally when the material is sectioned for inspection and evaluation. The material exhibited excellent structural integrity in virgin material with no delaminations, cracks or surface irregularities (Figures 189 and 190).

The KF-418 canvas phenolic nose, tape wrapped parallel to centerline, exhibited fair to good performance. A high local erosion occurred at station -8.0 decreasing to a uniform erosion at station -5.0 as shown below.

	Erosion Rate M/S		Char Rate M/S	
	Sta -8.0	Sta -5.0	Sta -8.0	Sta -5.0
Plane 2-1	13.93	8.19	15.57	9.51
2-3	16.88	9.02	18.03	11.31
3-1	27.05	11.15	28.68	12.78

As mentioned above, a characteristic of the material is a weak thin char layer. As shown in Figure 190, the char layer was lost locally by spalling during static test between station -6.0 to 0.0. A local gouge area started in the canvas phenolic nose char layer and extended into the silica cloth inlet char layer as shown in Figure 191. The structural integrity of the virgin material was excellent.

The silica phenolic inlet, a flat laminate 90 deg to centerline, showed a fair to good performance. A high local erosion occurred at station -8.0, decreasing to a uniform erosion at station -4.0 as shown below.

	Erosion Rate M/S		Char Rate M/S	
	Sta -8.0	Sta -4.0	Sta -8.0	Sta -4.0
Plane 2-1	17.05	19.67	18.36	21.60
2-3	31.96	23.93	33.77	24.75
3-1	28.68	19.67	30.49	20.98

A characteristic of the material is a thin hard char with no delaminations or cracks. The structural integrity of the char and virgin material is rated good and excellent, respectively.

The silica phenolic throat, a 45 deg to centerline downstream layup, showed good performance. The material exhibited a high uniform erosion as shown below by station -3.0 data.

	Erosion Rate M/S	Char Rate M/S
Plane 2-1	19.67	20.98
2-3	20.98	22.13
3-1	17.70	18.36

The material exhibited local spalling at station -3.0 (Figures 191 and 193), but no delaminations existed in the char or virgin layers. The local gouge that started in the nose and inlet ended in the throat at station -3.0. The structural integrity of the char and virgin material was excellent.

The 23-RPD asbestos phenolic forward exit cone, a parallel to centerline tape wrap, exhibited poor performance. The material showed a high uniform erosion/char rate as reflected below by station +7.0 data.

	Erosion Rate M/S	Char Rate M/S
Plane 2-1	23.75	24.60
2-3	21.31	22.13
3-1	22.95	24.59

Between station +7.0 and +26.0 all the asbestos liner material was lost and the canvas phenolic backup insulation was lost down to the surface of the steel shell. After static test only a triangular wedge of liner and backup insulation aft of the throat ring was left to evaluate as shown in Figures 192 and 193.

The deep erosion and subsequent loss of the 23-RPD asbestos phenolic liner and KF-418 canvas phenolic backup insulation in the forward exit cone was documented by a series of five-thrust augmentation blips after 42.0 sec of motor operation (Figure 198).

A review of the test motion films indicated that during the last half of the motor test, the exhaust plume became ragged and the number of sparks leaving the exit cone increased. No large objects were seen leaving the nozzle. Examination of the test bay area after the motor test revealed only small pieces of the aft exit cone material.

Following the poor performance of the 23-RPD material in the forward exit cone, a number of tests were performed on the tag end sample of this material, removed from the cone as it was machined for final assembly. The purpose of retests was to check the quality of the material as fabricated. The tests consisted of density, compressive strength, residual volatiles, and acetone extraction. Table 47 contains the resultant data. Density and compression data were compared to control specimen results previously obtained. No significant differences could be detected.

The MXS-198 silica epoxy novolac aft exit cone, tape wrapped parallel to center-line, showed good performance. The material exhibited a uniform erosion/char as shown below by station +27.0 data.

	Erosion Rate M/S	Char Rate M/S
Plane 2-1	4.10	7.38
2-3	5.24	8.03
3-1	4.92	7.86

The forward surface of the material interface (forward-to-aft exit cone) exhibited spalling and a local gouge which resulted from the performance of the forward exit cone material. However, the material stopped the excessive liner erosion in a short axial length and the gas flow returned to the initial exit cone wall as shown in Figures 192 and 193. The char layer showed many ply delaminations which made the internal wall surface rough. The structural integrity of virgin material was excellent and the integrity of the char material was good.

The exit cone backside insulation, KF-418 canvas phenolic tape wrapped parallel to centerline, was very satisfactory. The material prevented the loss of the steel shell when the 23-RPD forward exit cone material was lost. The canvas phenolic was lost between stations +7.0 to +18.0. At station +18.0 the insulation helped the MXS-198 return the gas flow to the initial exit cone wall surface. Local gouging occurred around the circumference of the canvas at station +18.0. No local delaminations were evident in the material (Figure 193).

The inlet/throat backside insulation SP-8030-96 silica phenolic, tape wrapped parallel to centerline, also proved to be very satisfactory with no delaminations while supporting the throat ablative liner of silica cloth (Figure 193).

In summary, it is recommended that three materials, KF-418, SP-8030-96, and MXS-198 be further evaluated for the 260 in. nozzle in the areas where tested. In addition, it is recommended not to consider 23-RPD as a forward exit cone material

until more test data are obtained. The recommendations are all based on erosion/char performance, the structural integrity and the comparison of actual to predicted erosion rates (Figure 148).

Nozzle No. 5 post-test inspection. - Five low cost materials evaluated in the screening tests and one standard Nomad AFRPL material were applied to the following seven ablative and two backup insulation liner areas.

Submerged OD	KF-418	Canvas phenolic
Nose	SP-8030-96	Silica phenolic
Inlet	LCCM-2626	Graphite particle phenolic
Throat	LCCM-2626	Graphite particle phenolic
Forward exit	LCCM-2626X	Graphite particle phenolic
Middle exit	LCCM-4120	Graphite particle phenolic
Aft exit	LCCM-4120	Graphite particle phenolic
Exit cone insulation	1581	Glass phenolic
Inlet/throat insulation	23-RPD	Asbestos phenolic - cork filled

In addition, an end retainer ring of KF-418 canvas phenolic was used to insulate the steel end plate from the low cost carbonaceous material. The test motor pressure versus time trace showed the following operating conditions:

Maximum pressure	489 psia
Average web time pressure	446 psia
Web time	58.4 sec

The nozzle post-test evaluation was fair to good with all materials exhibiting good performance in at least one nozzle area. Figures 199, 200, and 201 show the submerged liners and exit cone as received from the AFRPL testing facility. Figure 202 and 203 shows one of the three nozzle section profiles of the submerged and exit cone liners. The circumferential white arrows (Figure 200) point out the joints in the segmented throat while the axial white arrows (Figure 201) show the interfacing joints between the exit cone rings.

The main performance difference between Nozzle No. 1, standard material. nozzle, and this nozzle is the partial loss of the forward exit cone ablative liner by high nonuniform erosion and the higher erosion depths for the SP-8030-96 silica cloth phenolic nose.

The actual erosion/char profiles, depths, and rates for the ablative liners in three planes are shown in Figures 204 thru 206. The notes on the figures indicate the data changes since last reported in the monthly reports. The erosion/char rates are summarized for the three nozzle profile planes in Figure 207. The notes document the data changes, the lack of charline in graphite particle phenolic material, and definition of the erosion/char depths.

A performance summary of each nozzle component as discussed below is contained in Table 48.

The KF-418 canvas cloth phenolic submerged liner, tape wrapped parallel to centerline, showed good performance. The material exhibited a uniform erosion/char rate as shown below with station 9.0 data.

	Erosion Rate M/S	Char Rate M/S
Plane 1-1	6.51	8.91
2-2	9.42	12.34
3-3	10.28	12.85

A characteristic of the material is a weak char layer which breaks away locally when the material is sectioned for inspection and evaluation. The structural integrity of the virgin material was excellent with no ply delaminations or cracks (Figures 199 and 202).

The SP-8030-96 silica phenolic nose, tape wrapped parallel to centerline, showed good performance. The material exhibited local high erosion at station -8.0, decreasing to a uniform erosion at station -1.0 as shown below.

	Erosion Rate M/S		Char Rate M/S	
	Sta -8.0	Sta -1.0	Sta -8.0	Sta -1.0
Plane 1-1	13.71	5.99	13.88	8.57
2-2	18.85	9.94	21.42	11.65
3-3	19.71	9.94	22.28	12.34

The material showed a characteristic thin, hard char. The char showed the lowest level of delamination at station -8.0 and 0.0. The internal wall surface was smooth and uniform. The structural integrity of the char and virgin material was excellent.

The LCCM-2626 graphite particle phenolic inlet (molded at 1,000 psi and 320° F) showed very good performance. The material exhibited a uniform erosion rate as shown below. Station -8.0 shows the effect of the local high erosion of the silica nose, while station -7.0 is more representative of the material low uniform erosion rate.

	Erosion Rate M/S	
	Sta -8.0	Sta -7.0
Plane 1-1	13.71	9.59
2-2	15.42	7.71
3-3	17.14	8.74

The material exhibited localized light surface spalling on the wall at station -8.0 next to the silica cloth nose ring (Figures 199 and 200). The sectioned wall (Figure 202) shows local internal delaminations from station -8.0 to -4.0 parallel to the internal wall surface. The inlet/nose material selection is unique, since it was the only high erosion (silica) to low erosion (graphite particle phenolic) material interface evaluated in the six nozzle inlet/nose test matrix. The OD surface showed two axial cracks. The structural integrity of the LCCM-2626 was good.

The LCCM-2626 graphite particle phenolic four-segment throat molded at 1,000 psi and 320°F showed fair to good performance. The material exhibited uniform erosion as shown below by the station -1.0, 0.0, +2.0, +4.0 data.

<div align="center">

Erosion M/S

	Sta -1.0	Sta 0.0	Sta +2.0	Sta +4.0
Plane 1-1	7.37	8.05	10.62	11.65
2-2	9.42	9.94	14.39	16.28
3-3	11.99	12.34	14.56	11.65

</div>

The erosion rate aft of the throat plane, station +2.0 and +4.0, were higher than the inlet (station -1.0) and throat (station 0.0) erosion rates. The Nozzle No. 2 subscale throat (LCCM-2626) also showed locally higher erosion rates aft of the throat plane at station +2.0. The throat component materials of Nozzle No. 1 (carbon phenolic), Nozzle No. 3 (carbon phenolic), and Nozzle No. 4 (silica phenolic) showed locally higher erosion rates forward of the throat at station -3.0.

The throat material showed wall surface spalling and internal delaminations aft of the throat plane from station +1.0 to +4.0 as reflected in Figure 202. Figure 208 reflects the four segment throat ring orientation to the test motor propellant starpoint and star valley. The erosion rate of the LCCM-2626 material in the throat of this nozzle was approximately 30 percent higher than the rate experienced in the throat of Nozzle No. 2. The variation in performance may be within the natural erosion range of the material. However, there were some indications that the segmented throat design may have had a degrading effect upon the performance of the material. The structural integrity of the material was good.

The LCCM-2626X forward exit cone, molded at 850 psi and 320°F, showed poor to fair performance. The material exhibited high nonuniform erosion as shown below by the station +10.0 and +12.0 data.

<div align="center">

Erosion Rate M/S

	Sta +10.0	Sta +12.0
Plane 1-1	27.76	Liner material lost
2-2	20.56	29.80
3-3	17.65	17.48

</div>

The liner material was lost over 40 percent of the nozzle circumference between station +11.0 to +18.0 (Figure 201). Also, a portion of the glass phenolic insulation (overwrap) was eroded just aft of the throat segment joint, exposing the steel nozzle shell (Figure 209). The LCCM-2626X material performance in the forward exit cone of this nozzle and in Nozzle No. 5 may represent the natural range of material erosion under similar test conditions. However, the performance of the material in this nozzle was probably influenced by the higher erosion of the segmented throat between station +2.0 and +4.0.

The material showed local internal wall delaminations parallel to the internal wall surface from station +5.0 to +17.0 (Figure 203). In addition, the inside wall showed spalling and gouging. The structural integrity of the material was only poor to fair.

The erosion pattern and loss of material in the forward exit cone is documented by a series of eight thrust variations 13 sec after motor ignition (Figure 210). The same thrust variations were evident also in Nozzles No. 2 and 4 when a deep erosion pattern formed in the forward exit cone with LCCM-2626X segmented and 23-RPD materials. No significant thrust variations were noticed, with normal erosion patterns of the forward exit cone in Nozzles No. 1, 3, and 6 using SP-8050 carbon, SP-8057 carbon, and KF-418 canvas materials, respectively. Examination of the test bay area after the motor test revealed only small particles of the LCCM-2626X, indicating no material chunking.

The LCCM-4120 graphite particle phenolic middle exit cone (molded at 12.4 psi and 170°F) showed fair to good performance. The material exhibited low uniform erosion as shown below by station +27.0 data.

	Erosion M/S
Plane 1-1	1.55
2-2	1.19
3-3	0.00

The erosion rates are the lowest of the exit cone materials evaluated. However, between station +19 and +24 the liner lost a considerable amount of material while returning the exhaust flow lines to the original exit cone wall dimensions as a result of the forward exit cone material high nonuniform erosion. The liner surface spalled and gouged between stations +19.0 to +24.0, but showed excellent appearance between stations +27.0 to +31.0.

The LCCM-4120 material showed internal delaminations in the radial and axial directions. The outside diameter of the cone also showed a connected series of axial and circumferential cracks. The internal delaminations are shown in Figure 203, while the OD surface cracking is shown in Figure 211. The structural integrity of the material was only fair.

The LCCM-4120 graphite particle phenolic aft exit cone (molded at 12.4 psi and 170°F) showed good performance. The material exhibited the lowest uniform erosion of all the materials tested in this nozzle area as shown below by station +32.0.

Erosion Rate M/S

Plane 1-1	0.68
2-2	0.51
3-3	0.51

The material internal wall surface was very uniform, with no delaminations or cracking. However, in the internal wall radial delaminations were apparent for two-thirds of the wall thickness as measured from the outside liner surface (Figure 203). The outside surface again showed a connected series of axial and circumferential cracks. The structural integrity of the component was rated fair.

The end ring of KF-418 canvas phenolic, tape wrapped parallel to centerline, was very satisfactory. The material prevented the loss of the steel shell when the LCCM-2626X was locally eroded to the insulation. In addition, no delaminations were visible.

The inlet/throat backside insulation, 23-RPD asbestos phenolic tape wrapped parallel to centerline, was satisfactory in supporting the throat liner while exhibiting only local fine delaminations.

In summary, all five materials are recommended for evaluation in the 260 in. nozzle in the areas where tested except the LCCM-2626X material in the forward exit cone. The recommendations are based on the erosion/char rates, the overall structural integrity, and the comparison of actual to predicted erosion rates (Figure 149).

Nozzle No. 6 post-test evaluation. - Four materials, two from the AFRPL-Nomad program and two low cost materials evaluated in the screening task, were applied to the following six ablative and two backup insulation liner nozzle areas.

Submerged OD	SP-8030-96	Silica phenolic
Nose	FM-5272	Paper phenolic
Inlet	SP-8030-96	Silica phenolic
Throat	SP-8057	Carbon phenolic
Forward exit	KF-418	Canvas phenolic
Aft exit	FM-5272	Paper phenolic
Exit cone insulation	FM-5272	Paper phenolic
Inlet/throat insulation	KF-418	Canvas phenolic

The test motor pressure versus time trace showed the following operating conditions.

Maximum pressure   495 psia
Average web time pressure   - 446 psia
Web time   .58.3 sec

The post-test nozzle condition was good, with all four materials exhibiting fair to very good performance in all nozzle areas. Figures 212 thru 215 show the submerged liners and exit cone as received from AFRPL testing facility. Figure 216 shows one of the three nozzle section profiles for the submerged and exit cone liners. In comparison to Nozzle No. 1, the standard Nomad material nozzle, the materials in this nozzle compared favorably. The major performance differences were in the nose/inlet area and the forward exit cone area, where the erosion rates were higher, since canvas, silica, and paper phenolic were used in lieu of carbon cloth phenolic.

The three plane ablative liner actual erosion/char profiles, depths, and rates are shown in Figures 217, 218, and 219. The notes indicate the data changes made after publication of the monthly reports, the fabrication changes, the loss of material during disassembly operations. The erosion/char rates are summarized for the three nozzle profile planes in Figure 220.

The performance of each nozzle liner is summarized in Table 49 and discussed by component in greater detail below.

The SP-8030-96 silica cloth phenolic submerged liner, tape wrapped parallel to the nozzle centerline, showed good performance as reflected in Figure 212. The material exhibited a uniform erosion and char rate as shown by the station 0.0 values below.

	Erosion Rate M/S	Char Rate M/S
Plane 1-1	6.52	8.92
1-2	10.30	10.64
1-3	7.21	9.44

Local ply delaminations occurred in the char layer between station 0.0 to +3.0. The outside diameter surface was coated with solidified silicon dioxide (SiO_2) melt and residual gas exhaust products such as aluminum oxide (Al_2O_3). Several local axial ply delaminations occurred in the virgin material (Figure 216).

During the 500° F oven heat nozzle disassembly operation, the silica phenolic liner cracked axially, starting at station +15.0 and extending to station +3.0. Cracking was due to the expansion of the steel nozzle shell. The structural integrity of the liner was good.

The FM-5272 paper phenolic nose, tape wrapped parallel to centerline, showed fair to good performance. The material exhibited local high erosion at station -8.0, decreasing to a uniform erosion at station -3.0.

	Erosion Rate M/S		Char Rate M/S	
	Sta -8.0 Est	Sta -3.0 Est	Sta -8.0	Sta -3.0
Plane 1-1	15.77	6.86	14.05	5.14
2-2	28.32	11.16	26.60	9.44
3-3	22.32	10.14	20.60	8.42

A characteristic of the material is a loose, very weak char layer. The char layer spalled locally as shown in Figure 213. Later, during the forced air oven heating (500°F) nozzle disassembly operation, all the char layer was blown off the component. An estimated average char thickness of 0.100 in. was used to show the erosion rates at station -8.0 and -3.0.

The FM-5272 surface under the char layer was subjected to the 500°F oven heat that caused surface-crazing cracks and delaminations. The material performance was comparable to carbon cloth (WB-8217) from a gouging and spalling standpoint as seen by comparing Figure 157 at station -8.0. The same statement holds true for the other low cost nose components of SP-8030-96 silica cloth and KF-418 canvas cloth. However, the low cost materials do experience local high erosion in the plane of the propellant star valley.

The virgin material shows many internal delaminations that were probably the result of the fabrication process (Figure 216). The structural integrity of the char and virgin material was rated fair and very good, respectively.

The SP-8030-96 silica phenolic inlet, tape wrapped parallel to centerline, showed good performance. The material exhibited a local high erosion at station -8.0, decreasing to a uniform erosion rate at station -4.0. The erosion/char data for these two stations are shown below.

	Erosion Rate M/S		Char Rate M/S	
	Sta -8.0	Sta -4.0	Sta -8.0	Sta -4.0
Plane 1-1	13.54	15.75	15.60	17.35
2-2	22.80	20.25	25.41	22.32
3-3	19.02	18.80	20.75	20.50

The material exhibits a characteristic thin, hard char and a smooth internal wall surface as shown in Figures 214 and 216. The liner material exhibited no delaminations, cracks, spalling or gouging. From this standpoint the SP-8030-96 was superior to the other material tested in the nozzle inlet area. The structural integrity of the material is excellent.

The SP-8057 carbon cloth phenolic throat, laid up 45 deg to centerline downstream, showed excellent performance (Figures 214 and 216). The material exhibited a uniform erosion as shown below with station -3.0 and -2.0 data.

	Erosion Rate M/S		Char Rate M/S	
	Sta -3.0	Sta -2.0	Sta -3.0	Sta -2.0
Plane 1-1	10.62	9.44	13.38	12.87
2-2	11.98	10.64	16.13	14.59
3-3	12.50	10.98	15.75	15.05

The material erosion at station -2.0 was more of an indication of the material performance than station -3.0 since the inlet/throat interface was the only carbon/ silica material interface evaluated in the program in a high heat flux nozzle area. The char layer had a local delamination at station -3.0 and one fine circumferential ply delamination at the wall surface at station +2.0, extending into the virgin material. The internal wall surface was very smooth except for a slightly pitted area from station +1.0 to +4.0. The structural integrity of the char and virgin material was excellent.

The KF-418 canvas phenolic forward exit, tape wrapped parallel to centerline, exhibited good performance (Figures 215 and 216). The erosion pattern is illustrated below, with high uniform erosion/char rates at station +14.0 and with low uniform erosion/char rates at stations +5.0 and +23.0.

	Erosion Rate M/S			Char Rate M/S		
	Sta +5.0	Sta +14.0	Sta +23.0	Sta +5.0	Sta +14.0	Sta +23.0
Plane 1-1	6.86	18.20	5.49	9.95	18.52	6.00
2-2	6.50	16.82	3.60	9.44	17.50	4.29
3-3	6.53	16.86	6.52	10.30	17.50	7.55

This nozzle had the only carbon phenolic throat (low cost material canvas phenolic) to forward exit cone interface. The canvas phenolic material exhibited only one delamination and no cracks in the char and virgin material as shown by Figure 216. The fluted irregular wall surface was due to nonuniform loss of the thin, weak, char layer. The structural integrity of the material was very good.

The FM-5272 paper phenolic aft exit cone, tape wrapped parallel to centerline, exhibited good performance (Figures 215 and 216). The uniform erosion/char rates are illustrated by the values at station +27.0.

	Erosion Rate M/S	Char Rate M/S
Plane 1-1	4.29	5.14
2-2	3.43	4.29
3-3	6.00	6.52

The material exhibited a characteristic thin, loose, very weak char layer that was lost in an irregular surface pattern. In the sectioned wall many local ply delaminations were visible, that probably occurred during the material processing cycle. The structural integrity of the component was good.

The exit cone backside insulation, FM-5272 paper tape wrapped parallel to centerline, provided adequate performance. The material exhibited many local ply delaminations and radial cracks. The ply delaminations probably occurred during the fabrication process. The interface adhesive bond was lost during the oven heat (500°F) disassembly operations, showing wide separation (Figure 216) when thin sections were cut out of the exit cone.

The inlet/throat insulation KF-418 canvas, tape wrapped parallel to centerline, was very satisfactory with no delaminations or cracks. It provided a good throat support and steel insulation (Figure 216).

In summary, all four materials are recommended for evaluation in the 260 in. nozzle in the areas where tested. The materials were acceptable based on their good ablative performance (erosion/char integrity) and the comparison of actual to predicted erosion rates (Figure 150).

Subscale Nozzle
Overall Test Analysis Summary

The six nozzle tests encompassed an evaluation of 36 ablative liners and 12 backup insulative liners.fabricated from 14 materials. Seven carbonaceous materials (WB-8217, MX-4926, SP-8050, SP-8057, 4C-1686, LCCM-2626, LCCM-4120 including LCCM-2626X, with a process variant not fully characterized) and seven low or noncarbonaceous materials (KF-418, FM-5272, 23-RPD, MXA-6012, SP-8030-96, MXB-6001, MXS-198) were evaluated by erosion/char performance and structural integrity and rated poor to excellent as reflected in Table 50. It is noted that MXB-6001 (1581 glass phenolic tape), utilized as a backside insulative liner on the exit cone of Nozzles No. 2 and 5, had not been evaluated in Task I of this program.

With the exception of the LCCM-2626X (variant material) in the exit cone and the 23-RPD material in the forward exit cone, the above mentioned materials are recommended as satisfactory ablative liner candidates for evaluation in a 260 in. motor nozzle design in the areas in which they were tested. When evaluated as backup insulative liners (low or noncarbonaceous material only), five of the six materials are recommended as satisfactory candidates for evaluation in a 260 in. nozzle in the areas in which they were tested. Paper phenolic FM-5272 was eliminated as a candidate material. Table 51 reflects the recommended ablative liner and insulative materials by nozzle area location.

Achievements of the subscale nozzle task as related to stated objectives are discussed in the following paragraphs.

Demonstrate the suitability of low cost ablative nozzle concepts by static testing. - The low cost materials tested in six nozzles as tape wrapped or molded segments proved to be highly successful in terms of fabrication, performance prediction, and test evaluation. A comparison of successful low cost materials versus typical standard materials in terms of raw material cost is shown below.

Nozzle Type	Submerged Liner	Nose	Inlet	Throat	Forward Exit	Aft Exit
Standard production material nozzle	MX-2600 $6.50/lb	MX-4926 $21.00/lb	MX-4926 $21.00/lb	MX-4926 $21.00/lb	MX-4926 $21.00/lb	MX-2600 $6.50/lb
Standard Nomad material nozzle	FM-4272 paper $2.00/lb	WB-8217 carbon $20.97/lb	WB-8217 carbon $20.97/lb	MX-4926 carbon $21.00/lb	SP-8050 carbon $16.50/lb	KF-418 canvas $1.50/lb
Low cost material nozzle	KF-418 canvas $1.50/lb	KF-418 canvas $1.50/lb	LCCM-2626 graphite $0.75/lb	LCCM-2626 graphite $0.75/lb	KF-418 canvas $1.50/lb	LCCM-4120 graphite $0.75/lb

68

The original high cost standard production materials ranging from $6.50 to $21.00/lb could be replaced with lower cost materials ranging from $0.75 to $1.50/lb or the standard Nomad nozzle materials ranging from $1.50 to $20.97/pound.

Correlation of material properties and fabrication with nozzle performance. – The available data from this program and several previously conducted Air Force material programs when tabulated indicates that predictable theories relating fabrication techniques and material properties to material test performance are still undefined but trends may be indicated as shown in Table 52.

The tests indicated that the carbon and graphite tape wrapped and molded throat materials with low ultimate compressive strength and thermal conductivity will erode at a higher rate than the standard MX-4926 throat material. More data are needed for low or noncarbonaceous materials in the throat before any statement can be made. It is interesting to note, however, that the silica with a lower compressive strength and thermal conductivity also has a higher erosion rate.

The structural integrity of the tested throat components appear to be good to excellent for both types of materials with varying fabrication techniques and material properties.

Of the low or noncarbonaceous tape wrapped materials tested in the OD submerged liner, a low ultimate compressive strength and thermal conductivity also seems to indicate erosion at a higher rate. The structural integrity of the tested components appears to be good to excellent except the standard FM-5272 paper phenolic for the various material properties.

Of the low or noncarbonaceous materials tested in the aft exit cone, no trend of compressive strength and thermal conductivity is apparent when compared to the standard KF-418 canvas as shown below.

	Higher Comp Strength Lower K Than Std Mtl	Lower Comp Strength Lower K Than Std Mtl	Higher Comp Strength Higher K Than Std Mtl	Lower Comp Strength Higher K Than Std Mtl
Lower erosion rate than std mtl	--	--	--	--
Higher erosion rate than std mtl	SP-8030 silica	--	FM-5272 paper phenolic	--

Two materials, SP-8030 silica and FM-5272 paper, showed higher erosion rates with higher compressive strength and a higher or lower thermal conductivity (K). One other material that could have provided another matrix data point was not laboratory tested for (K). More data are needed to show any trend for the low or noncarbonaceous materials.

The structural integrity of the low or noncarbonaceous materials was good to very good for the varying fabrication techniques and material properties.

The graphite particle phenolic materials also need more data before any trend statement can be made. It is interesting to note, however, that the best performing material in the aft exit cone, LCCM-4120 graphite particle phenolic, showed a lower erosion rate with a lower compressive strength and higher thermal conductivity.

The structural integrity of the two graphite particle phenolic materials was only fair due to material delaminations and OD surface cracking.

While no definite statement can be made correlating the material property and fabrication technique to the material test performance, a preliminary evaluation of the submerged liner and throat indicates that the higher compressive strength and higher thermal conductivity materials will show better test performance than lower strength and lower thermal conductivity materials. A preliminary evaluation of the aft exit cone is unreasonable at this time.

Verification of design procedures (erosion predictions versus performance). - The comparison of material predicted erosion versus test erosion performance was good considering that a submerged nozzle with thin liner walls (2.0 in.) will exhibit higher erosion rates than an external nozzle with thick liner walls (3.0 to 4.0 in.) as exemplified by the high heat sink graphite particle phenolic materials.

The predicted erosion was obtained from material design curves using TU-379 and TU-622 motor erosion rate data versus a calculated convective heat transfer coefficient or total heat flux (Figures 57 thru 66) for carbonaceous materials and in Figures 71 thru 78 for low or noncarbonaceous materials.

The actual to predicted erosion rates for the materials in the nozzle areas where tested were good except for LCCM-2626X graphite particle phenolic in the forward, middle, and aft exit cone and the 23-RPD asbestos in the forward exit cone. The reasons for the elimination of these materials were unacceptable erosion rates and nonreproducibility.

No comparison of actual to predicted erosion rates were made for the six Nomad program nozzle materials (MX-4926, SP-8050, FM-5272, MXA-6012, KF-418, WB-8217) fired in the nozzles, because they were not tested in the TU-622 motor to obtain material performance design curves.

Material erosion/char performance data to design a full scale nozzle. - The material erosion/char performance data are tabulated in the post-test evaluation section of this report. Each nozzle was cut in three planes (propellant starpoint, star valley, and between the propellant starpoint and the star valley). The eroded

and charred profile lines were then overlaid on the subscale nozzle design drawing which had been updated to reflect fabrication deviations. The erosion/char depths and rates (using the web time) were calculated for each nozzle at 53 stations over six nozzle areas in each of the three sectioned nozzle planes. The TU-622 material erosion design curves (Figures 57 thru 66 and 71 thru 78) will be updated with the subscale erosion rate data and be used for the 260 in. nozzle material erosion prediction in the next section of this report – Material Performance and Prediction – 260 In. Nozzle.

FABRICATION TECHNIQUES STUDIES

Because of the great variety of materials investigated in this program and because most of them were new or recently developed, it was necessary to develop fabrication techniques for those materials which were low cost and yet produced optimum or near-optimum properties in a finished component. It was also necessary that such techniques be applicable to the fabrication of full sized nozzles for 260 in. diameter solid rocket motors.

Fabrication techniques were developed for each of the 14 materials employed in the fabrication and testing of the six subscale nozzles discussed in the previous section. Each of these materials will be discussed separately in this section.

One of the most significant costs encountered in the fabrication of large nozzle components was the cost of pressure curing facilities of the size required. Consequently, one of the primary objectives of this study was to eliminate this need, either through the use of materials requiring a lower pressure cure or through the design and incorporation of more reasonably sized high pressure molded components. Both areas of this objective were successfully met in this program.

With one exception, all materials utilized in the six subscale nozzles were fabricated at autoclave pressures or lower, thereby eliminating the requirement for large, costly hydroclaves or presses. Two materials were fabricated under vacuum bag only, at one atmosphere pressure, eliminating an autoclave requirement as well.

The one material still requiring high pressure was fabricated into small segments or bricks (Subscale Nozzles 2 and 5). Such segments can easily be tailored in size to accommodate existing presses and handling equipment. The concept was thoroughly proven in this program and is discussed in detail in the section of this report dealing with the six subscale nozzles.

Combined with low pressure curing cycles, tape wrapping was found to be an entirely feasible method of fabricating large nozzle components. Basically, tape wrapping is a most desirable technique in part fabrication which produces highly satisfactory results. The only detrimental facet has been the costly high pressure curing facilities required for large, monolithic tape wrapped parts. Reducing the pressure requirements to autoclave range or lower has successfully eliminated this detriment. A summary of the conditions employed in the fabrication of the tape wrapped components is contained in Table 53. General comments concerning the qualities and fabrication techniques developed for each material are listed below.

Materials and Fabrication Techniques

LCCM-2626 (Graphite particle phenolic produced by Thiokol). - This is the
only material employed which was press molded at high pressures (850 to 1,000 psi).
Being a dry powder molding compound, the material handled easily. A predetermined
quantity was simply added to a mold. Because of a relatively high bulk factor, it
was found that it was desirable to add the material to a mold in increments and debulk
at full pressure between additions. Staging of this material was not necessary. A
cured part of this material can be removed from a mold hot or cold.

LCCM-4120 (Graphite particle phenolic produced by Thiokol). - The material
is versatile with regards to curing, requiring only vacuum bag (1 atmosphere) pres-
sure. Cure temperature is from 170° to 300°F, with longer time at lower temperature
required. The material is easy to work with and can be used in a variety of applica-
tions. This material should not be staged.

SP-8030-96 (Heavyweight silica fabric phenolic produced by Armour Coated
Products). - This material is very easy to handle. Since it is a heavyweight fabric,
a fast thickness buildup is obtained during tape wrapping operations. A low amount
of heat is necessary to obtain proper tack during wrapping. Wrapping itself can be
performed at a high rate. The fabric tends to smooth out minor distortions during
wrapping, resulting in parts free from wrinkles, creases, or folds. If more than
one thickness is to be wrapped, each wrap should be debulked prior to addition of
the next wrap. Thick parts should be debulked and staged before final cure. During
cure, rate of heat rise is relatively unimportant, but rate of cooldown is critical.
Full pressure should be maintained on the part throughout cooldown, and the rate of
cooldown should not exceed 0.75°F per minute. The part should be cooled to a uniform
temperature of 160°F or lower before pressure is released. Once this temperature
is reached, the part may be removed from the mandrel or mold. It was further
found that a curing pressure of 225 psi (autoclave) yields completely satisfactory
results with this material.

SP-8050 (Carbon fabric phenolic produced by Armour Coated Products),
MX-4926 (Carbon fabric phenolic produced by Fiberite Corp), WB-8217 (Carbon
fabric phenolic produced by Western Backing). - These materials are all standard
carbon cloth phenolic materials and as such were handled in the conventional manner,
with the exception that an autoclave pressure of 225 psi produced entirely acceptable
parts with all three materials and, consequently, was used. The materials all
handled well as would be expected of fully developed materials.

SP-8057 (Pluton H-1 fabric phenolic produced by Armour Coated Products). - This material presented no fabrication difficulties. Having a resin content in excess of 50 percent, it requires moderate to high preheating when tape wrapped. The square weave of the fabric suggested that tape under tension might neck down during wrapping operations. Consequently, little or no tape tension was employed with completely satisfactory results. The material lends itself well to autoclave cure operations, requiring only 225 psi curing pressure to produce good, uniform parts. Staging of a part made of this material prior to actual cure is desirable. As with most tape wrapped parts, complete cooldown under pressure is also advisable.

4C-1686 (Carbon fabric polyphenylene produced by Coast Mfg & Supply). - No major fabrication problems were encountered with this material. Tack was somewhat difficult to obtain when tape wrapping, but application of moderate preheat temperature and high roller head pressure combined to provide adequate results. This material, with a polyphenylene resin system, must be cured half again longer at a cure temperature of 350°F than a comparable phenolic part. On the other hand, a cure pressure of only 225 psi produces entirely satisfactory parts.

23-RPD (Asbestos/cork phenolic produced by Raybestos-Manhattan). - Some fabrication difficulties were encountered with this material, due in some part to a Thiokol tendency to consistently underestimate the extremely high bulk factor of the material. It was determined that a tape wrapped part wrapped under a 250 lb/in. width head pressure will compress 20 percent in thickness during cure at 225 psi. However, if this factor is fully taken into consideration, fabrication of parts is simplified. This material also seems to be plagued by high volatiles, causing a lack of tack during wrapping. The best solution found for this difficulty was to apply a relatively high preheat during wrapping, followed by an immediate and thorough chill after application to the part being fabricated. This material will also cure adequately in an autoclave at 225 psi.

FM-5272 (Crepe paper phenolic produced by U. S. Polymeric, Inc). - This material was noted for its almost complete lack of tack during tape wrapping. All attempts to improve tacking qualities were unsuccessful. The most satisfactory method developed for wrapping this material was to use high preheat temperature, apply maximum head pressure, and maintain the wrapped part at a relatively high temperature. It was also expedient to vacuum bag and cure the wrapped component immediately following the wrap to prevent ply slippage. Autoclave curing this material at 225 psi is highly successful. Finished parts are entirely satisfactory. A part fabricated from this material must be removed from the mandrel while hot (180° to 200°F) to prevent freezing to the mandrel or cracking of the part. This is basically a good material from a handling standpoint, especially if the lack of tack poses no problems.

KF-418 (Canvas fabric phenolic produced by Fiberite Corp). - No problems were encountered with this material. It is easily fabricated into a wide variety of parts. No special treatment of the material is required and it can be successfully

cured at autoclave pressures. During tape wrapping, it should be moderately pre-
heated to achieve good tack and, after cure, it should be cooled to 160°F or lower
under pressure.

MXA-6012 (Crocidolite asbestos phenolic produced by Fiberite Corp). - This
material, basically an asbestos mat, handles well and presents no fabrication diffi-
culties. Only a slight amount of preheating is required to produce good tack. Use
of high head pressure when wrapping will effectively debulk the material, which can
subsequently be satisfactorily cured at autoclave pressures. A tendency towards
delamination can be effectively countered by extensive staging at 180°F and a gradual
heatup to cure temperature. Cooldown should be under pressure until the part
temperature reached 160°F or lower.

MXS-198 (Silica fabric epoxy novolac produced by Fiberite Corp). - This
material handled well during component fabrication. Little or no preheating of the
tape is required since sufficient tack is reached when the material is warmed to
room temperature. Curing is effected with only vacuum bag (1 atmosphere) pressure.
Staging of this material is unnecessary. It was further determined that a heavyweight
fabric should not be used with the epoxy novolac resin system since an insufficient
degree of flow seems to result, causing a tendency towards delaminations. Parts
fabricated of this material require a longer time at cure temperature than phenolic
materials in similar parts. As with most materials, parts fabricated of this material
should also be cooled to at least 160°F under pressure.

MATERIAL PERFORMANCE AND PREDICTION - 260 IN. NOZZLE

The purpose of the material performance and prediction study was to provide designs and component weight information for four 260 in. low cost material nozzles. A summary of this work is discussed briefly.

Fourteen subscale nozzle materials (LCCM-2626X included) were evaluated at different nozzle areas and rated by erosion/char and density. A material matrix for four 260 in. booster nozzles was formed from the best ranked subscale materials.

In addition, the erosion and char rates developed for 14 subscale nozzle materials were plotted against subscale nozzle wall convective heat transfer coefficient (carbon materials) and subscale nozzle wall total heat flux (canvas, paper, silica, and asbestos materials). Material design lines were drawn through the plotted erosion/char data for all materials.

A nozzle design computer program is used to produce a standard material nozzle design (carbon and silica cloth) including a design drawing, erosion/char rates, and a weight summary for a 260 in. solid rocket. The nozzle internal wall shape was produced from a standard nozzle computer input design criteria. An aerodynamic flow analysis computer program (see Appendix A) using the 260 in. grain, closure, and nozzle wall configuration computes the nozzle wall convective heat transfer coefficient and total heat flux. Entering the subscale material performance graphs with the 260 in. nozzle wall (h/cp) and (Q_T) values, the erosion/char performance prediction was readout for each of the four nozzle materials matrices.

From this standard material nozzle design base, optional input low cost material erosion/char scaling factors or rates were substituted for standard materials and erosion/char rates to produce four new low cost material nozzle designs and weight summaries.

An outline of the material performance and prediction effort is shown in Table 54.

Preliminary material selection - ablative materials. - Fourteen tested subscale nozzle materials were evaluated at different nozzle areas. The materials with erosion/char rates at selected stations in the six nozzle material areas are shown in Table 55. Two materials, SP-8057 (carbon) and SP-8030 (silica), were tested extensively in the subscale nozzles because of the low material cost and dependable TU-622 test data. The erosion/char rates are shown in Table 55 for two or three stations within each nozzle material area.

For each subscale nozzle area four to six different materials were ranked by a cost material rating (CMR) equation. The equation costs out the amount of erosion/char each material exhibits during static test.
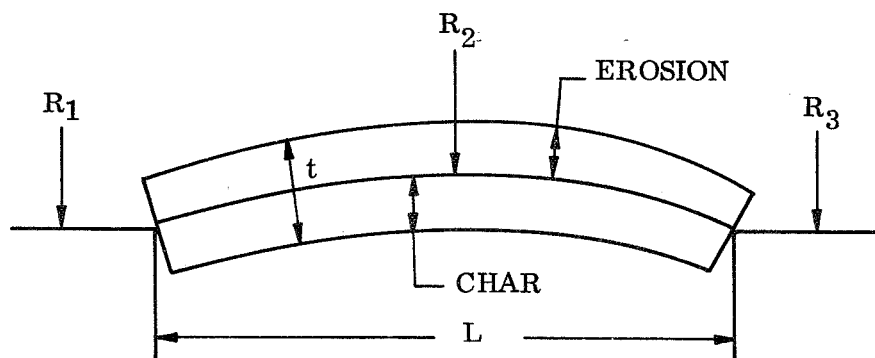
Material erosion/char cost $= 2\pi\, R\, tL\, \rho$ ($/lb)　　　　　　　(1)

$$R = \frac{R_1 + R_2 + R_3}{3} = R_{avg}$$

t of erosion and char $=$ [(erosion rate) (FS) + (char rate) (FS)] time motor operation

FS $=$ material factor of safety for nozzle design

$/lb $=$ dollars/pound raw material cost

ρ $=$ (specific gravity)

t $=$ char and erosion thickness

L $=$ component length

For each nozzle area material evaluation, R, time and L are considered constant. The material factors of safety vary from 1.0 to 1.5, depending on the nozzle area location. The final cost material rating (CMR) equation after substitution of (t) into equation (1) and replacing 2π, R and L with a constant (1.0) is:

Cost material rating $=$ [erosion rate (FS) + char rate (FS)] ρ ($/lb)　　(2)

The CMR index for each material in each nozzle area decides the best material and runners-up. The erosion and char rate factors of safety are also identified. The average corrected subscale erosion rate is an average of the two or three values listed in Tables 56 to 61 for each subscale nozzle area and corrected to the standard throat size, pressure and web time, e.g., Nozzle No. 1: $D_t = 8.12$ in., average web pressure = 471 psi, web time = 56.8 seconds.

77

The erosion rate is corrected to the standard conditions by the formula:

$$\text{corrected erosion rate for standard conditions} = \text{uncorrected erosion rate} \left(\frac{\left(\dfrac{p_s}{1,000}\right)^{1/1.25}}{\left(\dfrac{p^1}{1,000}\right)^{1/1.25}} \right)$$

p_s = 471 psia = standard motor pressure

p^1 = psia = motor pressure of uncorrected erosion rate

The char rate is corrected to the standard conditions by the formula:

$$\text{corrected char rate for standard conditions} = \text{uncorrected char rate} \left(\frac{(t_s)^{1/1.47}}{(t^1)^{1/1.47}} \right)$$

t_s = 56.8 sec = standard motor web time

t^1 = sec = motor web time of uncorrected char rate

The lowest CMR index number indicates the best material. The erosion/char design factors of safety are included to simulate a real design application of the material. The factor of safety for the six nozzle areas is as shown.

	FS Erosion	FS Char
Submerged liner	1.25	1.50
Nose	1.375	1.00
Inlet	1.50	1.00
Throat	1.50	1.00
Forward exit	1.25	1.00
Aft exit	1.25	1.00

For each subscale nozzle ablative liner area, the recommended materials (Table 51) are cost-effective rated by equation (2) as shown in Tables 56 thru 61. The material with the lowest CMR equation number is the most cost effective material.

The most cost effective material for each subscale nozzle area (Tables 56 to 61) is shown below.

Submerged liner	FM-5272 paper
Nose	KF-418 canvas
Inlet	LCCM-2626 graphite particle
Throat	LCCM-2626 graphite particle
Forward exit cone	KF-418 canvas
Aft exit cone	KF-418 canvas

The first through fourth cost effective ranking of materials were evaluated in the various nozzle areas where listed as shown in Table 62. In the case of the forward exit cone, only three qualified materials were available to be ranked.

A 260 in. diameter four nozzle material matrix was developed (Table 63). Nozzle No. 1 included all the standard (Nomad program) materials tested in subscale Nozzle No. 1. The next three low cost material nozzles, 2 thru 4, include as many of the first through fourth ranked materials as possible not used in Nozzle No. 1.

<u>Preliminary material selection - insulative backup materials.</u> - The five low cost backup insulation materials recommended for preliminary material selection were MXB-6001-1581 glass phenolic, KF-418 canvas phenolic, 23-RPD asbestos-cork phenolic, SP-8030-96 silica phenolic, and MXA-6012 asbestos phenolic (Table 51).

For each nozzle insulative area, i.e., throat/inlet backup and exit cone backup, the five materials were evaluated by a cost rating equation as defined below.
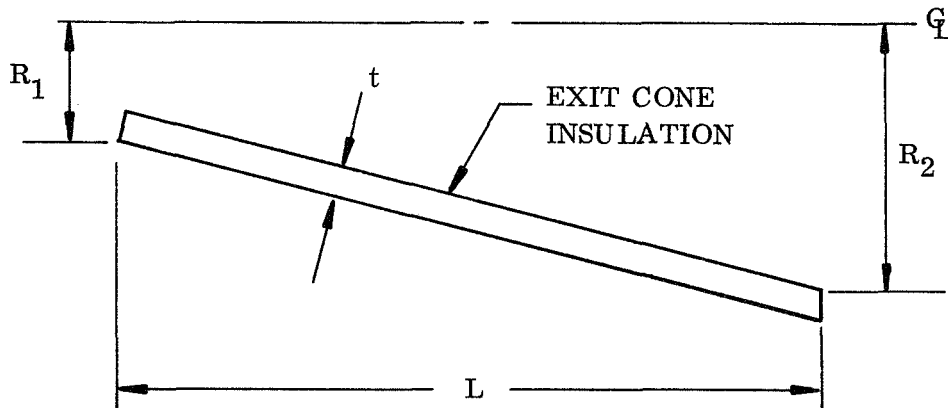
Cost rating equation = $2 \pi R_{avg} t L$ (lb/cu in.) ($/lb)

The cost rating (CR) equation includes material density, raw material cost per pound, and the component physical dimensions. Assuming that the length (L), thickness (t), 2π and average radius (R_{avg}) remain constant, the CR equation reduces to:

Cost rating equation = (lb/cu in.) ($/lb)

79

The backup material with the lowest numerical cost rating was the selected material. A chart of the materials cost rating for the exit cone and the inlet/throat backup insulation is given in Table 64.

The best material for both insulative areas is KF-418 canvas phenolic closely followed by the MXA-6012 asbestos. The FM-5272 paper cost rating is shown but not ranked because the material as an insulative liner was rated only adequate from a performance standpoint.

Based on the above evaluation the following 260 in. motor low cost insulative materials matrix was developed for four nozzles. In the throat and inlet areas of Nozzle No. 1, two commonly used standard materials, MXB-6001 glass and MX-2600 silica, were added to the matrix.
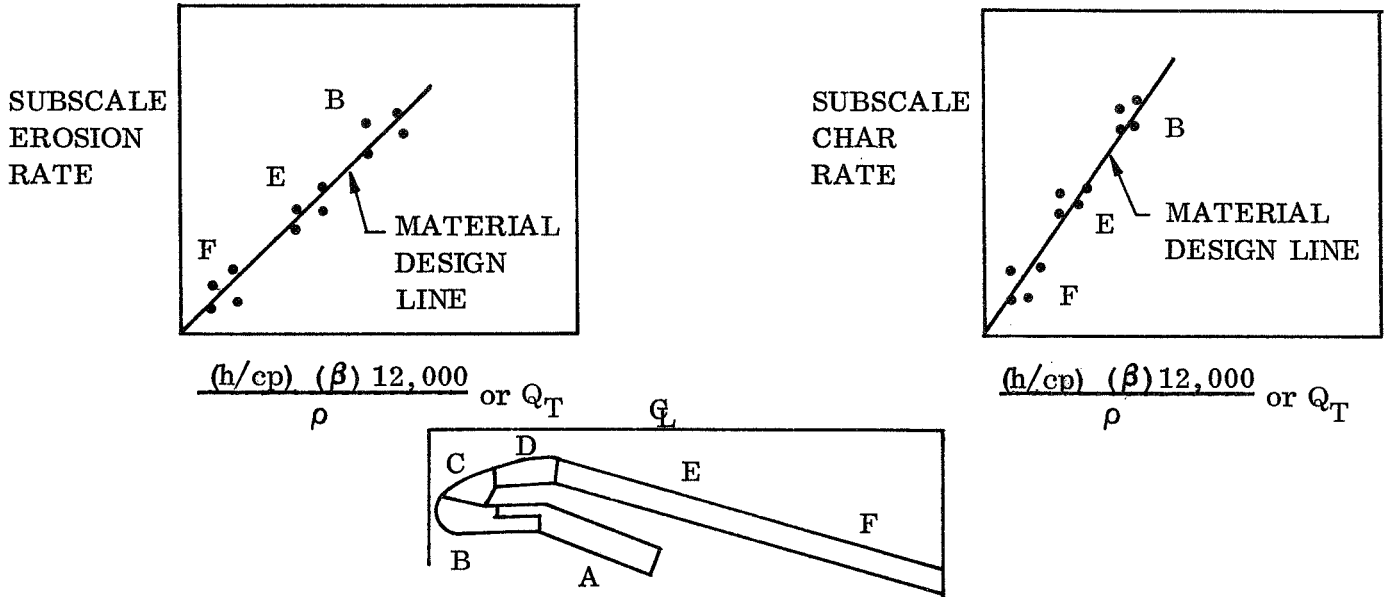
| Low Cost | Insulative Nozzle Areas | | |
Material Nozzle	Inlet	Throat	Exit Cone
1	MXB-6001 glass	MX-2600 silica	MXB-6001 glass
2	KF-418 canvas	KF-418 canvas	KF-418 canvas
3	KF-418 canvas	KF-418 canvas	KF-418 canvas
4	KF-418 canvas	KF-418 canvas	KF-418 canvas

Material Performance Prediction

Thirteen of the 14 tested subscale materials were applied to 36 nozzle ablative areas (six tests multiplied by six nozzle liner areas). The erosion char rates were determined for each of the 36 nozzle material areas and tabulated in the subscale post-test analyses. An aerodynamic flow analysis established the subscale nozzle wall liner convective heat transfer coefficient (h/cp) for carbonaceous materials and the wall total heat flux (Q_T) for silica asbestos, canvas, and paper in the subscale nozzle material performance prediction (Figures 141 thru 144).
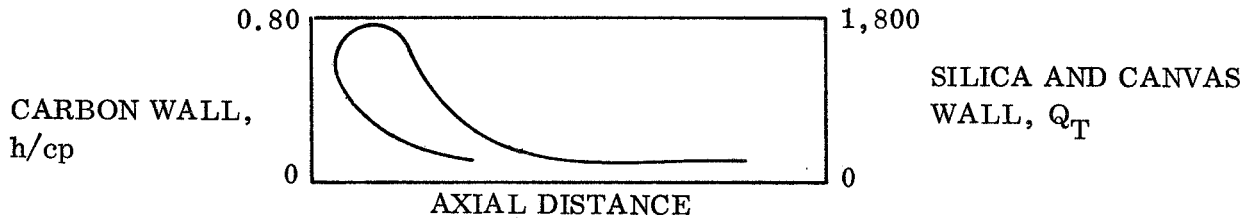
In a material performance graph, the erosion and char rates for each material were plotted versus $\dfrac{(h/cp\ (B)\ 12,000)}{\rho}$ or Q_T and marked for nozzle area location. The resulting data points were then connected by a material design line for use in predicting performance for the full scale 260 in. nozzle as shown below.

SUBSCALE
EROSION
RATE

B

E

F

MATERIAL
DESIGN
LINE

$$\frac{(h/cp)\ (\beta)\ 12{,}000}{\rho}\ \text{or}\ Q_T$$

SUBSCALE
CHAR
RATE

B

E

F

MATERIAL
DESIGN LINE

$$\frac{(h/cp)\ (\beta)\ 12{,}000}{\rho}\ \text{or}\ Q_T$$

C D

E

F

B

A

ρ = MATERIAL DENSITY

β = BLOWING COEFFICIENT OF THE EXHAUST GAS

0.80

1,800

CARBON WALL,
h/cp

SILICA AND CANVAS
WALL, Q_T

0

0

AXIAL DISTANCE

Material I, for example, was tested in the subscale nozzle at the nose Ⓑ , forward exit Ⓔ , and aft exit Ⓕ . The measured erosion/char rates at these nozzle areas are plotted versus the wall h/cp or Q_T. The plotted data are grouped together and defined as Ⓕ aft exit, Ⓔ forward exit, and Ⓑ nose. The connecting line between data groups is called a material design line for predicting erosion rates and char rates of the 260 in. nozzle.

The following 13 materials were graphed and material design lines drawn (Figures 221 to 244). The 14th material, LCCM-2626X, was not plotted.

Carbonaceous	Cellulosic	Silica	Asbestos
LCCM-2626	KF-418	SP-8030-96	23-RPD
LCCM-4120	FM-5272	MXS-198	MXA-6012
SP-8057	--	--	--
4C-1686	--	--	--
SP-8050	--	--	--
WB-8217	--	--	--
MX-4926	--	--	--

The carbonaceous material erosion and char graphs show three design lines: (1) the theoretical, (2) the TU-622 design line, and (3) the subscale design line. If the material was not tested in the TU-622, this line is not shown. The char graphs show only the subscale data line. The theoretical curve is when the erosion rate equals the h/cp (B) 12,000/p factor. No char graphs are shown for LCCM-2626 and LCCM-4120 because no char was visible.

The noncarbonaceous material erosion graphs show only: (1) the TU-622 design line, and (2) the subscale design line. If the material was not tested in the TU-622, this line is not shown. The char graphs show only the subscale data line.

The canvas KF-418, paper FM-5272, and silica MXS-198 erosion and char performance curves have two material subscale design lines. These two design lines reflect different erosion/char rates at the same total heat flux (Q_T) in different nozzle area locations like (D) submerged liner and (E) forward exit cone for KF-418 canvas.

The erosion/char rate is defined as indicated below for the char performance curves:
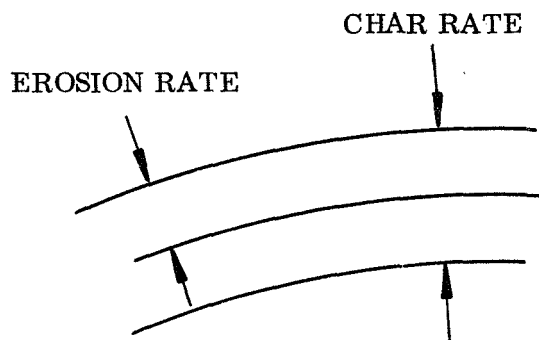
A review of the material performance curves for the 13 materials indicates several general statements.

1. For seven carbonaceous materials

    a. Three materials, SP-8050, WB-8217, and MX-4926 (carbons), subscale design erosion lines in good agreement with theoretical erosion design line

    b. Three materials, LCCM-2626 (graphite particle phenolic) and SP-8057, 4C-1686 (carbons) subscale design erosion lines were above the theoretical and TU-622 erosion design lines

    c. One material, LCCM-4120, subscale design erosion line was below TU-622 and theoretical erosion design lines

d. Char subscale design line for five materials (4C-1686, MX-4926, WB-8217, SP-8050, and SP-8057 carbons) shows a nonuniform line (nose char rate approaches throat char rate)

e. LCCM family (LCCM-2626, LCCM-4120) showed no visible char line but TU-622 char rate used for design approximations

f. Three materials had no TU-622 erosion design lines (SP-8050, WB-8217, and MX-4926 carbons)

2. For six low or noncarbonaceous materials

a. Three materials had no TU-622 design line comparison (KF-418 canvas, FM-5272 paper, and MXA-6012 asbestos)

b. Three materials had TU-622 erosion design lines (23-RPD, MXS-198, SP-8030-96); two subscale design lines (SP-8030-96 silica and MXS-198 silica) had higher subscale erosion design lines than TU-622 erosion design lines and one subscale material (23-RPD asbestos) had a subscale erosion line on top of TU-622 erosion design line

c. Three materials (KF-418, FM-5272, SP-8030-96) were tested in many different nozzle areas; two materials (KF-418, FM-5272) had a two level erosion and char design lines; higher erosion/char line for the nose, throat, and forward exit cone; lower erosion/char line for the submerged liner, part of nose, inlet, and aft exit

d. Subscale erosion/char design lines were uniform except for MXS-198 char line and KF-418 char line

Preliminary Design by Computer

A computer program has been developed by Thiokol and AFRPL that processes the input nozzle and motor design criteria. The output includes nozzle and material components weights, moments of inertia, thicknesses, and a nozzle drawing.

The computer program capability includes the design of both external and submerged nozzles, either of which can be fixed or movable. The movable nozzles can have the splitline in the supersonic region, the subsonic region, or on the chamber side of a submerged nozzle.

The nozzle can be designed without TVC, or for any of seven TVC types: (1) liquid injection, (2) hot gas injection (submerged or external injectors), (3) jet tab, (4) gimbal ring, solid or hollow, (5) hinged (four-nozzle motor), (6) ball and socket (omnivector), forward, center, or aft pivoted, or (7) flexible seal, forward or aft pivoted.

Preselected stored data applicable to as wide a range of designs as practical are stored in the program so they can be utilized with a minimum of input. In addition to specifying the type of nozzle and TVC system desired, the user need input only the following additional information to generate a rough order of magnitude design: (1) thrust vs time, (2) throat size, (3) expansion ratio, (4) firing duration, and (5) average chamber pressure.

For more exacting work, such as matching an existing design for subsequent parametric studies, several hundred items of optional input are available (such as material choices) which override the prestored values.

The program parallels the usual six step process followed by a designer: criteria, aerodynamic, thermal, and mechanical design, design modification, and final design (Figure 245).

Step 1. - Input nozzle and motor design criteria.

Step 2. - The aerodynamic configuration is calculated to fit the available envelope. Either a conical or contoured exit is calculated, as requested. Contoured exit envelope and thrust coefficients identical to those of a method of characteristics contour are calculated in a fraction of the time required for a characteristics net. The submerged nozzle entry (nose) is elliptical.

Step 3. - The liner required to withstand erosion and char and the backup insulation required to prevent heating of the structure are calculated in seven separate nozzle insulation sections. A different liner and backup material can be specified for each section. Erosion is calculated semi-empirically; char is calculated at 20 locations by the corrosion analogy. Erosion and char depth are calculated at 20 locations

84

in the nozzle to size insulation accurately. A different factor of safety can be applied in each insulation section.

Step 4. - The geometry of the rings and shells forming the nozzle structure is calculated, and if the nozzle is movable, the components which provide for nozzle motion are designed. A different material can be specified for each component, and individual factors of safety can be imposed. Structural components are designed individually by application of stress, deflection, and buckling criteria.

Step 5. - In response to console command, the nozzle input and output data, plus the computed designed nozzle, appear on a TV screen on the IBM-360 computer graphic display. The nozzle design can be changed on the computer graphics console by revising the input data by light pen and typewriter (Figure 246).

Step 6. - The final nozzle design output is printed by the IBM-360 data plotter (Figure 247) after completion of the design in Step 5 along with the output data sheets (Tables 65 thru 67). The output data sheets include nozzle and material component thickness, weight, center-of-gravity, and moment of inertia.

The standard baseline 260 in. nozzle as shown in Figure 247 uses standard materials MX-2600 silica and MX-4926 carbon for the six nozzle areas:

Submerged liner - MX-2600 silica
Nose   - MX-4926 carbon
Inlet   - MX-4926
Throat   - MX-4926
Forward exit   - MX-4926
Aft exit   - MX-2600

The standard nozzle was designed to the following design criteria:

Throat D_T = 89.1 in.
Exit cone half angle = 17.5 deg
Exit cone expansion = 11.00 in.
Inlet expansion = 2.16 in.

With the shape of the 260 in. standard nozzle defined by Figure 247, an aerodynamic flow analysis was completed as outlined in the Flow Field Calculations section of Appendix A. The flow analysis showed the convective heat transfer coefficient vs axial nozzle station for carbonaceous wall materials and the total heat flux vs axial nozzle station for asbestos, silica and paper-canvas wall materials. The resulting graphs are shown in Figures 248 thru 251. The six areas of the nozzle are defined on each graph for ① submerged nozzle, ② nose, ③ inlet, ④ throat, ⑤ forward exit, and ⑥ aft exit.

To computer design the four low cost nozzles, the selected materials at each nozzle area had an erosion and char rate calculated as shown in Table 68. An example of how the erosion/char rate was calculated is shown in Steps A, B, and C for a canvas cloth KF-418 nose.

Step A. - The minimum-maximum range of the total heat flux for a canvas nose wall was shown below to be 920 aft nose to 2,160 forward nose Btu/sq ft-sec using Figure 251.

STEP A
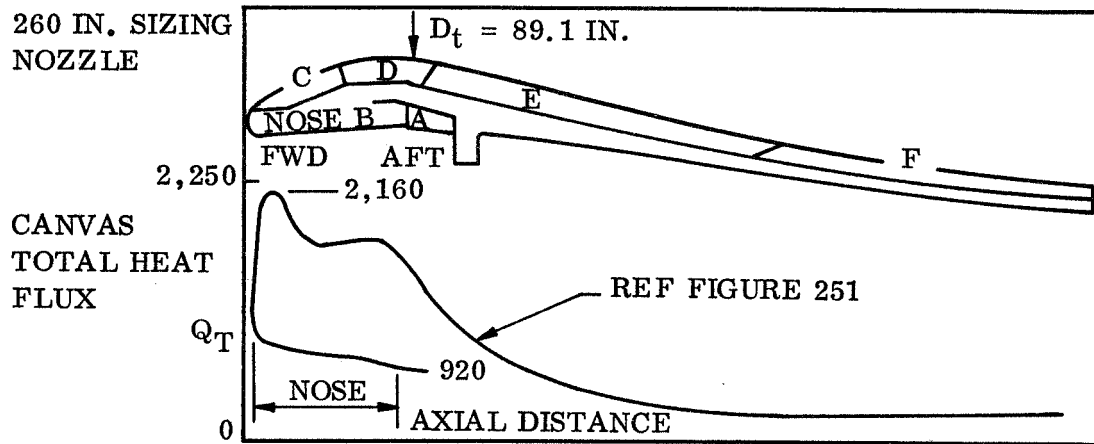
Step B. - Enter the KF-418 material erosion performance curve with the maximum total heat flux at forward nose. The KF-418 material erosion curve is shown in Figure 233. Line ① of the graph below is used for the forward nose Ⓑ and forward exit cone Ⓔ . Line ② of the graph is used for the aft nose Ⓑ , aft exit Ⓕ and submerged liner Ⓐ . The intersection of the vertical line (Q_T = 2, 160) with line ① gives a horizontal reading of erosion rate = 37 mil/sec.

STEP B   KF-418 MATERIAL PERFORMANCE

86
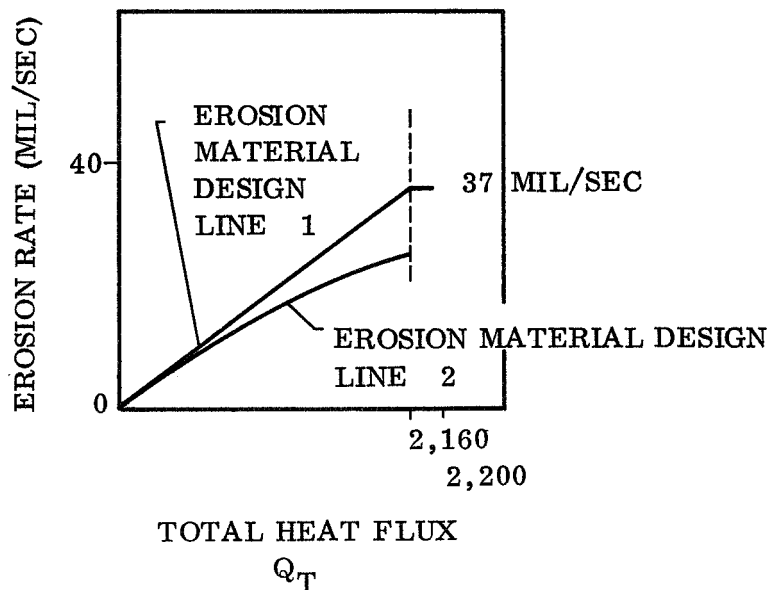
Step C. - Enter the KF-418 material char performance curve (Ref Figure 234) with the maximum total heat flux at the forward nose. Line ① of the graph is used for the forward nose Ⓑ and forward exit cone Ⓔ . Line ② of the graph is used for the aft nose Ⓑ , aft exit Ⓕ , and the submerged liner Ⓐ . The intersection of the vertical line (Q_T = 2, 160) with line ① gives a horizontal char rate reading of 40. 7 mil/sec as shown below:

KF-418 MATERIAL PERFORMANCE

STEP C
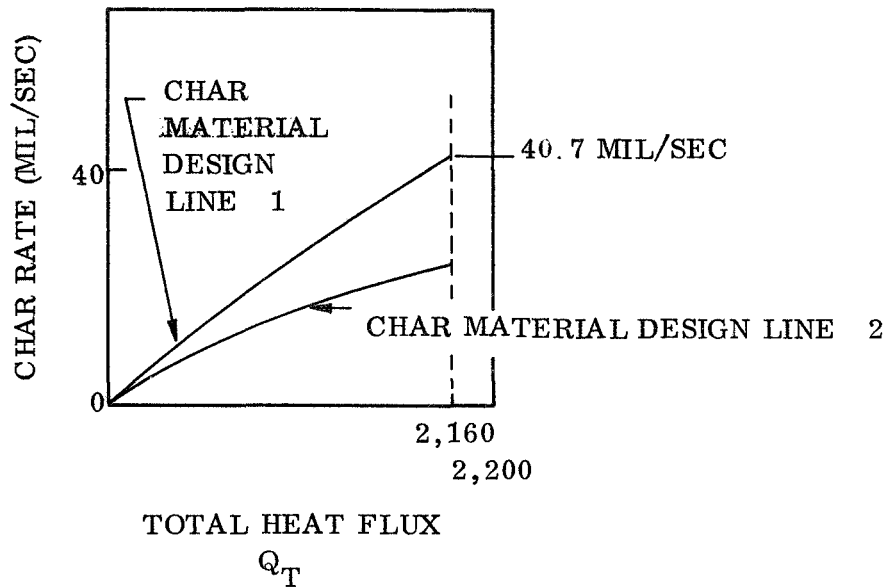
Thus at the forward nose location, the predicted nose erosion and char rate is shown by the sketch:

KF-418 NOSE
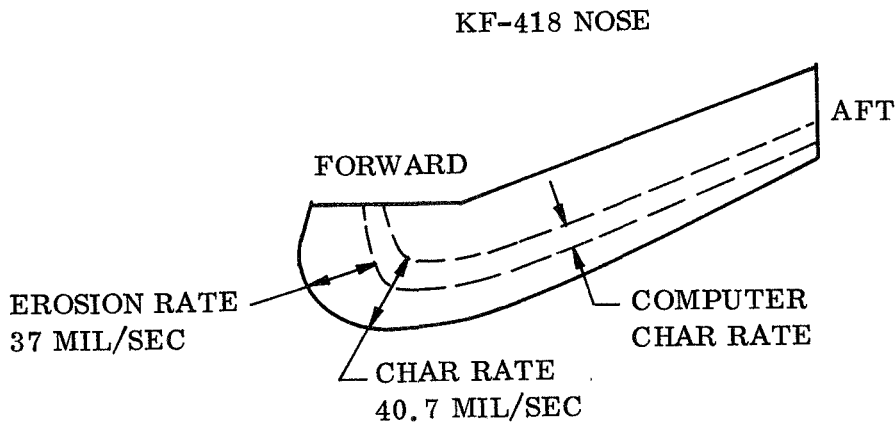
This same procedure is repeated for each material as applied to the six nozzle areas. Table 68 shows the low cost material erosion/char rate performance in each of the nozzle areas. The canvas KF-418 erosion and char rates are shown under nose column as 37.0 and 3.7 mil/sec. The computer design program defines char rate as the thickness of the final char layer, thus the computer char rate of 40.7-37.0 = 3.7 mil/sec. The materials shown in Table 68 are the same materials chosen for the four-nozzle ablative material matrix.

The standard 260 in. nozzle input data are changed to reflect the new materials, erosion/char rates and densities for each low cost material nozzle, 1 thru 4.

The nozzle computer design output shows the four low cost nozzles drawn to 1/5 scale in Figures 252 thru 255. The internal wall geometry, length, and flange location are exactly the same as on the standard 260 in. nozzle. The only changes are the increased wall thicknesses which reflect larger outside diameters over the entire length of the nozzle. The computer program output includes, in addition to the nozzle drawing, a nozzle and material weight, moments of inertia, and liner thickness.

The nozzle and material component weights are summarized in Table 69 for the standard baseline 260 in. nozzle and for the four low cost material 260 in. nozzle designs. The location of the structure and liner components is shown in Figure 247 for the standard 260 in. nozzle design. The standard nozzle is the lightest nozzle design at 32,875 lb. The steel weight remains fairly constant between 9,353 lb (standard nozzle) and 9,635 lb (low cost material Nozzle No. 3). The liner weight variations are the reason for the total weight difference between the standard nozzle at 32,875 lb and the heaviest low cost Nozzle No. 3 at 44,004 lb.

COST/PERFORMANCE EFFECTIVENESS STUDIES

The five full scale nozzle assemblies designed and analyzed in the Materials Performance and Prediction, 260 Inch Nozzle phase of this program, were also submitted to a cost performance effectiveness study. As discussed in the preceding section of the report, the nozzles under consideration consist of:

1. Standard baseline nozzle. This nozzle design utilizes conventional standard materials that have been commonly used as ablative liners and insulative materials in large solid propellant rocket motor nozzles in the past. MX-4926, carbon cloth phenolic, was used in the nozzle, nose, inlet, throat, and forward exit cone. MX-2600, silica cloth phenolic, was used in the submerged OD liner, aft exit cone, and as a throat backup material. MXB-6001, glass phenolic, was used as backup insulation in the inlet, throat, and exit cone. Hydroclave pressure cure was considered in the component manufacturing process.

2. Nozzle No. 1. This nozzle design utilizes the ablative liner materials that were selected from the Nomad program by NASA/Thiokol to establish a performance baseline for the Subscale Nozzle Material Evaluation phase of this program. The design, by definition, is not considered a low cost material nozzle. In general, standard family ablative liner materials were used. Carbon cloth phenolic materials, WB-8217, MX-4926, and SP-8050, were used in the nose, inlet, throat, and forward exit cone. However, a deviation to the typical large nozzle design was the use of a paper phenolic (FM-5272) in the submerged OD liner and a canvas phenolic (KF-418) in the aft exit cone areas. Silica and glass phenolic materials (MX-2600, MXB-6001) were used as insulative backup materials. Autoclave pressure cure was considered in the component manufacturing process.

3. Nozzles No. 2, 3 and 4. These nozzles, referred to as low cost material nozzles, utilized materials that are not commonly used in typical standard large nozzle designs. Canvas and asbestos phenolic materials were used in the submerged OD liners. Canvas, paper, and high resin content carbon phenolic materials were used in the nose. Silica, high resin content carbon, and low cost graphite particle phenolic materials were used in the inlets of the nozzles. The throats included low cost graphite particle, silica, and carbon phenolic materials. High resin

content carbon, canvas, and carbon phenolic materials were
used in the forward exit cone area. The nozzle aft exit cones
utilized low cost graphite particle phenolic, paper phenolic, and
silica epoxy novolac materials.

A complete cost and weight breakdown of each nozzle assembly was developed
(Tables 71 thru 80). Table 70 summarizes this breakdown and includes a cost/
performance index (CPI) calculated for each nozzle from a formula derived for this
purpose in an effort to comparatively rate the nozzle assemblies.

All pertinent factors concerning the cost and performance of nozzles were
incorporated into this formula, which can be simply expressed by:

$$CPI = (cost) \, K_1 + (weight) \, K_2.$$

Further definitions of the factors involved in this formula are as follows:

1. Cost = materials cost + tooling cost + facilities cost
   + labor cost + burden.

   Materials cost = ($/lb x density) (volume of part + volume
   of scrap).

   Tooling cost = cost of tooling per nozzle amortized over
   six nozzles per year for 5 yr.

   Facilities cost = cost of fabrication facility + cost of cure
   facility amortized over six nozzles per
   year for 5 yr.

   Labor cost = $/hr x total hours required for fabrication
   of nozzle.

   Burden = division general + corporate G & A + fee.

2. Weight = total net weight of completed nozzle assembly.

The cost breakdown is, of course, self-explanatory. Performance data are
included in the weight figure since the design of the four nozzles was based upon
performance data input to the computer, and the resulting net weight of the nozzles
reflects the optimization of these data.

In determination of values for the constants K_1 and K_2, the standard com-
puter output nozzle was used as a baseline. Employing the computer design of this
nozzle, cost and weight factors were determined (Table 72). Using these factors,
the constants were then calculated in the following manner:

$$CPI = (cost) \, K_1 + (weight) \, K_2$$

For the baseline nozzle let CPI = 100

Also assume cost to be two times as important as weight,
then, $100 = 66.66 + 33.33$

(Cost) $K_1 = 66.66$

$K_1 = 5.14 \times 10^{-5}$

Cost = $\$1,296,807$

(Weight) $K_2 = 33.33$

$K_2 = 10.1 \times 10^{-4}$

Weight = 32,875 lb

therefore, CPI = (cost) (5.14×10^{-5}) + (weight) (10.1×10^{-4}).

In the derivation of the above formula, the constants K_1 and K_2 were employed to balance the cost and weight factors and to place them in proper perspective to each other. Cost is expressed in millions while weight is in thousands. Without the use of constants to proportion the two factors, the relative value of cost to weight as expressed in the formula would be excessive. In the calculation of K_1 and K_2, the assumption was made that cost was twice as important as weight and the constants were calculated to express this relative importance. It is entirely possible, however, that for a specific application the relative importance between the two factors would be different. In this case, a different set of constants would be determined reflecting this.

The same constant values were then used in the calculation of CPI values for the remaining four nozzles. Those nozzles having CPI values lower than the baseline nozzle value of 100 are theoretically superior to the baseline nozzle. It must be remembered, however, that a simple basic design was employed in the standard nozzle and that each of the four other nozzles represents a direct substitution of a material into the baseline design without regard for possible redesign. Each nozzle could be optimized with resultant weight savings and additional cost savings.

The five full scale nozzle assemblies are ranked below in order of their cost/performance effectiveness:

Rank	Nozzle No.	CPI
1st	2	88.00
2nd	3	88.83
3rd	4	96.38
4th	1	96.39
5th	Standard (baseline)	100.00

91

The most cost/performance effective complete nozzle assembly (Nozzle No. 2) represents a cost savings of 28 percent ($362,835) over the standard baseline nozzle which was estimated at a cost of $1,296,807. This nozzle assembly has a calculated 20.4 percent increase in weight over the standard nozzle weight of 32,875 lb. Nozzle No. 3 is the most cost effective design with a 33.4 percent cost savings over the standard nozzle; whereas, the standard nozzle is the most performance effective design with a weight reduction of 6.6 percent when compared to the next ranked contender, Nozzle No. 1.

However, from a program objective standpoint, a comparison of two cost factors (1) nozzle ablative insulation raw materials and (2) manufacturing process (Tables 71 thru 80) is of more significance than the cost/performance effectiveness comparison which took into consideration a more comprehensive list of nozzle assembly cost and performance factors. A comparison of these two factors shows that materials cost can be reduced by up to 69.8 percent ($241,549) while materials plus processing cost [materials + (labor + facilities + tooling)] can be reduced by up to 42.0 percent ($339,312) depending upon nozzle design selection when compared to the standard nozzle.

Cost Comparison, Materials, and Process

Nozzle No.	Material Cost Reduction (%)	Material + Processing Cost Reduction (%)
Standard (Baseline)	Base	Base
1	+2.6	-10.9
2	-53.5	-35.0
3	-69.8	-42.0
4	+1.9	-11.4

This evaluation was further extended to include an insulation material cost and weight comparison between full scale nozzle factors supplied by NASA-Lewis and this program's computer designed nozzle factors.

By considering the NASA-Lewis supplied 260 in. motor nozzle design factors, i.e., material cost and weight, as the baseline nozzle, rather than the Thiokol computer design, an even greater cost savings in material can be realized depending on design selection.

Comparison, Material Cost and Weight

Nozzle No.	Material Cost ($)	Material Cost Reduction (%)	Material Weight (lb)	Material Weight Change (%)
NASA design	434,490	Base	30,290	Base
Standard	345,184	-20.6	23,523	-22.3
No. 1	354,223	-18.5	25,406	-19.4
No. 2	160,370	-63.0	30,064	-0.7
No. 3	103,635	-76.1	34,369	+13.5
No. 4	351,653	-19.0	25,918	-14.4

Based on the above, disregarding design variations between the NASA-Lewis supplied nozzle and the Thiokol computer design nozzles, it can be concluded that a 76.1 percent cost savings in material is feasible with a 13.5 percent weight penalty through the use of the low cost materials evaluated in this program.

In comparing the NASA nozzle design with the most cost/performance effective computer design nozzle (Nozzle No. 2), a 63.0 percent cost savings can be realized in material cost with a 0.7 percent material weight savings through the use of the low cost materials evaluated in this program. As in the preceding evaluation, design variations were not considered in this comparison.

No attempt was made in this program to produce an optimum design. The four computer designed full scale low cost nozzles presented contain specific materials in specific locations which were actually tested and evaluated in the Sub-scale Nozzle Evaluation phase of this program and are intended to be used as illustrations only and not as optimum designs. A large number of materials were tested in this program and all possible combinations of these materials in various locations should be examined in the derivation of an optimum nozzle design. The locations of component joints or interfaces should also be examined and optimized. For example, the forward exit-aft, exit cone interface was arbitrarily located at a 4:1 expansion ratio in the nozzles tested in this program. It is likely that this could be optimized at 3:1 or even 2:1. Such combinations would result in a very large number of nozzles, many of which would undoubtedly be more cost and performance effective than those employed in this report as illustrations or examples. Such an optimization would be quite involved, however, and was beyond the intent and scope of this program.

SUMMARY OF RESULTS

Introduction

This program involved the development of low cost ablative nozzles for large solid propellant rocket motors, 260 in. in diameter. The general requirements associated with this scope of work involved:

1. Selection of materials through an evaluation of factors affecting the performance of these materials, and selection of nozzle fabrication techniques.

2. Evaluation of the most promising ablative system candidates on subscale motors which closely duplicated the environment imposed by the full scale motor.

3. Performance prediction of candidate materials in a 260 in. diameter rocket motor nozzle design.

Summary

In satisfaction of the program requirements, a comprehensive ablative system evaluation program was conducted. An extensive supplier and thorough survey of literature concerning low cost ablative materials was conducted. This survey encompassed the review and consideration of 43 different materials. Based on this review and subsequent consultation with NASA-Lewis, 21 materials were selected for materials screening and evaluation testing.

Materials screening and evaluation tests consisting of physical and mechanical property testing at temperatures up to 600°F, motor static firing erosion, and char performance tests were conducted. Approximately 54 materials screening motors were static fired, nozzle erosion and char measurements were made, and erosion and char rates were calculated in evaluation of the materials. Ten of the most promising materials were selected for followon evaluation.

In evaluating the most promising materials, ten relatively large material evaluation motor assemblies were manufactured and static fired to ascertain nozzle material erosion and char performance when evaluated in a more severe environment. In addition, thermal properties tests (up to 1,500°F) were performed on five materials, and six materials were exposed to compression tests at temperatures up to 2,000°F.

Six subscale (8 in. diameter throat) nozzles were designed, tested, and evaluated using materials performance data obtained from this program and available data taken from other materials development and evaluation programs. A total of 14 materials were evaluated in 36 nozzle component parts. Low cost nozzle fabrication techniques applicable to full scale nozzle manufacture were employed in the production of the nozzles. In addition, material design curves were developed.

Using the data obtained from the materials evaluated in the subscale nozzle evaluations, four preliminary 260 in. motor nozzle designs were produced, as well as a baseline design consisting of commonly used standard ablative materials. These designs were used in support of a nozzle cost/performance effectiveness study.

Conclusions

Based on the work performed in this program and on the results obtained, a number of significant conclusions may be drawn.

1. Cost savings in nozzle liner and insulative materials of from 69.8 to 76 percent can be realized through the utilization of low cost materials evaluated in this program. Based on a cost comparison between NASA-Lewis supplied nozzle factors and a Thiokol designed nozzle incorporating a combination of low cost materials, a cost savings of 76 percent ($330,855) can be realized. Whereas, a cost savings of 69.8 percent ($241,549) can be achieved by comparing a baseline nozzle design utilizing standard materials with the same design modified to reflect a combination of low cost materials. The use of the base nozzle eliminates design variation effects, thus providing a directly comparable design base for cost comparison.

2. By taking into consideration the cost of fabrication and processing factors as well as liner and insulative backup materials cost, the cost of a 260 in. motor nozzle liner assembly can be reduced by approximately 42 percent ($339,312). By taking into consideration the total nozzle assembly performance effectiveness as well as cost effectiveness, cost can be reduced by approximately 28 percent ($362,835). The above conclusions are based on a comparative examination between the Thiokol 260 in. motor nozzle baseline design using standard conventional materials and the same design modified only through incorporating a combination of low cost materials evaluated in this program.

3. Of the low cost material 260 in. motor nozzles designed in this program, the most cost/performance effective nozzle utilized KF-418 canvas phenolic in the nozzle submerged OD liner and

nose areas, LCCM-2626 in the inlet and throat areas, SP-8057 in the forward exit cone area, and LCCM-4120 in the aft exit cone area.

4. The most cost effective materials, by nozzle area location, evaluated in the six subscale nozzles are FM-5272 paper phenolic - submerged OD liner, KF-418 canvas phenolic - nose, LCCM-2626 graphite particle phenolic - inlet and throat, and KF-418 - forward and aft exit cone. The above evaluation is based on analysis of the subscale nozzle material performance data and the cost of material rating equation that was developed by Thiokol.

5. All materials evaluated as ablative liner components in the six subscale (8 in. diameter throat) nozzles were considered as satisfactory candidates for design evaluation in a 260 in. motor nozzle in the areas in which they were tested with the exception of LCCM-2626X graphite particle phenolic as an exit cone liner and 23-RPD asbestos phenolic as a forward exit cone liner. The above conclusion is based upon the materials erosion/char rate performance, overall structural integrity, and the comparison of actual to predicted erosion rates.

6. A considerable savings in nozzle cost can be realized through selective utilization of ablative materials within the same material family. For example, the carbon cloth phenolic materials evaluated as throat components in the subscale nozzles had a price range of $4/lb whereas the erosive performance of the materials were nearly identical with a calculated erosion rate variance of only 1.69 mil/sec.

7. Low cost reinforced materials such as canvas, paper, and asbestos phenolics can be successfully used as aft exit cone and submerged OD liners in place of the commonly used silica phenolic materials with a resulting cost savings of up to 70 percent.

8. In selective nozzle areas the graphite particle phenolic materials demonstrated erosion resistance equivalent to that of the carbon cloth phenolic materials; however, in general, the performance reproducibility of this material family requires further improvement.

9. Significant cost savings can be realized in the manufacture of large nozzles through the use of several fabrication methods and design advances that were developed and/or verified in the manufacture of the subscale nozzles.

a. With the exception of two materials (LCCM-2626 and LCCM-2626X), it was demonstrated that all phenolic resin system materials evaluated in the subscale nozzles can be satisfactorily cured at a maximum autoclave pressure of 225 psi. The low pressure cure demonstration de-emphasizes the requirement for costly and extensive hydroclave and press facilities, resulting in a substantial cost reduction.

b. Through the successful performance evaluation of nozzle components produced from materials (MXS-198 and MXSC-198) containing the epoxy-novolac resin system and cured under vacuum at 1 atmosphere pressure only, it was demonstrated that the need for large autoclave facilities can be reduced, resulting in additional cost savings.

c. As demonstrated in this program, nozzle components fabricated from a number of smaller segments or "building blocks" assembled together and containing both longitudinal and radial joints perform equally as well as components fabricated as one monolithic piece. When applied to a large nozzle component, this concept becomes economically advantageous since it eliminates the need for very large monolithic components. The smaller segments can be fabricated with the more commonly available facilities, reducing the need for large specialized facilities.

Recommendations

Through the work performed in this program and the conclusions drawn as a result of this work, the following recommendations are in order.

1. Larger nozzles, with a throat diameter in the range of 15 to 20 in., incorporating the better performing materials and processes from this program should be fabricated and evaluated. Such nozzles would adequately evaluate scaleup factors and increase the base of low cost liner material nozzle application data without incurring the very high costs attendant to a full scale nozzle for a 260 in. solid rocket motor.

2. Additional development work should be performed on the low cost graphite particle phenolic materials to lower their density and improve their mechanical properties. Although these materials

generally performed well in this present program, optimization through characterization of the resin, reinforcement, and filler systems may provide materials applicable to all nozzle application areas.

3. A fabrication techniques study should be initiated, in which alternate processing parameters are employed with the materials evaluated in this program, and other forms or combinations of these materials are evaluated. For example, molding compound versions of the tape and broadgoods materials should be evaluated, and reinforcement-resin variations such as canvas-epoxy novolac should also be evaluated. In this manner, each process and material form can be optimized.

4. It is also recommended that additional small material screening motor nozzles be fabricated in which some or all of the components are constructed of segments molded of materials not previously segmented, such as canvas-phenolic or Pluton H-1 epoxy novolac. The concept of segmenting was proven feasible in this current program. It now remains to be optimized through proper material selection and placement.

5. A unique nozzle design study should be conducted that will take maximum advantage of the low cost ablative insulation material and fabrication techniques. The study should take into consideration, for example, a low cost multiple composite reinforced plastic shell that would provide all the required design functions of erosion and thermal barriers, as well as structural support, with the possible exception of a small metal flange.

APPENDIX A

NOZZLE PERFORMANCE PREDICTION

A vital part of the program to develop low cost materials for large nozzles was the development of methods to accurately predict the performance of these materials in the 260 in. motor environment. Reliable techniques are essential for two related applications: (1) prediction of 260 in. performance based on smaller motor performance and (2) prediction of changes in material performance due to changes in motor environment when 260 in. test data become available. Motor environment alteration would result from changes in design pressure, propellant composition, and throat area.

An essentially theoretical technique that was proven accurate is the introduction of empirical data to supplement theory. Other more advanced programs were available, but were not used due to the cost limitations of the program.

This analysis method is described step-by-step in the following pages. An example of the application of the technique to a nozzle tested on a TU-622 motor is described in this appendix and the theoretical performance predictions are compared to the measured data.

The theoretical analysis of the material performance in a nozzle considers the several steps in defining the flow field and the environmental conditions near the wall and the response of the materials to these environments.

This analysis is programed for high speed digital computers in four* of the seven separate steps as shown below.

1. Thermochemical analysis*

2. Nozzle configuration

3. Wall material properties

4. Flow field calculation*

5. Boundary layer*

6. Wall erosion prediction

7. Wall transient temperature*

This method of analysis, while essentially theoretical does provide for the introduction of empirical data (wall erosion prediction) and design information (nozzle configuration and wall material properties) to supplement theory. Each of the analyses steps are discussed and summarized in Figure A-1.

Thermochemical Analysis

From the basic propellant formulations and specified chamber pressure, the equilibrium and/or frozen composition and thermodynamic properties are calculated during gas expansion. The original version of the program in use at Thiokol was based on one by Zeleznik and Gordon described in NASA TND-1454. The analysis is primarily based on satisfying conservation of mass, Dalton's Law of partial pressures, adiabatic combustion, and an isentropic combustion process. The enthalpy, heat of formation, and free energy data are obtained from an up-to-date file of JANAF data. The species system is usually set to allow every gaseous species, including ions if desired, to be in the system of products that are selected from the thermodynamic tape. Gaseous or liquid species are allowed to change phase at their equilibrium temperature.

The output parameters which are subsequently used in the aerothermo analysis are the gas thermodynamic properties, the composition, and the blowing coefficient.

Nozzle Configuration

The nozzle configuration as inlet, throat and exit diameter, inlet ellipse radii and exit cone half angle defines the boundaries for the wall erosion prediction and flow field calculations.

Wall Material Properties

To provide erosion, char and material temperature profiles, the following material properties versus temperature must be provided for all the nozzle liner materials to be used as input for the one-dimensional char and ablation program.

1. Density

2. Specific heat
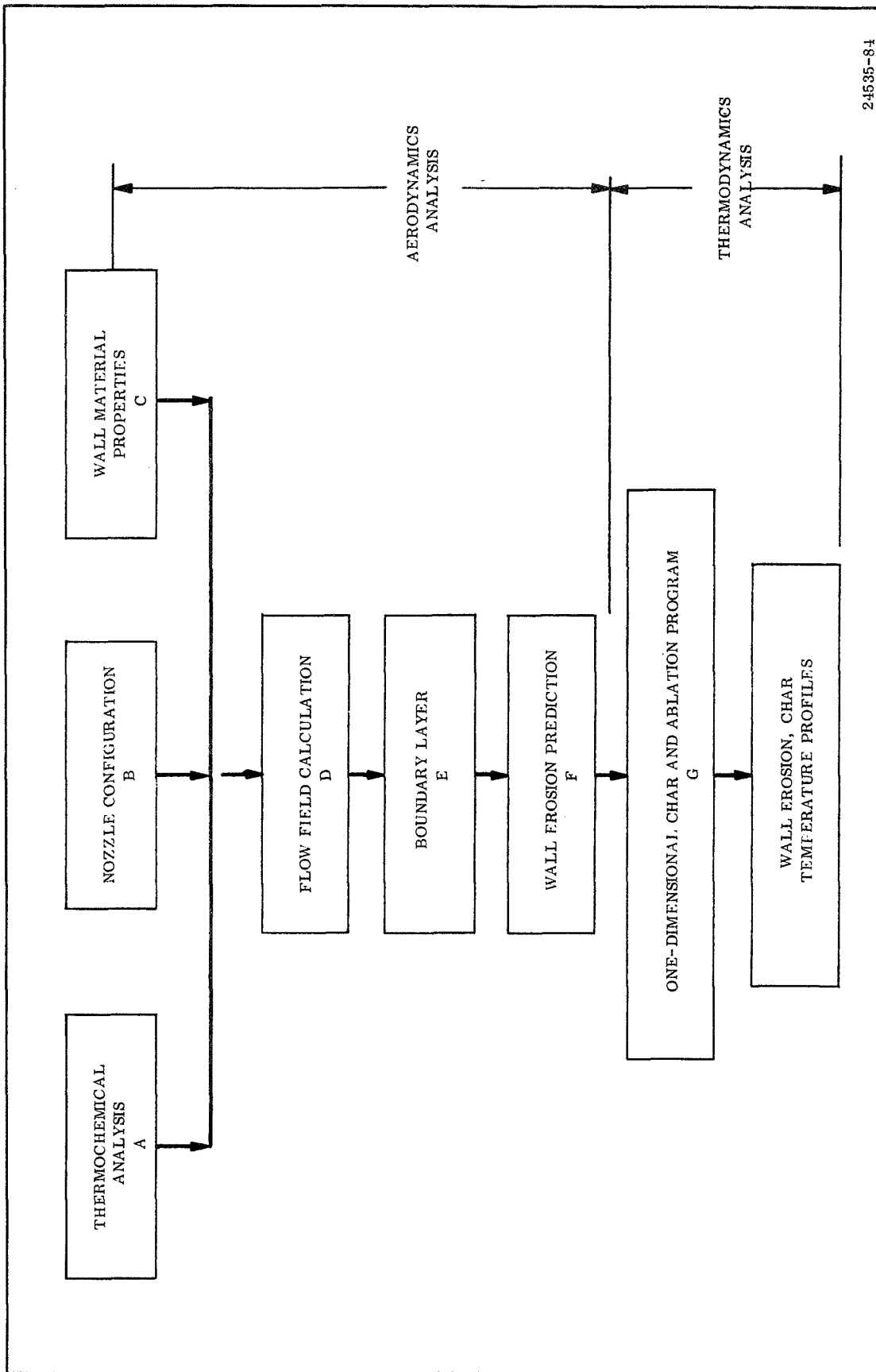
3. Thermal conductivity

4. Emissivity

Figure A-1. Aerothermo Analysis in Wall Material Response Calculations

24535-84

Flow Field Calculation

The flow field is divided into three regimes of subsonic (2 cases) and supersonic flow in calculating the wall flow conditions. The TU-379 and TU-622 external nozzle analysis required only two regimes: subsonic and supersonic. However, the submerged subscale and full scale nozzle analysis required one additional subsonic run for the submerged OD liner surface in a separate flow area.

Subsonic flow regime. - The subsonic flow analysis from the case propellant surfaces to the nozzle throat was defined for the initial uneroded nozzle and unburned propellant surfaces of four motors, TU-379, TU-622, Stage II Minuteman and the 260 in. motor. This detailed flow analysis was conducted using a potential flow solution programed on a digital computer.[a] This program calculates flow streamlines, Mach numbers, static temperatures, and static pressures in an axisymmetric subsonic compressible potential flow field.

The values obtained from this program are valid up to fairly high subsonic Mach numbers (0.8) whereupon the accuracy decreases as it approaches the supersonic condition. The surface of transition (locus of the points at which the Mach number is equal to one) occurs near the geometrical throat and is the division between subsonic and supersonic regimes.
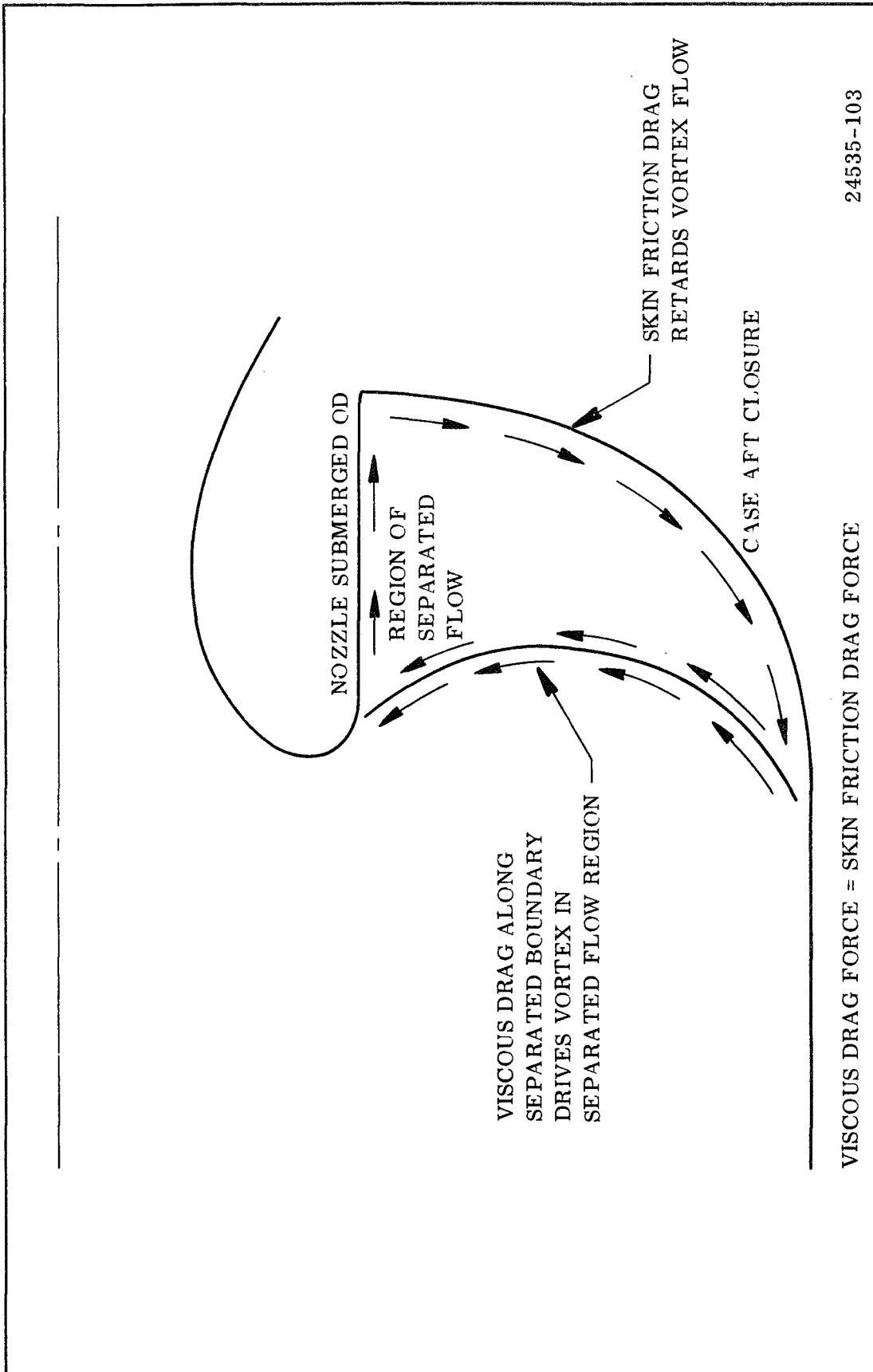
Case aft closure, submerged nozzle backside: The nozzle backside was analyzed at both the initial and post-test conditions. Although the inviscid flow analogy accurately predicts nozzle entrance conditions, this type of analysis is inadequate in the aft case area between the motor case and the backside of the nozzle. Analytical and cold flow studies conducted by the Wasatch Division have indicated this region is a region of separated flow.[b] This becomes a region of separated flow when the grain burns back and the flow deceleration produces a region of separated flow in the large area between the aft case wall and the backside of the nozzle.

Prediction of the flow properties in this separated region was achieved by equating the drag force driving the secondary flow and the wall drag length (momentum balance) as shown in Figure A-2. This relationship defines the velocity on the backside of the nozzle nose. Using the velocities calculated in this manner, the boundary layer and heat transfer coefficients were determined.

The convective heat transfer coefficient from the final separated condition best represents the environment on the backside of the nozzle during motor operation.

---

[a] "Two Dimensional or Axisymmetric Subsonic Flow and Particle Trajectories with Compressibility Improvement," Thiokol Chemical Corporation, Wasatch Division, Program S3241.

[b] "Investigation of Flow in the Aft Case of Motors with Submerged Nozzles," Thiokol Chemical Corporation, Wasatch Division, TWR-1380, 22 Sep 1965.

Figure A-2. Description of Viscous and Skin Friction Drag Parameters

NOZZLE SUBMERGED OD

REGION OF SEPARATED FLOW

SKIN FRICTION DRAG RETARDS VORTEX FLOW

CASE AFT CLOSURE

VISCOUS DRAG ALONG SEPARATED BOUNDARY DRIVES VORTEX IN SEPARATED FLOW REGION

VISCOUS DRAG FORCE = SKIN FRICTION DRAG FORCE

24535-103

The initial unseparated flow exists for only a very short period of time, and therefore, would not appreciably affect the erosion rate. The adiabatic wall temperature is equal to the gas temperature in this region.

Nozzle inlet: The nozzle inlet was analyzed for both the initial and final surface condition using the subsonic flow analysis.

The subsonic flow field is calculated by a solution of the Euler equation, the continuity equation, the condition of irrotational flow, and an expression for the speed of sound in an isentropic flow.

The inviscid, steady state flow field is calculated by a relaxation solution of the finite difference equation in terms of the stream function. The density is corrected at each mesh point in the calculation to account for compressibility.

Arbitrarily prescribed inlets, outlets, and channel boundaries are allowed with few restrictions. Mass addition (from burning or ablation) is allowed along any boundary and is input as a gradient in the stream function. This is particularly useful where the propellant surface is near the nozzle. The output consists of streamlines for specified values of the stream function and values of velocity, flow angle, pressure ratio, and Mach number along the streamlines.

An option allows the calculation of the uncoupled particle trajectories for any diameter and density and for any set of starting conditions at an inlet. The program calculates the trajectory and the conditions at impact (if necessary).

This program well defines the inviscid flow field at the edge of the boundary layer.

Supersonic flow regime. - On a conical nozzle, the wall flow conditions are not widely different from a one-dimensional analysis, so this assumption was used for the exit cone. The exit cone was analyzed at both the initial and final surface condition.

Turbulent Boundary Layer

In solid rocket motors, the boundary layer is generally turbulent in the critical areas for analysis; therefore, this discussion considers turbulent boundary layer only. In a nozzle evaluation, the Reynolds number is checked to insure turbulent flow.

The boundary layer program calculates boundary-layer thicknesses, skin friction, and heat flux in axisymmetric nozzles. The method solves simultaneously the integral momentum and energy equations. Boundary layer shape parameters are based on a one-seventh power profile of velocity and stagnation temperature.

The program is based on a program developed by Elliott, Bartz, and Silver at JPL on Contract NAS7-100.[a]

The program either calculates one-dimensional Mach numbers or accepts input values from the subsonic, transonic, and supersonic flow calculations. The output is displacement thickness, momentum thickness, convective heat transfer coefficient, convective and radiative heat fluxes, skin friction coefficient, and the wall shear force.

Wall Erosion Prediction

To provide wall erosion predictions, the following motor information must be available.

1. Grain configuration

2. Propellant blowing coefficient

3. Nozzle configuration

4. Throat diameter

5. Average web pressure

6. Liner materials selected.

Two erosion prediction methods were used: (1) aerodynamic material performance curves and (2) a method for preliminary sizing of nozzle liner.[b] During the program contract period, both erosion prediction methods were used.

Method 1. -

1. Calculate initial (uneroded) and final (eroded) convective heat transfer coefficient (h/cp) for the nozzle internal wall surface. Reference Figure A-3 for the initial (h/cp) of the TU-379 nozzle with carbonaceous liner materials. An average (h/cp) is used in further calculations.

2. Measure and tabulate the wall material erosion and char rate from past test nozzles.

---

[a]Elliott, D. G. et al.: Calculation of Turbulent Boundary Layer Growth and Heat Transfer in Axisymmetric Nozzles, JPL Technical Report No. 32-387, February 1963.
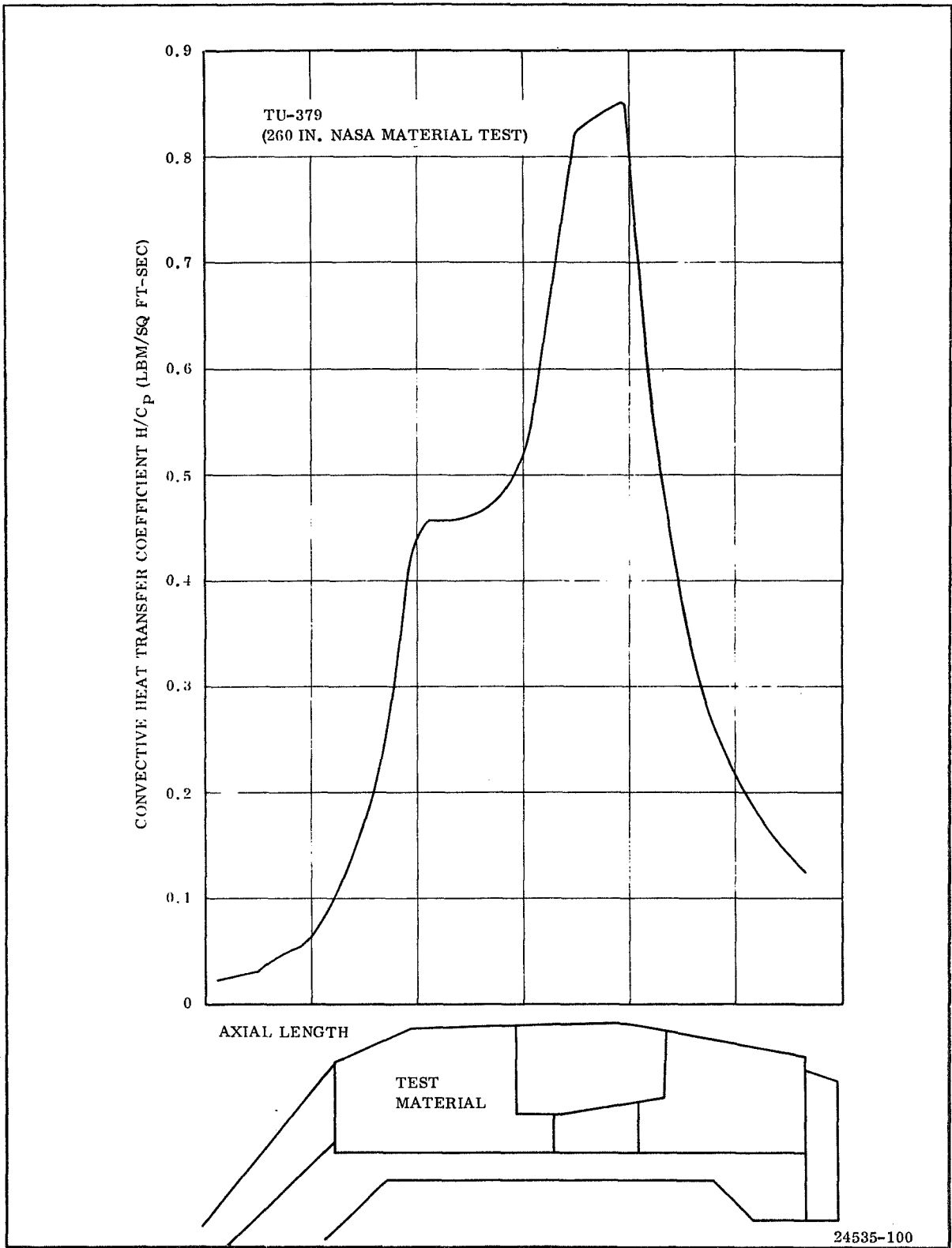[b]Thiokol-Wasatch Document TWR-1710.

Figure A-3. TU-379 h/cp vs Axial Length

3. Plot a material performance design curve by plotting the wall erosion rate versus the average h/cp times $\beta \dfrac{(12,000)}{\rho}$ at that wall location.

β = Propellant blowing coefficient
ρ = Wall material density (lb/cu ft)

4. Draw the theoretical and actual design line through the plotted data (Figure A-4). Theoretical erosion rates are calculated based on the theory describing the surface chemical reaction between the carbonaceous wall and the oxidizing species in the exhaust. The actual design line may be on, above, or below the theoretical design line.

5. To predict the erosion rate for SP-8057 in the larger TU-622 nozzle, enter the TU-379 SP-8057 material performance curve with the wall erosion parameter $\dfrac{(h/cp)\ \beta\ 12,000}{\rho}$ and read out the predicted erosion rate. The h/cp for the TU-622 nozzle versus axial distance is shown in Figure A-5.

Method 2. – The following steps are followed to predict the wall material erosion rate along the nozzle axial length (Figure A-6).

1. Enter Bartz simplified convective heat transfer coefficient chart with the area ratio of the wall plane where the erosion rate is required and read out the convective heat transfer coefficient for the reference conditions of 1,000 psi, D_t = 10.00 in., blowing coefficient = 0.108, and wall temperature = 5,790° F.

2. Modify the convective heat transfer coefficient to the required motor average web pressure and throat diameter as shown.

$$\text{Modified h/cp} = (h/cp)_{1,000\ psi}\left(\frac{P}{1,000}\right)^{1/1.25}\left(\frac{10}{D_t}\right)^{1/5}$$

$$D_t = 10\ \text{in.}$$

3. Enter a material performance graph of the same material as the liner wall material with the modified convective heat transfer coefficient and read out the predicted wall erosion rate.
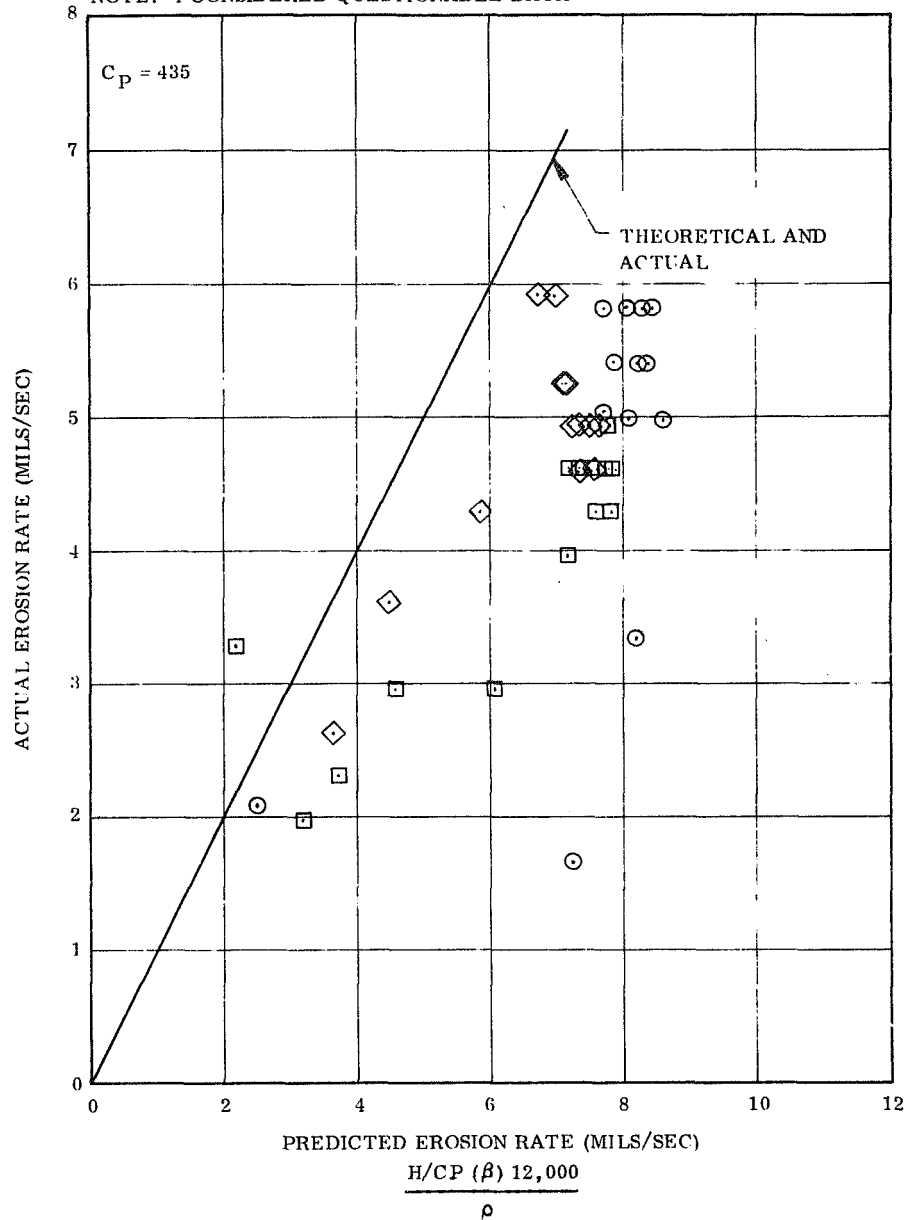
Figure A-4. TU-379 Erosion Performance, SP-8057 (Pluton H-1 Phenolic)

$D_t = 1.74$

$C_p = 435$

UNERODED CONFIGURATION
CARBONACEOUS MATERIALS

CONVECTIVE HEAT TRANSFER
COEFFICIENT (H/CP (LBM/SQ FT-SEC)

AXIAL DISTANCE (IN.)

MODIFIED
CONFIGURATION

THROAT

MODIFIED
CONFIGURATION
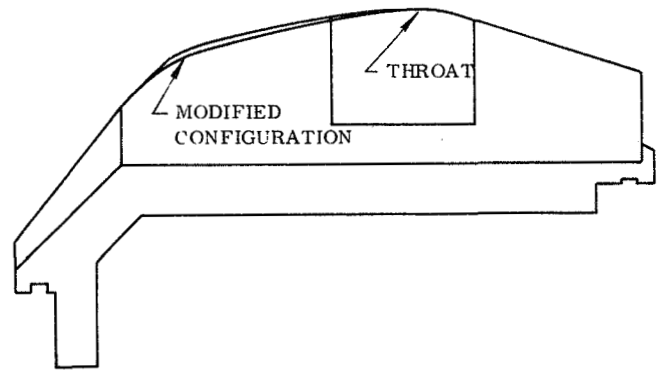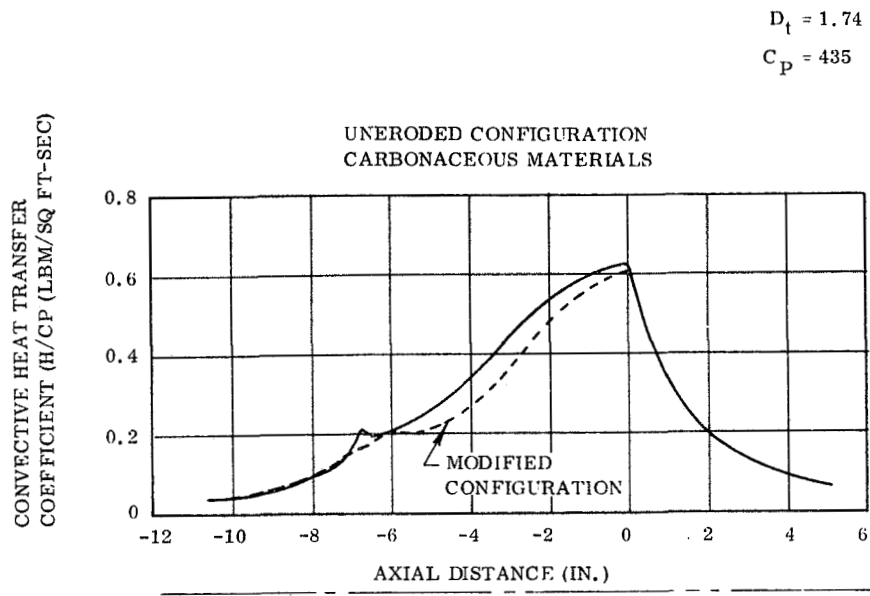
24535-102

Figure A-5. TU-622 Boundary Layer Parameters

A-11

Figure A-6. Wall Erosion Rate Prediction Calculation Steps

4. Modify the predicted erosion rate by the grain shape factor (GSF), end burner, star or CP, the propellant blowing coefficient (PBC) and the nozzle shape factor (NSF) external, submerged and type of TVC control.

$$\text{Modified erosion rate} = \text{erosion rate (GSF)} \left(\frac{PBC}{0.108} \right) \text{(NSF)}$$

Wall Transient Temperature

The material response program is called the One-Dimensional Char and Ablate Program (3132). The program is used to predict nozzle liner wall thermal gradients from internal gas heating.

The program provides an explicit, finite difference solution for the transient transport of thermal energy in a one-dimensional axisymmetric body, which can experience decomposition in depth. The program energy balance considers resin pyrolysis and surface regression (erosion).

The ablating surface boundary condition is permitted in two forms:

Option 1, general convection, radiation heating with coupled mass transfer, assuming unity Lewis number.

Option 2, specified surface temperature and surface recession rate.

Option 2 was used for the wall temperature gradient predictions.

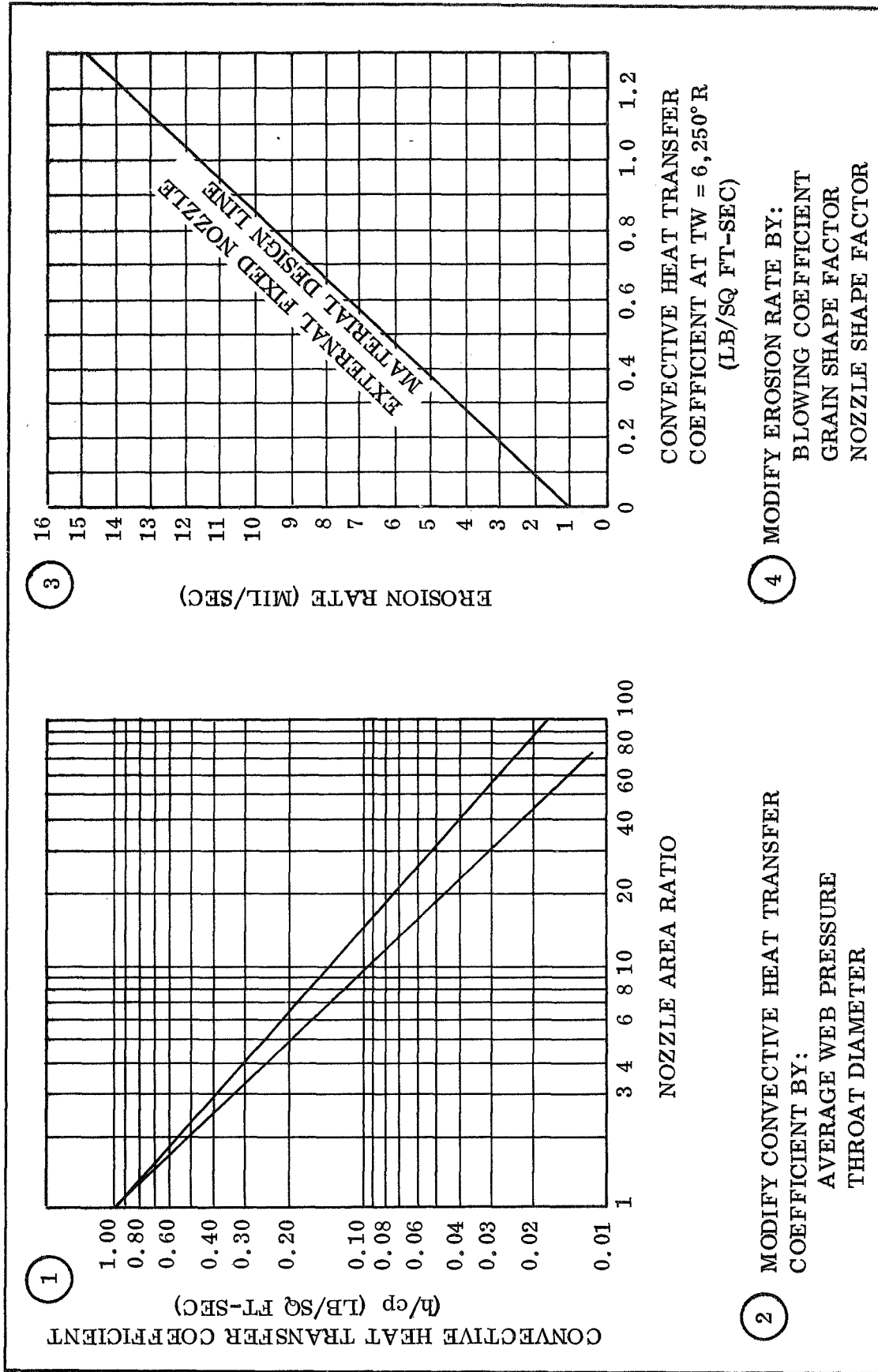The program input includes wall material properties, convective heat transfer coefficients, predicted wall erosion rates, and wall material thicknesses.

The program output includes internal wall temperatures which are plotted versus radial wall thickness. In addition, erosion and char depths are marked off at the internal wall diameter and at the 500° F temperature line (Figure A-7).

Sample Analysis

To illustrate the results of this type of analysis procedure, an example is included for a TU-622 materials test motor. Some of the vital motor parameters are:

Motor Designation	TU-622
Propellant	TP-H1011 16% Al, 86% solids HB binder - endburner - uncured

A-13
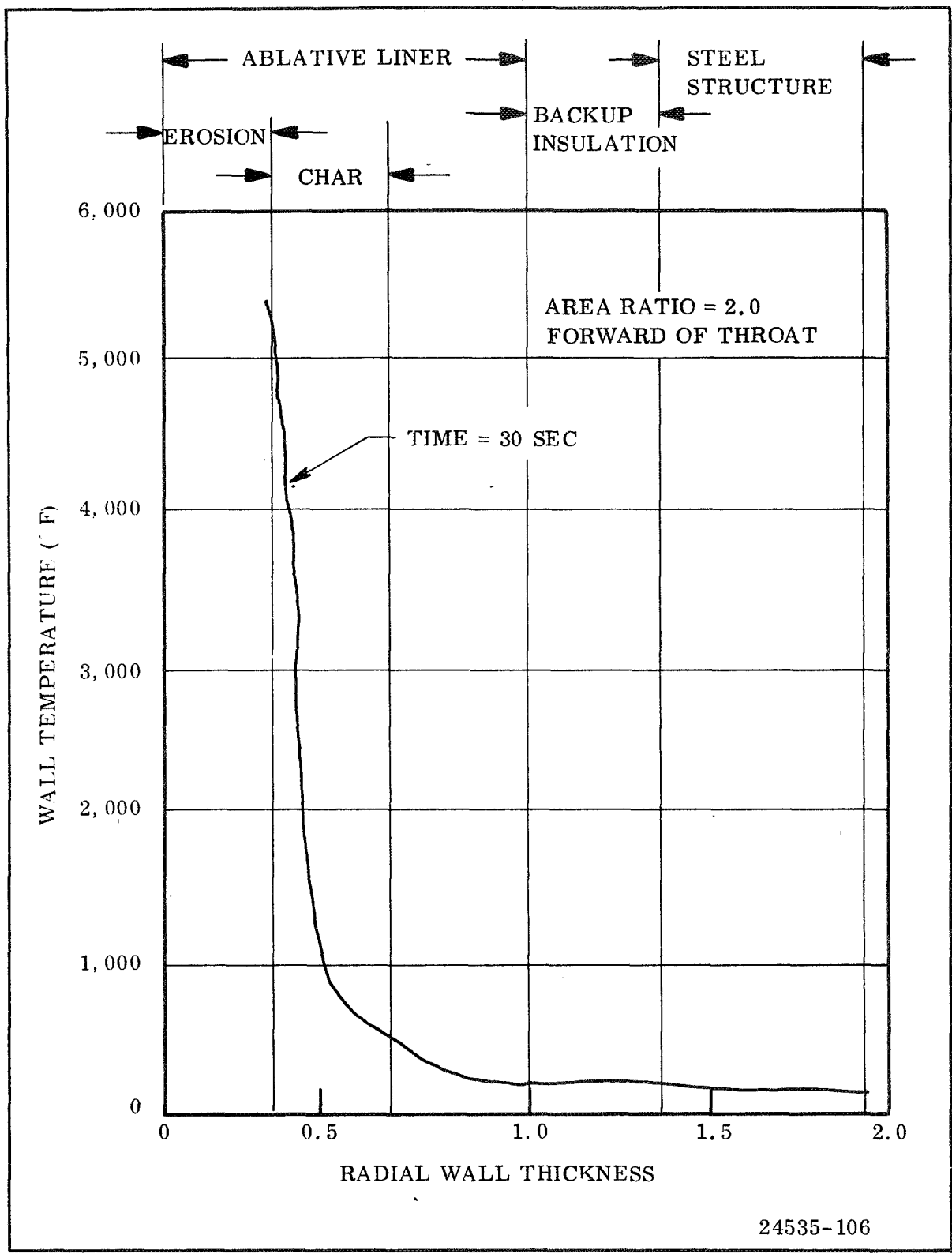
Figure A-7. Wall Temperature Profile

24535-106

Throat Diameter (in.)	1.74
Propellant Weight (lbm)	250
Burn Time (sec)	35
Chamber Pressure (psi)	400

A cross section of the tested nozzle is shown in Figure A-8 with a carbon cloth (SP-8057) used in all three nozzle locations (inlet, throat, and exit). The wall Mach numbers for the uneroded configuration are shown in Figure A-9. The propellant gas thermodynamic properties and composition used were:

	Chamber	Throat
Enthalpy Mixture (cal/gm)	-459.6	-587.5
Enthalpy Gas (cal/gm)	327.7	237.3
Molecular Weight	28.382	28.636
Heat Capacity (cal/gm°K)	0.8949	0.8188
Gamma	1.1397	1.1416
Blowing Coefficient	0.11	0.108
C*	5,162.5	--

Species present in mole fraction above 0.01.

	Chamber	Throat
CO	0.277	0.277
CO_2	0.016	0.016
Cl	0.013	0.011
HCl	0.128	0.135
H	0.039	0.032
OH	0.010	0.007
H_2	0.256	0.261

Figure A-8. TU-622 Material Test Nozzle and Measured Erosion-Char
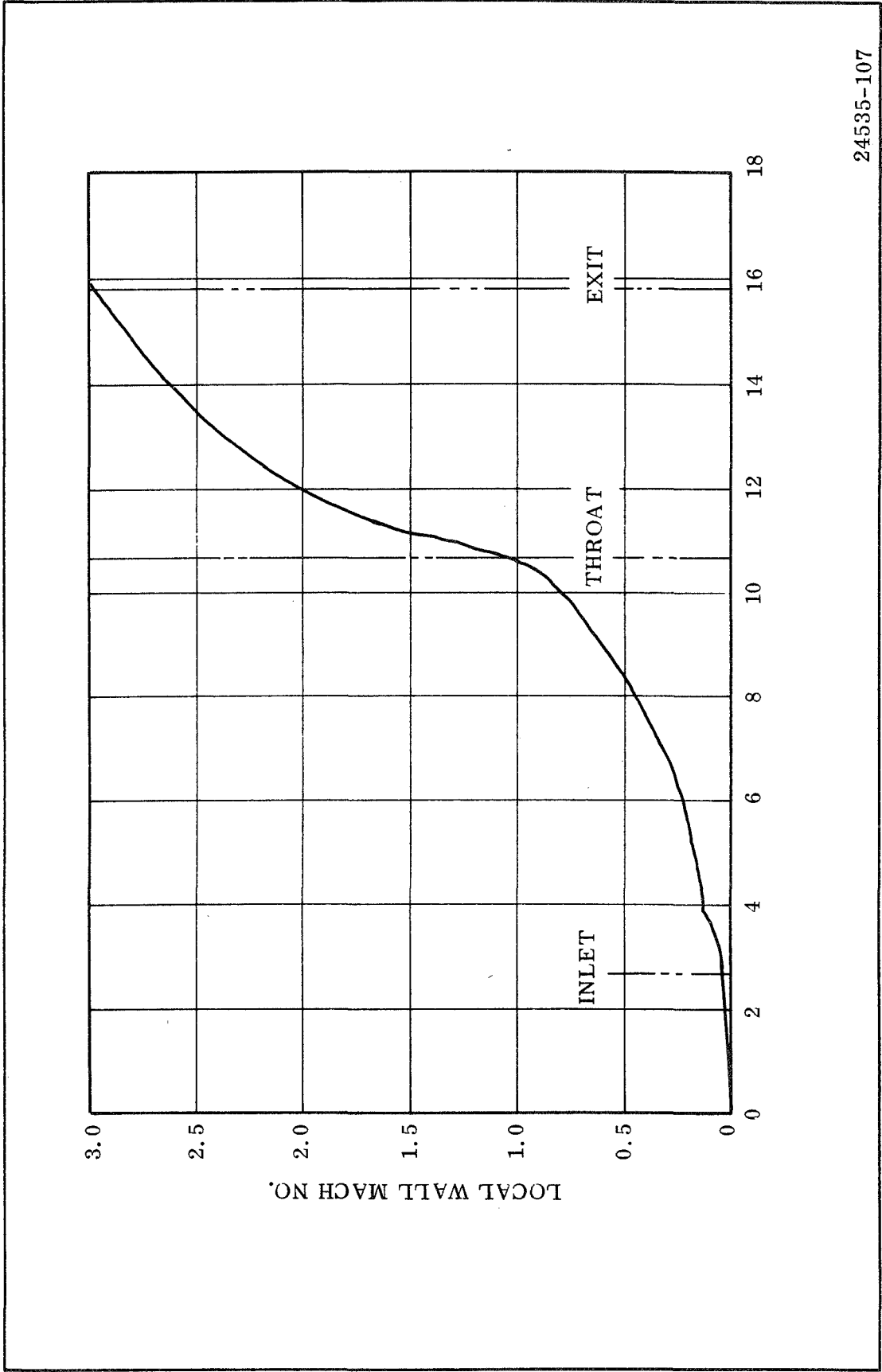
24535-105

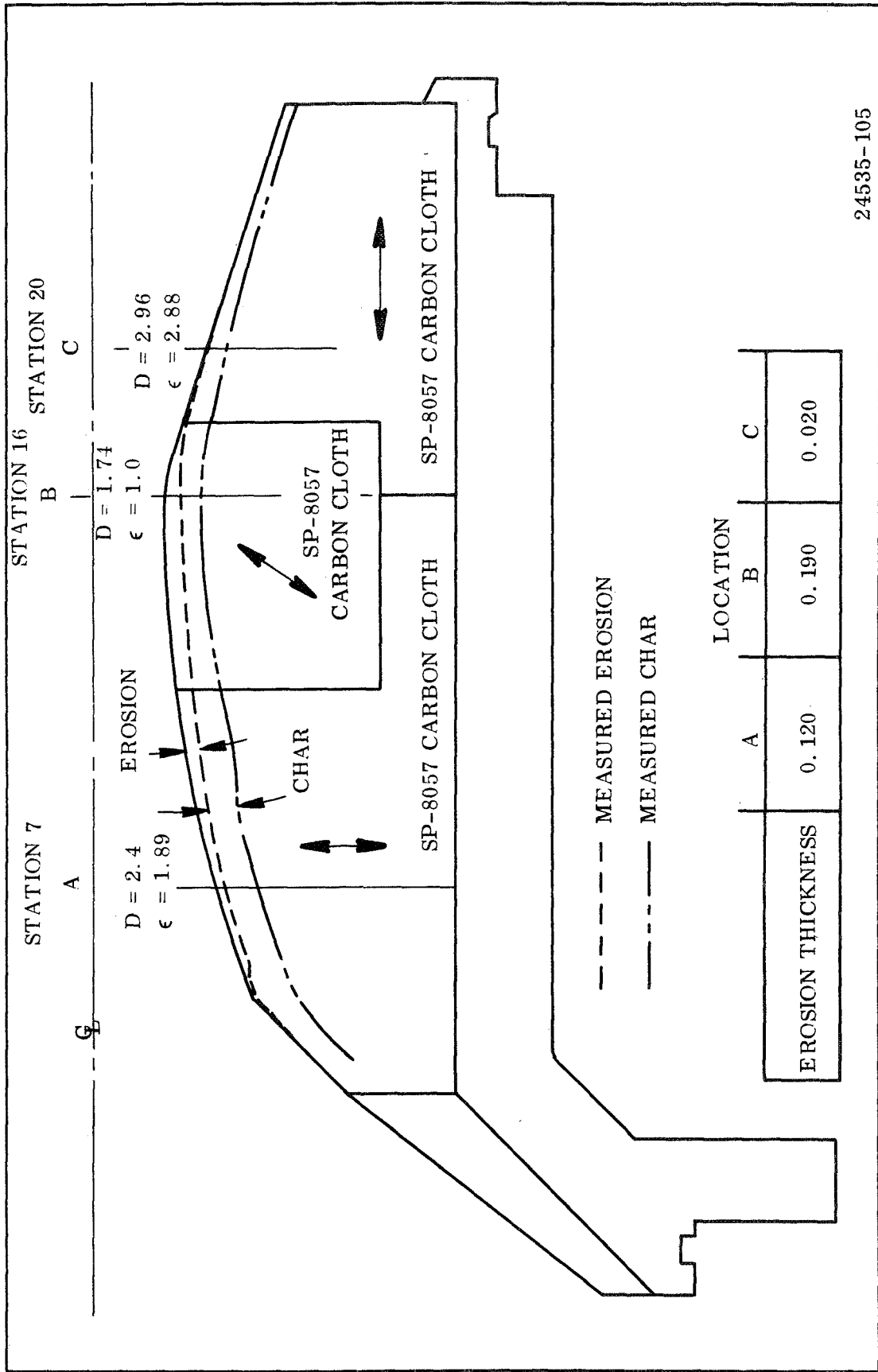Figure A-9. Material Test Nozzle (TU-622) Mach No. Profile

24535-107

	Chamber	Throat
H_2O	0.143	0.143
N_2	0.080	0.081
$Al_2O_3(1)$	0.076	0.078

The species which were considered in the carbon cloth oxidation are CO_2, H_2, and H_2O. These three species were considered in the material response analysis.

The predicted erosion depth for the TU-622 SP-8057 liner nozzle is calculated by the two erosion prediction methods and are shown in Figure A-10. The erosion prediction methods at the three stations either bracket the actual erosion depth on the high and low side (inlet, throat) or are both larger than the actual erosion depth (exit).

The one-dimensional char and ablate program output provides internal wall temperatures that are plotted versus radial wall thickness as shown in Figure A-11. The profiles are of particular interest for the predicted depth of heat penetration to insure that the steel structural shell remains at room temperature throughout the motor static test.
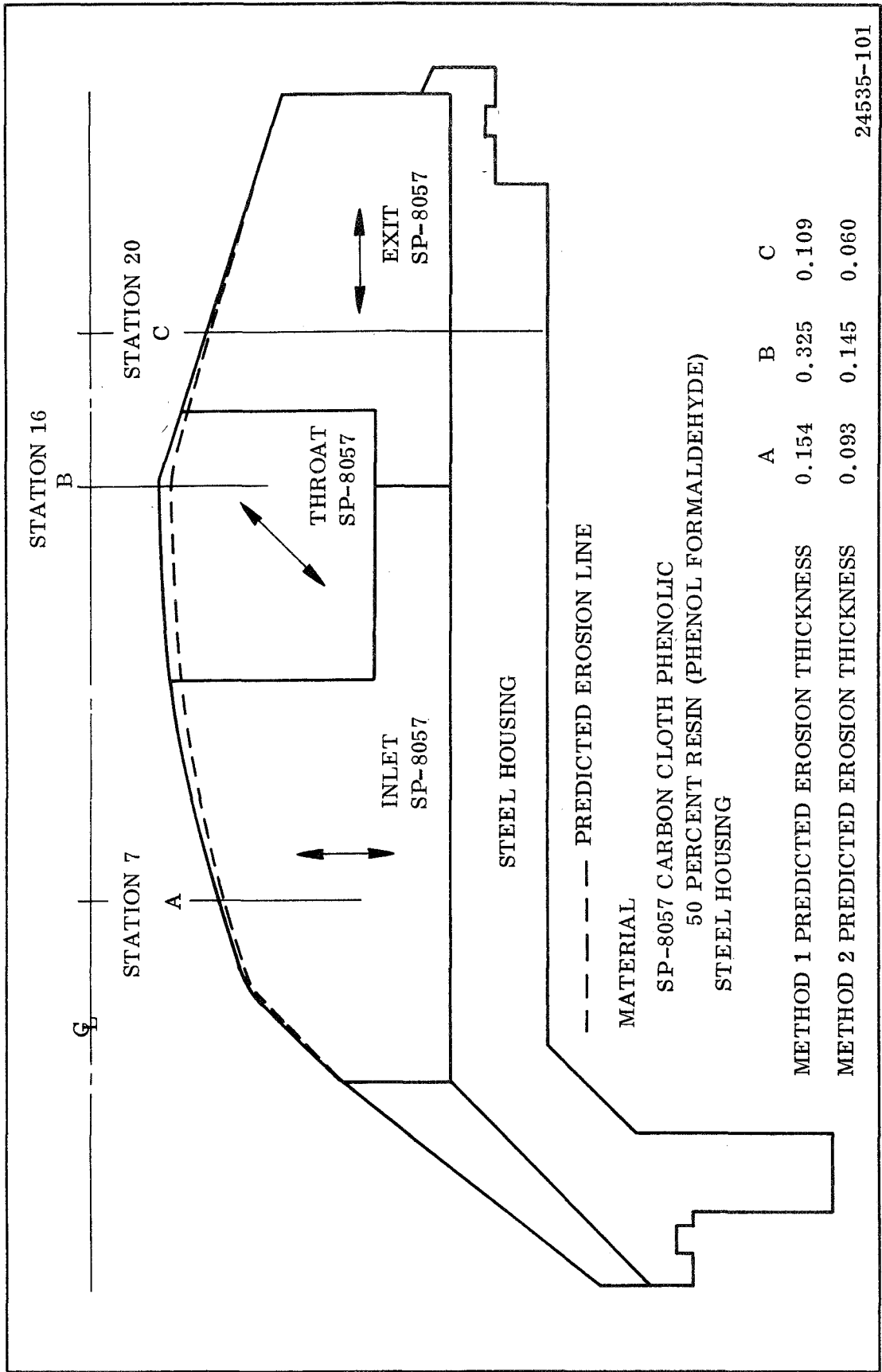
Figure A-10. TU-622 Material Response Prediction

24535-101

	A	B	C
METHOD 1 PREDICTED EROSION THICKNESS	0.154	0.325	0.109
METHOD 2 PREDICTED EROSION THICKNESS	0.093	0.145	0.060

PREDICTED EROSION LINE

MATERIAL
SP-8057 CARBON CLOTH PHENOLIC
50 PERCENT RESIN (PHENOL FORMALDEHYDE)
STEEL HOUSING

STATION 7

STATION 16

STATION 20

INLET SP-8057

THROAT SP-8057

EXIT SP-8057

STEEL HOUSING
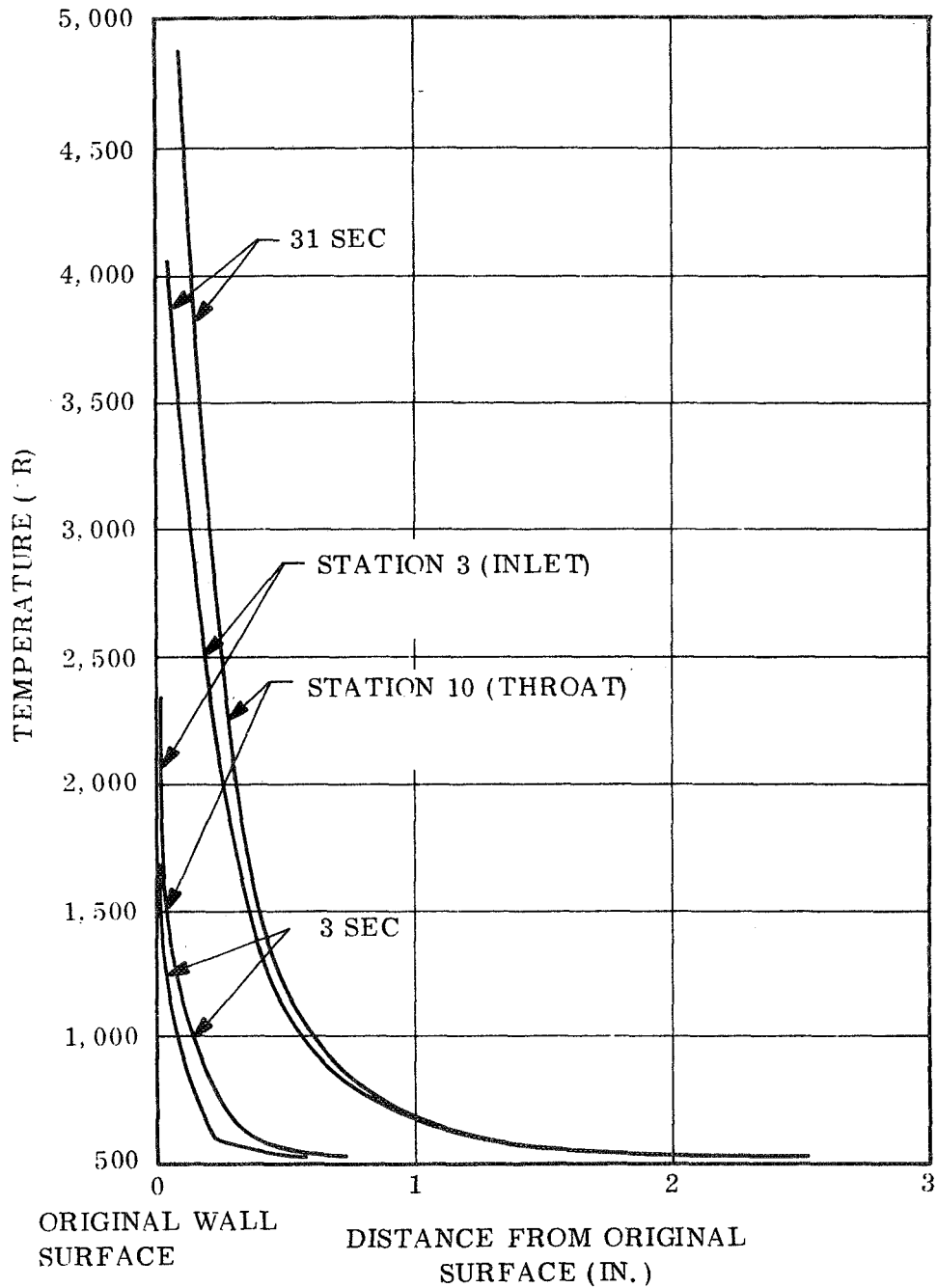
Figure A-11. TU-622 Material Temperature Profiles

24535-104

APPENDIX B

MATERIALS PROPERTY TEST METHODS

The test methods utilized in the conduct of materials property testing are listed in Table B-I. ASTM and Federal Specification methods of test were utilized in obtaining all materials properties with the exception of specific heat and thermal conductivity. Thiokol Standard Laboratory Procedures SLP-526, Determination of Thermal Conductivity of Solid Nonconductive Materials (Attachment No. 1) and SLP-527, Determination of Specific Heat of Various Materials (Attachment No. 2) were used in obtaining the above thermal properties.

TABLE B-I

MATERIAL TEST METHODS

Material Properties	Test Method	Test Specimen State	Test Specimen Ply Orientation (deg)
Specific Heat	Thiokol Std Lab Procedure SLP-527	Virgin	--
Thermal Conductivity	Thiokol Std Lab Procedure SLP-526	Virgin	Normal - 90
Coefficient of Thermal Expansion	ASTM D696	Virgin	Parallel - 0
Ultimate Compressive Strength	ASTM D695	Virgin	Warp - 0 Fill - 90
Ultimate Tensile Strength	ASTM D638	Virgin	Warp - 0 Fill - 90
Ultimate Interlaminar Shear Strength	Fed Spec L-P-406 Method 1042	Virgin	Warp - 0 Fill - 90
Young's Modulus Tension	ASTM D638	Virgin	Warp - 0 Fill - 90
Specific Gravity	Fed Spec L-P-406 Method 5012	Virgin	---
Hardness Shore "D"	ASTM D1706	Virgin	---

ATTACHMENT NO. 1

Thiokol Standard Laboratory Procedure SLP-526 Determination of
Thermal Conductivity of Solid Nonconductive Materials

1.0   PURPOSE

        This procedure provides a method for determining the thermal conductivity
        of solid, nonconductive materials.

2.0   SCOPE

        This procedure defines the method by which all thermal conductivity
        determination will be performed of cured propellants at the Thiokol Chemical
        Corporation, Wasatch Division.

3.0   APPARATUS

3.1   Cenco-Fitch Heat Conductivity Apparatus, Cat. No. 77555.

3.2   Cenco Immersion Heater, Cat. No. 16554 or equivalent.

3.3   Linear scale microammeter, millivolt potentiometer, or recording milli-
        volt potentiometer.

3.4   Vernier calipers.

3.5   Two aluminum plates 8 in. x 8 in. x 1/8 in. with centered 4 in. diameter
        holes.

3.6   Constantan wire.

3.7   Small copper wire.

3.8   Weight (about 4 kg).

4.0   METHOD

4.1   Samples suitable for testing must have a minimum size of 2 in. x 2 in. and
        be between 1/4 in. and 1/2 in. thick. Thicker specimens give low values
        for thermal conductivity as a result of heat loss from the edges.

        The specimens should be uniform in thickness with smooth surfaces permitting
        maximum surface contact between the sample, the source vessel, and receiver.

4.2   Connect the two constantan thermocouple binding posts on the source and
        receiving vessels with a short piece of constantan wire. With a piece of
        copper wire, connect the copper terminals of the thermocouples to the poles
        of the microammeter or potentiometer.

4.3   Place the sample to be tested on a clean flat surface, such as a bench top.
        Fill source vessel with water and place over the sample. Place the immersion
        heater in the water to heat the water and to maintain a constant, boiling
        temperature. Care should be exercised to prevent the grounded heater cover
        from coming in contact with the walls or bottom of the source vessel. The
        receiver should be approximately at room temperature. At this condition the
        maximum deflection of the microammeter or potentiometer will be noted.

        NOTE: When successive determinations are to be made using the same
              equipment, the copper receiving plug can be cooled to room
              temperature rapidly by placing an aluminum weighing dish filled
              with ice on top of it.

4.4   When the ammeter or potentiometer is steady, TURN OFF and remove the
        heater.

        NOTE: The immersion heater must not be left on after it has been removed
              from the water.

4.5   Place the sample over the receiving plug, and place the source vessel on top
        of the sample. Care should be taken to prevent the source and receiver from
        being grounded or from touching each other. Place the weight (4 kg) on top
        of the source vessel to insure intimate contact of the sample with the source
        and receiver. Place the immersion heater in the water, turn it on, and
        maintain the water at boiling temperature.

4.6   Record the ammeter or potentiometer reading at regular intervals (one, two,
        or three minutes) according to the rate of the change in the reading. A
        series of about 10 readings should be taken. If a recording potentiometer
        is used, allow sufficient time to elapse after a near-constant rate of change
        is noted, to give 10 readings at regular time intervals.

4.7   Remove the sample slab from the apparatus. Measure the thickness of the sample using a pair of vernier calipers. Care must be taken to apply about the same pressure to the sample as is applied in the apparatus during the determination. Measurement of this thickness is facilitated if an aluminum plate with a 4 in. diameter section removed from it is centered and glued to the bottom of the source vessel and a similar one fixed to the top of the receiving vessel. A measurement of the actual separation of the bottom of the source vessel and the top of the receiving plug during the conductivity determination is then made possible. It will, however, first be necessary to calibrate the separation of the plates with a solid block of material of known thickness.

4.8   Plot a graph of the data using time as the ordinate and the logarithm of the ammeter or potentiometer reading as the abscissa. Draw the best fitting straight line. Plotting this graph may be simplified by the use of semilog graph paper.

4.9   Calculate the slope of the line as follows:

$$m = \frac{td_c}{d_i}$$

Where: m = slope of the line

t = time in seconds

d_c = length of one cycle on the similog graph paper in cm

d_i = length of abscissa from initial reading of ammeter or potentiometer (i_o) to final reading (i_t) at time (t)

For example:
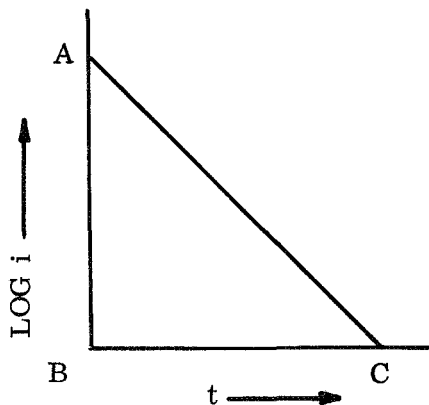
$$m = \frac{BC\ (sec)}{AB\ (cm)} \times \text{length of one cycle (cm)}$$

5.0 CALCULATIONS

Calculate the thermal conductivity (K) by use of the equation:

$$K = \frac{LMc}{mA}$$

Where:
K = thermal conductivity of sample $\left(\dfrac{cal\text{-}cm}{cm^2\text{-}sec\text{-}°C} \right)$

L = thickness of sample (cm)

M = mass of copper plug on receiver (g)

c = specific heat of copper plug = 0.093 cal/g-°C

m = slope (sec) (from 2.9 above)

A = upper surface area of the copper plug

5.1 Report the value of K to the nearest 0.01×10^{-4}

$$\frac{cal\text{-}cm}{cm^2\text{-}sec\text{-}°C}$$

Thiokol Standard Laboratory Procedure SLP-527,
Determination of Specific Heat of Various Materials

1.0   PURPOSE

This procedure provides a method, utilizing the Parr calorimeter, for determining the specific heat of various materials used in rocket motor manufacturing by Thiokol Chemical Corporation, Wasatch Division.

2.0   SCOPE

This procedure applies to cured solid propellant, insulation, liner, and other similar solids materials which go into Thiokol rocket motors.

3.0   PROCEDURE

3.1.0   Apparatus

3.1.1   Parr calorimeter and accessories.

3.1.2   Constant temperature drying oven.

3.1.3   Analytical balance capable of weighing to nearest milligram.

3.1.4   Torsion balance capable of weighing to nearest 0.5 gram.

3.2.0   Calibration of Calorimeter

3.2.1   Using a torsion balance, weigh 2,000 ± 0.5 grams of cold tap water into the calorimeter bucket. Replace the bucket in the calorimeter, close the lid and lower the thermometer into the water. Start the stirrer and take temperature readings one minute apart. Do this until three consecutive readings agree within ± 0.01°C. Record this temperature for calculation purposes.

3.2.2   Weigh 250 ± 0.5 grams of hot water at about 60°C into a 600 ml beaker. Open the calorimetric lid, measure the hot water temperature to the nearest 0.1°C, record this temperature, and pour the water into the bucket. Replace the lid, start the stirrer, and read the temperatures as previously until three consecutive readings agree within ± 0.01°C. Record this temperature.

3.2.3   Calculations

The heat capacity of the calorimeter plus the 2,000 grams of water are calculated according to the following formula:

$$Qc = G_W \times S_W \times T_W = Cal/°C$$

Where: Qc = Heat capacity of calorimeter plus 2,000 grams of water

G_W = grams of hot water added

S_W = specific heat of water

T_W = change in temperature of hot water in °C equal to initial water temperature minus final calorimeter temperature

T_c = change in temperature of calorimeter in °C

4.0   SAMPLE ANALYSIS

4.1   The sample should be approximately 3 in. by 3 in. by 0.5 in. and should preferably weigh between 100 and 300 grams.

4.2   Weigh the sample to the nearest 0.01 gram. Place in a constant temperature oven at about 110°C for at least 30 minutes before analyzing.

4.3   Weigh 2,000 ± 0.5 grams of cold tap water into the calorimeter bucket. Replace the bucket in the calorimeter, close the lid and lower the thermometer into the water. Start the stirrer and take temperature readings one minute apart. Do this until consecutive readings agree within ± 0.01°C. Record this temperature for calculation purposes.

4.4   Record the temperature of the sample conditioning oven to ± 0.1°C. Open the lid to the calorimeter and quickly transfer the sample from the oven to the calorimeter bucket. Close the calorimeter lid and take the temperature readings as previously until three consecutive readings agree within ± 0.01°C. Record this temperature.

4.5   Calculations

The specific heat of the sample is calculated according to the following formula:

$$S_s = \frac{Q_c \times T_c}{G_s \times T_s} = cal/gm°C$$

Where: S_s = specific heat of sample

Q_c = heat capacity of calorimeter plus 2,000 grams of water (see para 2.1.3)

T_c = change in temperature of calorimeter in °C

G_s = weight of sample in grams

T_s = change in temperature of sample in °C; equal to initial sample temperature minus final calorimeter temperature

4.6   Report the specific heat to the nearest hundredth as calories per gram per degree centigrade.

DISTRIBUTION LIST

Recipient	Copies
NASA Lewis Research Center	
21000 Brookpark Road	
Cleveland, Ohio 44135	
Attn: Contracting Officer	
Mail Stop 500-313	(1)
Solid Rocket Technology Branch	
Mail Stop 500-205	(8)
Technical Library	
Mail Stop 60-3	(2)
Tech. Report Control Office	
Mail Stop 5-5	(1)
J. Kennard	
Mail Stop 3-17	(1)
Tech. Utilization Office	
Mail Stop 3-19	(1)
Patent Counsel	
Mail Stop 500-311	(1)
National Aeronautics and Space Administration	
Washington, D.C. 20546	
Attn: RPM/William Cohen	(3)
RPS/Robert W. Ziem	(1)
ATSS-AL/Technical Library	(2)
NASA Ames Research Center	
Moffett Field, California 94035	
Attn: Technical Library	(1)
NASA Langley Research Center	
Langley Station	
Hampton, Virginia 23365	
Attn: Robert L. Swain	(1)
Technical Library	(1)
NASA Goddard Space Flight Center	
Greenbelt, Maryland 20771	
Attn: Technical Library	(1)
NASA Manned Spacecraft Center	
2101 Webster Seabrook Road	
Houston, Texas 77058	
Attn: Technical Library	(1)

Recipient	Copies
NASA George C. Marshall Space Flight Center	
Redstone Arsenal	
Huntsville, Alabama 35812	
Attn: Technical Library	(1)
R-P & VE-PA/K, Chandler	(1)
Jet Propulsion Laboratory	
California Institute of Technology	
4800 Oak Grove Drive	
Pasadena, California 91103	
Attn: Richard Bailey	(1)
Technical Library	(1)
Scientific & Technical Information Facility	
NASA Representative	
P. O. Box 33	
College Park, Maryland 20740	
Attn: CRT	(6)
GOVERNMENT INSTALLATIONS	
AF Space Systems Division	
Air Force Unit Post Office	
Los Angeles, California 90045	
Attn: Col. E. Fink	(1)
AF Research and Technology Division	
Bolling AFB, D.C. 20332	
Attn: Dr. Leon Green, Jr.	(1)
AF Rocket Propulsion Laboratory	
Edwards AFB, California 93523	
Attn: RPM/Mr. C. Cook	(2)
AF Materials Laboratory	
Wright-Patterson AFB, Ohio 45433	
Attn: MANC/D. Schmidt	(1)
MAAE	(1)
P. F. Pirrung	(1)

Recipient	Copies	Recipient	Copies
AF Ballistic Missile Division P. O. Box 262 San Bernardino, California 92402 Attn: WDSOT	(1)	Chemical Propulsion Information Agency Applied Physics Laboratory 8621 Georgia Avenue Silver Spring, Maryland 20910	(1)
Structures Division Wright-Patterson AFB, Ohio 45433 Attn: FDT/R. F. Hoener	(1)	Defense Documentation Center Cameron Station 5010 Duke Street Alexandria, Virginia 22314	(1)
Army Missile Command Redstone Scientific Information Center Redstone Arsenal, Alabama 35809 Attn: Chief, Document Section	(1)	Defense Materials Information Center Battelle Memorial Institute 505 King Avenue Columbus, Ohio 43201	(1)
Ballistic Research Laboratory Aberdeen Proving Ground, Maryland 21005 Attn: Technical Library		Materials Advisory Board National Academy of Science 2101 Constitution Ave., N.W. Washington, D.C. 20418 Attn: Capt. A. M. Blamphin	(1)
Picatinny Arsenal Dover, New Jersey 07801 Attn: Technical Library		Institute for Defense Analysis 1666 Connecticut Ave., N.W. Washington, D.C. 20009 Attn: Technical Library	(1)
Navy Special Projects Office Washington, D.C. 20360 Attn: H. Bernstein		Advanced Research Projects Agency Pentagon, Room 3D154 Washington, D.C. 20301 Attn: Technical Information Office	(1)
Naval Air Systems Command Washington, D.C. 20360 Attn: AIR-330/Dr. O. H. Johnson		Naval Research Laboratory Washington, D.C. 20390 Attn: Technical Library	(1)
Naval Propellant Plant Indian Head, Maryland 20640 Attn: Technical Library		INDUSTRY CONTRACTORS	
Naval Ordnance Laboratory White Oak Silver Spring, Maryland 20910 Attn: Technical Library		Aerojet-General Corporation P. O. Box 296 Azusa, California 91702 Attn: Technical Library	(1)
Naval Ordnance Test Station China Lake, California 93557 Attn: Technical Library C. J. Thelen			

Recipient	Copies	Recipient	Copies

Aerojet-General Corporation
P. O. Box 1168
Solid Rocket Plant
Sacramento, California 94086
Attn: Dr. B. Simmons
      Technical Information Center
      Space Booster Department
	
	(1)
	(1)
	(8)
		Lockheed Missiles & Space Company
		P. O. Box 504
		Sunnyvale, California 94088
		Attn: Technical Library
			
			(1)

Aerospace Corporation 2400 East El Segundo Boulevard El Segundo, California 90245 Attn: Technical Library Solid Motor Dev. Office	 (1) (1)	Lockheed Propulsion Company P. O. Box 111 Redlands, California 93273 Attn: Bud White	 (1)
Aerospace Corporation P. O. Box 95085 Los Angeles, California 90045 Attn: Technical Library		Martin Marietta Corporation Baltimore Division Baltimore, Maryland 21203 Attn: Technical Library	 (1)
Atlantic Research Corporation Shirley Highway at Edsall Road Alexandria, Virginia 22314 Attn: Technical Library		Mathematical Sciences Corporation 278 Renook Way Arcadia, California 91107 Attn: M. Fourney	 (1)
Battelle Memorial Library 505 King Avenue Columbus, Ohio 43201 Attn: Edward Unger		Philco Corporation Aeronutronics Division Ford Road Newport Beach, California 92660 Attn: Technical Library	 (1)
The Boeing Company P. O. Box 3999 Seattle, Washington 98124 Attn: Technical Library		Rocketdyne Solid Propulsion Operations P. O. Box 548 McGregor, Texas 76657 Attn: Technical Library	 (1)
Chrysler Corporation Space Division Michoud Operations New Orleans, Louisiana 70150 Attn: Technical Library		Rocketdyne 6633 Canoga Avenue Canoga Park, California 91304 Attn: Technical Library	 (1)
Hercules, Inc. Allegany Ballistics Laboratory P. O. Box 210 Cumberland, Maryland 21502 Attn: Technical Library	 (1)	Rohm and Haas Redstone Arsenal Research Division Huntsville, Alabama 35807 Attn: Technical Library	 (1)
		Douglas Missiles & Space Systems Huntington Beach, California 92647 Attn: T. J. Gordon	 (1)

Recipient	Copies	Recipient	Copies
Hercules Company Bacchus Works P. O. Box 98 Magna, Utah 84044 Attn: Technical Library	(1)	Rohr Corporation Space Products Division 8200 Arlington Boulevard Riverside, California 92503	(1)
Thiokol Chemical Corporation Elkton Division Elkton, Maryland 21921 Attn: Technical Library	(1)	Raybestos-Manhattan, Inc. 4651 Pacific Building Los Angeles, California 90053	(1)
Thiokol Chemical Corporation Huntsville Division Huntsville, Alabama 35807 Attn: Technical Library	(1)	Narmco Materials Division Whittaker Corporation 600 Victoria Street Costa Mesa, California 92627	(1)
Minnesota Mining & Mfg Company 2501 Hudson Road St. Paul, Minnesota 55101	(1)	Hexcel Corporation Coast Division 11711 Dublin Boulevard Dublin, California 94566	(1)
US Polymeric, Inc. 700 E. Dyer Road Santa Ana, California 92707	(1)	HITCO 1602 West 135 Street Gardena, California 90249	(1)
Ferro Corporation 3512-20 Helms Avenue Culver City, California 90230	(1)	AVCO Corporation 201 Lowell Street Wilmington, Massachusetts 01887	(1)
Fiberite Corporation 645 No. Cypress Street Orange, California 92666	(1)	TRW, Inc. Structures Division 23444 Euclid Avenue Cleveland, Ohio 44117 Attn: L. Russell	(1)
United Technology Center P. O. Box 358 Sunnyvale, California 94088 Attn: Technical Library	(1)	TRW Systems One Space Park Redondo Beach, California 90278 Attn: M. Lipow	(1)

Recipient	Copies
Thiokol Chemical Corporation	
Wasatch Division	
Brigham City, Utah 84302	
Attn: C. Hickox	
Mail Stop 284	(2)
R. Ellis	
Mail Stop 284	(1)
R. Laramee	
Mail Stop 284	(1)
W. Allen	
Mail Stop 268	(1)
E. Gray	
Mail Stop 240	(1)
P. Russell	
Mail Stop 240	(1)
J. Mathis	
Mail Stop 240	(1)
E. Bennion	
Mail Stop 315	(1)
U. Garrison	
Mail Stop 310	(1)
Library	
Mail Stop 125C	(1)
W. Skidmore	
Mail Stop 712	(1)